

1 **Cemdata18: A chemical thermodynamic database for hydrated Portland cements and alkali-**
2 **activated materials**

3

4 Barbara Lothenbach^{1*}, Dmitrii A. Kulik², Thomas Matschei³, Magdalena Balonis⁴, Luis Baquerizo⁵, Belay
5 Dilnesa⁶, George D. Miron², Rupert J. Myers^{7,8}

6

7 ¹ Empa, Laboratory for Concrete & Construction Chemistry, CH-8600 Dübendorf, Switzerland

8 ² Paul Scherrer Institut, Laboratory for Waste Management, 5232 Villigen PSI, Switzerland

9 ³ HTW Dresden University of Applied Sciences, Department of Civil Engineering, 01069 Dresden, Ger-
10 many

11 ⁴ Department of Materials Science and Engineering, University of California Los Angeles, Los Angeles,
12 CA, USA

13 ⁵ Lafarge Centre de Recherche, 38291 Saint-Quentin Fallavier, France

14 ⁶ BASF Schweiz AG, 5082 Kaisten, Switzerland

15 ⁷ University of Sheffield, Department of Materials Science and Engineering, Sheffield, S1 3JD, UK

16 ⁸ Current address: University of Edinburgh, School of Engineering, Edinburgh, EH9 3FB, UK

17

18 * Corresponding author. Tel: +41 58 765 47 88; barbara.lothenbach@empa.ch

19 Keywords: thermodynamic modelling, cement, database, solubility, C-S-H

20

21

22 Accepted by Cement and Concrete Research April 2018.

23 Lothenbach, B., Kulik, D., Matschei, T., Balonis, M., Baquerizo, L., Dilnesa, B.Z., Miron, D.G.,
24 Myers, R. (in press) Cemdata18: A chemical thermodynamic database for hydrated Portland
25 cements and alkali-activated materials *Cement and Concrete Research*,
26 <https://doi.org/10.1016/j.cemconres.2018.04.018>

27

28

29

30 **Abstract**

31 Thermodynamic modelling can reliably predict hydrated cement phase assemblages and chemical
32 compositions, including their interactions with prevailing service environments, provided an accurate
33 and complete thermodynamic database is used. Here, we summarise the Cemdata18 database, which
34 has been developed specifically for hydrated Portland, calcium aluminate, calcium sulfoaluminate and
35 blended cements, as well as for alkali-activated materials. It is available in GEMS and PHREEQC com-
36 puter program formats, and includes thermodynamic properties determined from various experimental
37 data published in recent years. Cemdata18 contains thermodynamic data for common cement hy-
38 drates such as C-S-H, AFm and AFt phases, hydrogarnet, hydrotoalcite, zeolites, and M-S-H that are val-
39 id over temperatures ranging from 0 to at least 100°C. Solid solution models for AFm, AFt, C-S-H, and
40 M-S-H are also included in the Cemdata18 database.

41

42 **1 Introduction**

43 Numerous studies have shown that chemical thermodynamic modelling, coupled with accurate and
44 complete thermodynamic databases, can reliably predict hydrated cement phase assemblages and
45 chemical compositions. One of the most interesting aspects of applying thermodynamics to hydrated
46 cements has been the discovery that the chemical compositions of $\text{Al}_2\text{O}_3\text{-Fe}_2\text{O}_3$ mono (AFm) and
47 $\text{Al}_2\text{O}_3\text{-Fe}_2\text{O}_3$ tri (AFt) phases are very sensitive to the presence of carbonate [1-3] and temperature [4-
48 6], thus demonstrating that these factors may significantly modify hydrated cement phase assemblag-
49 es. Experiments have shown that compositions of hydrate cement phase assemblages can alter rapidly,
50 often within weeks or months, reflecting changing system compositions and temperatures. Thus,
51 thermodynamic calculations and experiments support each other: on the one hand, calculations enable
52 more complete interpretations of limited experimental datasets and help to identify key experiments
53 to perform; and on the other hand, experiments provide the data that are needed to validate calcula-
54 tion results and model parameters.

55 The quality of thermodynamic modelling results depends directly on the accuracy and completeness of
56 the input thermodynamic properties of substances and phases, which are usually supplied from a
57 thermodynamic database. Relevant thermodynamic data for solid cementitious substances, such as the
58 solubility products of ettringite or hydrogarnet, have been compiled in several specific "cement data-
59 bases" such as (1) the Cemdata07 and Cemdata14 databases [1, 7-12] (<http://www.empa.ch/cemdata>),
60 which are available for GEMS [13, 14], (2) the Thermoddem (<http://thermoddem.brgm.fr/>) database
61 [15, 16] available for the Geochemists Workbench® [17](<https://www.gwb.com/>) and PHREEQC [18] or
62 (3) HATCHES database [19] available for PHREEQC [18]. Data in the first two databases are generally
63 comparable, although some differences exist, as discussed in more detail in Damidot et al. [20]. Our
64 experience applying Cemdata in thermodynamic modelling applications underlines the importance of
65 a careful data selection and evaluation process, and of including sensitivity analyses into the analysis
66 and discussion of results.

67 Additional experimental data, and thermodynamic properties derived from these data, have become
68 available since the first compilation of Cemdata07 in 2007/2008 and subsequent compilation of
69 Cemdata14 in 2013/2014 [1, 7, 21]. Cemdata18 provides a significant update to both Cemdata07 and
70 Cemdata14. Cemdata18 is written into a format supporting the GEM-Selektor code [13, 14] and is fully
71 compatible with the freely available GEMS-Selektor version of the PSI-Nagra 12/07 TDB [22, 23]
72 (<http://gems.web.psi.ch/>). PSI/Nagra 12/07 TDB [22] contains the same entries for aqueous spe-
73 cies/complexes relevant to cement systems as the PSI/Nagra 01/01 [24], with only slight changes: the
74 thermodynamic properties of $\text{Si}_4\text{O}_8(\text{OH})_4^{4-}$ and $\text{AlSiO}_3(\text{OH})_4^{3-}$ were added, while the complex Al-
75 $\text{SiO}(\text{OH})_6^-$ was removed. The GEMS version of the PSI/Nagra 12/07 TDB includes further changes to the
76 thermodynamic properties of Al bearing species/complexes and the addition of Helgeson-Kirkham-
77 Flowers equation of state parameters to account for changes in temperature and pressure [25, 26].
78 Cemdata18 includes a comprehensive selection of cement hydrates commonly encountered in Port-
79 land cement (PC) systems in the temperature range of 0 to 100°C, including calcium silicate hydrate (C-
80 S-H), magnesium silicate hydrate (M-S-H), hydrogarnet, hydrotalcite-like phases, some zeolites, AFm
81 and AFt phases, and various solid solutions used to describe the solubility of these phases. Solubility
82 constants have generally been calculated based on critical reviews of all available experimental data
83 and from additional experiments made either to obtain missing data or to verify existing data. Addi-
84 tional solubility data were measured and compiled using temperatures ranging from 0 to 100°C in
85 many instances, as documented in [9, 12, 27, 28]. Numerous solid solutions among AFm and AFt
86 phases, siliceous hydrogarnets, hydrotalcite-like phases, C-S-H, and M-S-H have been observed and
87 are included in Cemdata18.

88 Several C-S-H solid solution models, as well as two models for hydroxide-hydrotalcite are available in
89 Cemdata18. The CSHQ model from [11] and the OH-hydrotalcite end member with $\text{Mg/Al} = 2$ are well
90 adapted for PC. Although the CSHQ model is able to describe the entire range of Ca/Si ratios encoun-
91 tered, it is best used for high Ca/Si C-S-H, as it still lacks the ability to predict aluminium uptake, which
92 is of less importance for Portland cements than for blended cements. For alkali activated binders, the
93 calcium (alkali) aluminosilicate hydrate (C-(N-)A-S-H) gel model, with lower calcium but higher alu-
94 minium and alkali content than in the C-S-H type phase which exists in hydrated PC, and a Mg-Al lay-
95 ered double hydroxide with variable Mg/Al ratio, are available.

96 This paper summarises Cemdata18, which includes the most important additions to the Cemdata07
97 and Cemdata14 databases in recent years. It also discusses the relevance and implications of these ad-
98 ditions, and compares Cemdata07 and Cemdata18, accounting for their main differences. Summaries
99 of the thermodynamic data compiled in the Cemdata18 database are available in formats supported
100 (readable) by the computer programs GEM-Selektor [13, 14] and PHREEQC [18]. Both of these Cemda-
101 ta18 variants can be freely downloaded from <http://www.empa.ch/cemdata>.

102

103 **2 Thermodynamic data for cements**

104 Recent experimental data has enabled the Cemdata07 and Cemdata14 databases to be extended and
105 refined [1, 7, 21]. We report this more comprehensive and refined dataset here as Cemdata18, com-

106 piled in several tables. Cemdata18 has been developed to predict changes in chemistry that occur dur-
 107 ing the hydration of Portland, blended and alkali activated cements, and also their interactions with
 108 service environments during use.

109 Table 1 reports the thermodynamic properties of minerals important for cementitious systems, while
 110 Table 2 reports their solubility products referring to the dominate species present at the high pH val-
 111 ues of cementitious systems. The data for hydrotalcite-like phases and detailed discussions of the dif-
 112 ferent models for C-S-H are given in sections 2.6 and 2.7. Standard thermodynamic data for minerals
 113 such as calcite, brucite and aqueous and gaseous species already documented in the PSI-Nagra chem-
 114 ical thermodynamic database [22] are not repeated in these tables, but given only in summary tables in
 115 Appendix B and D. To enable users to model cementitious systems using the Cemdata18 dataset with
 116 the law of mass action (LMA) geochemical modelling package PHREEQC [18], a variant of the Cemda-
 117 ta18 dataset has been generated as documented in Appendix B.

118

119 Table 1: Cemdata18 database: Standard thermodynamic properties at 25°C and 1 bar. Update of
 120 Cemdata07 [1, 7, 29]. The data are compatible with the GEMS version of the PSI/Nagra 12/07 TDB [22,
 121 23]. Standard properties of master species and properties of reactions of forming product species out
 122 of master species, commonly used in LMA programs such as PHREEQC, are compiled in the Appendix
 123 B.

	$\Delta_f G^\circ$	$\Delta_f H^\circ$	S°	a_0	a_1	a_2	a_3	V°	Ref
	[kJ/mol]	[kJ/mol]	[J/K/mol]	[J/K/mol]	[J/mol/K ²]	[J K/mol]	[J/K ^{0.5} /mol]	[cm ³ /mol]	
Solids									
<i>AFt-phases</i>									
128	(Al-)jetttringite ^{a,b,c}	-15205.94	-17535	1900	1939	0.789	-	707	[1, 7]
129	C ₆ As ₃ H ₃₀ ^c	-14728.1	-16950.2	1792.4	1452	2.156	-	708	[30]
130	C ₆ As ₃ H ₁₃	-10540.6	-11530.3	1960.4	970.7	1.483	-	411	[30]
131	C ₆ As ₃ H ₉	-9540.4	-10643.7	646.6	764.3	1.638	-	361	[30]
132	tricarboaluminate ^a	-14565.64	-16792	1858	2042	0.559	-7.78·10 ⁶	650	[1, 7]
133	Fe-ettringite ^b	-14282.36	-16600	1937	1922	0.855	2.02·10 ⁶	717	[1, 21]
134	Thaumasite	-7564.52	-8700	897.1	1031	0.263	-3.40·10 ⁶	330	[28]
<i>Hydrogarnet</i>									
137	C ₃ AH ₆ ^d	-5008.2	-5537.3	422	290	0.644	-3.25·10 ⁶	150	[9, 12]
138	C ₃ AS _{0.41} H _{5.18} ^{*d}	-5192.9	-5699	399	310	0.566	-4.37·10 ⁶	146	[9]
139	C ₃ AS _{0.84} H _{4.32} ^{*e}	-5365.2	-5847	375	331	0.484	-5.55·10 ⁶	142	[9]
140	C ₃ FH ₆ ^{***f}	-4122.8	-4518	870	330	1.237	-4.74·10 ⁶	155	[9]
<i>Al-Fe siliceous hydrogarnet (solid solution)</i>									
143	C ₃ FS _{0.84} H _{4.32} ^{e,f}	-4479.9	-4823	840	371	0.478	-7.03·10 ⁶	149	[9]
144	C ₃ A _{0.5} F _{0.5} S _{0.84} H _{4.32} ^e	-4926.0	-5335	619	367	0.471	-8.10·10 ⁶	146	[9]
146	C ₃ FS _{1.34} H _{3.32}	-4681.1	-4994	820	395	0.383	-8.39·10 ⁶	145	[9]
<i>AFm-phases</i>									
149	C ₄ AH ₁₉	-8749.9	-10017.9	1120	1163	1.047	-	369	[12, 31]
150	C ₄ AH ₁₃ ^g	-7325.7	-8262.4	831.5	208.3	3.13	-	274	[31]
151	C ₄ AH ₁₁	-6841.4	-7656.6	772.7	0.0119	3.56	1.34·10 ⁻⁷	257	[31]
152	C ₂ AH _{7.5}	-4695.5	-5277.5	450	323	0.728	-	180	[12]

153	CAH ₁₀	-4623.0	-5288.2	610	151	1.113	-	3200	193	[12]
154	C ₄ AC _{0.5} H ₁₂	-7335.97	-8270	713	664	1.014	-1.30·10 ⁶	-800	285	[1, 7]
155	C ₄ AC _{0.5} H _{10.5}	-6970.3	-7813.3	668.3	0.0095	2.836	1.07·10 ⁻⁷	-	261	[31]
156	C ₄ AC _{0.5} H ₉	-6597.4	-7349.7	622.5	0.0088	2.635	9.94·10 ⁻⁸	-	249	[31]
157	C ₄ ACH ₁₁	-7337.46	-8250	657	618	0.982	-2.59·10 ⁶	-	262	[1, 7]
158	C ₄ ACH ₉	-6840.3	-7618.6	640.6	192.4	2.042	-	-	234	[31]
159	C ₄ AsH ₁₆	-8726.8	-9930.5	975.0	636	1.606	-	-	351	[31, 32]
160	C ₄ AsH ₁₄	-8252.9	-9321.8	960.9	1028.5	-	-	-	332	[31, 32]
161	C ₄ AsH ₁₂ ^{g, h}	-7778.4	-8758.6	791.6	175	2.594	-	-	310	[31, 32]
162	C ₄ AsH _{10.5}	-7414.9	-8311.9	721	172	2.402	-	-	282	[31, 32]
163	C ₄ AsH ₉	-7047.6	-7845.5	703.6	169	2.211	-	-	275	[31, 32]
164	C ₂ ASH ₈ ⁱ	-5705.15	-6360	546	438	0.749	-1.13·10 ⁶	-800	216	[1, 7]
165	C ₂ ASH ₇ ^j	-5464.0	-6066.8	487.6	0.0063	1.887	7.12·10 ⁻⁸	-	215	[31]
166	C ₂ ASH _{5.5}	-5095.2	-5603.4	454.8	0.0057	1.685	6.36·10 ⁻⁸	-	213	[31]
167	C ₄ As _{0.5} ClH ₁₂	-7533.4	-8472 ^j	820	557	1.141	-1.02·10 ⁶	751	289	[27, 33]
168	C ₄ ACl ₂ H ₁₀ ^k	-6810.9	-7604	731	498	0.895	-2.04·10 ⁶	1503	272	[33, 34]
169	C ₄ A(NO ₃) ₂ H ₁₀	-6778.1	-7719.3	821	580	1.02	-2.77·10 ⁶	872	296	[34, 35]
170	C ₄ A(NO ₂) ₂ H ₁₀	-6606.8	-7493.1	799	565	0.99	-2.24·10 ⁶	703	275	[34-36]
171										
172	C ₄ FH ₁₃ ^{**}	-6438.6	-7435	630	694	1.113	2.02·10 ⁶	1600	286	[9]
173	C ₄ FC _{0.5} H ₁₀	-5952.9	-6581	1270	308	1.201	-9.08·10 ⁵	3200	273	[8]
174	C ₄ FcH ₁₂	-6674.0	-7485	1230	612	1.157	-5.73·10 ⁵	-	292	[8]
175	C ₄ FsH ₁₂ ^h	-6873.2	-7663	1430	577	1.234	2.02·10 ⁶	-	321	[10]
176	C ₂ FSH ₈				not stable					[37]
177	C ₄ FCl ₂ H ₁₀ ^k	-5900.1	-6528 ^l	1286	481	0.961	-1.61·10 ⁴	1503	278 ^l	[37]
178										
179	<u>Sulfates</u>									
180	Cs (anhydrite)	-1322.12	-1434.60	106.7	70.2	-0.099	-	-	46	[22, 23]
181	CsH ₂ (gypsum)	-1797.76	-2023.36	193.8	91.4	-0.318	-	-	75	[22, 23]
182	CsH _{0.5} (hemihyd)	-1436.34 ^m	-1575.3 ^m	134.3	124.1	-	-	-	62	[38]
183	syngenite	-2884.91	-3172	326	201	0.308	-1.78·10 ⁶	-	128 ⁿ	[29]
184										
185	<u>(Hydr)oxides</u>									
186	Al(OH) ₃ (am)	-1143.2	-		not defined				32	[1]
187	Al(OH) ₃ (mic)	-1148.4	-1265.3 ^o	140 ^o	36	0.191	-	-	32	[12]
188	Al(OH) ₃ (gibbsite)*	-1151.0	-1288.7	70.1	36.2	0.191	-	-	32	[22, 23]
189										
190	Fe(OH) ₃ (am)	-700.1			not defined					[22, 23]
191	Fe(OH) ₃ (mic)	-711.6			not defined					[22, 23]
192	FeOOH(mic)	-480.14	-551.1	60	1.25	-0.233	-3.14·10 ⁵	-	21	[9, 22]
193	FeOOH(goethite)*	-497.26	-568.2	60	1.25	-0.233	-3.14·10 ⁵	-	21	[22, 23]
194										
195	CH (portlandite)	-897.01	-985	83	187	-0.022	-	-1600	33	[22, 23]
196	SiO ₂ (am)	-848.90	-903	41	47	0.034	-1.13·10 ⁶	-	29	[1, 7]
197	SiO ₂ (quartz)*	-854.79	-909	41	47	0.034	-1.13·10 ⁶	-	29	[22, 23]
198										
199	<u>Hydrotalcite-pyroaurite (solid solution)</u>									
200	½M ₆ AcH ₁₃ ^P	-4339.85	-4875.9	411	512.6	-	-	-	115	[39]
201	½M ₆ FcH ₁₃ ^P	-3882.60	-4415.1	423	521.7	-	-	-	119	[39]
202										
203	<u>M-S-H (solid solution)</u>									
204	Mg/Si=0.75									
205	M _{1.5} S ₂ H _{2.5} ^q	-3218.43	-3507.52	270 ^r	318 ^r	-	-	-	95	[40]
206	Mg/Si = 1.5									
207	M _{1.5} SH _{2.5} ^q	-2355.66	-2594.22	216 ^r	250 ^r	-	-	-	74	[40]
208										
209	<u>Zeolites</u>									
210	Zeolite P(Ca)*	-5057.8	-5423	779	753	-	-	-	153 ^s	[41]
211	Natrolite*	-5325.7	-5728	360	359	-	-	-	169 ^s	[41]

212	Chabazite	-7111.8	-7774	581	617	-	-	-	251 ^s	[41]
213	Zeolite X(Na)	-5847.5	-6447	566	586	-	-	-	214 ^t	[41]
214	Zeolite Y(Na)	-7552.5	-8327	734	739	-	-	-	283 ^u	[41]
215										
216	<u>Clinkers</u>									
217	C ₃ S	-2784.33	-2931	169	209	0.036	-4.25·10 ⁶	-	73	[1, 7, 42]
218	C ₂ S	-2193.21	-2308	128	152	0.037	-3.03·10 ⁶	-	52	[1, 7, 42]
219	C ₃ A	-3382.35	-3561	205	261	0.019	-5.06·10 ⁶	-	89	[1, 7, 42]
220	C ₁₂ A ₇	-18451.44	-19414	1045	1263	0.274	-2.31·10 ⁷	-	518 ^v	[42]
221	CA	-2207.90	-2327	114	151	0.042	-3.33·10 ⁶	-	54 ^w	[42]
222	CA ₂	-3795.31	-4004	178	277	0.023	-7.45·10 ⁶	-	89 ^x	[42]
223	C ₄ AF	-4786.50	-5080	326	374	0.073	-	-	130	[1, 7, 42]
224	C (lime)	-604.03	-635	39.7	48.8	0.0045	-6.53·10 ⁵	-	17	[43]
225										
226	Ks (K ₂ SO ₄ arcanite)	-1319.60	-1438	176	120	0.100	-1.78·10 ⁶	-	66	[44]
227	K (K ₂ O)	-322.40	-363	94	77	0.036	-3.68·10 ⁵	-	40	[43]
228	Ns (Na ₂ SO ₄ thenardite)	-1269.80	-1387	150	58	0.023	-	-	53	[44]
229	N (Na ₂ O)	-376.07	-415	75	76	0.020	-1.21·10 ⁶	-	25	[43]

230 a_0, a_1, a_2, a_3 are the empirical coefficients of the heat capacity function: $C_p^\circ = a_0 + a_1T + a_2T^{-2} + a_3T^{-0.5}$; heat capacity functions for
231 cement hydrates are typically valid up to 100°C only; "-" = 0. Cement shorthand notation is used: A = Al₂O₃; C = CaO; F = Fe₂O₃;
232 H = H₂O; M = MgO; S = SiO₂; c = CO₂; s = SO₃;

233 * precipitates very slowly at 20°C, generally not included in calculations; ** tentative value;

234 ^a, non-ideal solid solutions; miscibility gap: $X_{SO_4, solid} = 0.1-0.55$ reproduced with the dimensionless Guggenheim interaction param-
235 eters $\alpha_0 = 1.67$ and $\alpha_1 = 0.946$; downscaled in this paper to 1CO₂ : 1SO₃ replacement, instead of the 3CO₂ : 3SO₃ used in [4, 7].^b

236 non-ideal solid solution; miscibility gap: $X_{Al, solid} = 0.25-0.65$ reproduced with the dimensionless Guggenheim interaction param-
237 eters $\alpha_0 = 2.1$ and $\alpha_1 = -0.169$ [45].^{c,d,e,f,i,k,p,q} ideal solid solutions c.f. [9, 11, 30, 39].^g non-ideal solid solutions; miscibility gap:

238 $X_{OH, solid} = 0.50-0.97$ reproduced with the dimensionless Guggenheim interaction parameters $\alpha_0 = 0.188$ and $\alpha_1 = 2.49$ [7].^h non-
239 ideal solid solutions; miscibility gap: $X_{Al, solid} = 0.45-0.95$ reproduced with the dimensionless Guggenheim interaction parameters α_0

240 = 1.26 and $\alpha_1 = 1.57$ [10].^j typing error in [27], recalculated from G_r° and S from [27].^l typing error in [37], recalculated from G_r°
241 and S from [37]. Volume calculated from XRD data [37].^m recalculated from ΔG_r° of -20500 J/mol [38].ⁿ calculated from density

242 data from [33, 46].^o valid up to 60°C only, estimated to describe solubility of microcrystalline Al(OH)₃ aged for 19 months be-
243 tween 5 to 60°C [12].^r Estimated from C_p and S of talc, chrysotile and H₂O using data from [43].^s volume from [47].^t calculated

244 from XRD data: pdf 00-038-0237 [48];^u calculated from XRD data; pdf 00-039-1380 [49],^v [50],^w [51],^x [52]

245

246

247 Table 2: Equilibrium solubility products of solids and formation constants for calcium-silica complexes

248 at 1 bar, 25°C in Cemdata18 (as given in Table 1).

249 Mineral	log K ₅₀	Dissolution reactions used to calculate solubility products.	
250 Solids			
251 (Al-)ettringite	-44.9	Ca ₆ Al ₂ (SO ₄) ₃ (OH) ₁₂ ·26H ₂ O	→ 6Ca ²⁺ + 2Al(OH) ₄ ⁻ + 3SO ₄ ²⁻ + 4OH ⁻ + 26H ₂ O
252 tricarboaluminate	-46.5	Ca ₆ Al ₂ (CO ₃) ₃ (OH) ₁₂ ·26H ₂ O	→ 6Ca ²⁺ + 2Al(OH) ₄ ⁻ + 3CO ₃ ²⁻ + 4OH ⁻ + 26H ₂ O
253 Fe-ettringite	-44.0	Ca ₆ Fe ₂ (SO ₄) ₃ (OH) ₁₂ ·26H ₂ O	→ 6Ca ²⁺ + 2Fe(OH) ₄ ⁻ + 3SO ₄ ²⁻ + 4OH ⁻ + 26H ₂ O
254 thaumasite	-24.75	Ca ₃ (SiO ₃)(SO ₄)(CO ₃)·15H ₂ O	→ 3Ca ²⁺ + H ₃ SiO ₄ ⁻ + SO ₄ ²⁻ + CO ₃ ²⁻ + OH ⁻ + 13H ₂ O
255			
256 C ₃ AH ₆	-20.50	Ca ₃ Al ₂ (OH) ₁₂	→ 3Ca ²⁺ + 2Al(OH) ₄ ⁻ + 4OH ⁻
257 C ₃ AS _{0.41} H _{5.18} ⁺	-25.35	Ca ₃ Al ₂ (SiO ₄) _{0.41} (OH) _{10.36}	→ 3Ca ²⁺ + 2Al(OH) ₄ ⁻ + 0.41 SiO(OH) ₃ ⁻ + 3.59OH ⁻ - 1.23H ₂ O
258 C ₃ AS _{0.84} H _{4.32} ⁺	-26.70	Ca ₃ Al ₂ (SiO ₄) _{0.84} (OH) _{8.64}	→ 3Ca ²⁺ + 2Al(OH) ₄ ⁻ + 0.84 SiO(OH) ₃ ⁻ + 3.16OH ⁻ - 2.52H ₂ O
259 C ₃ FH ₆	-26.30 ^{**}	Ca ₃ Fe ₂ (OH) ₁₂	→ 3Ca ²⁺ + 2Fe(OH) ₄ ⁻ + 4OH ⁻
260 C ₃ FS _{0.84} H _{4.32}	-32.50	Ca ₃ Fe ₂ (SiO ₄) _{0.84} (OH) _{8.64}	→ 3Ca ²⁺ + 2Fe(OH) ₄ ⁻ + 0.84 SiO(OH) ₃ ⁻ + 3.16OH ⁻ - 2.52H ₂ O
261 C ₃ (F,A)S _{0.84} H _{4.32}	-30.20	Ca ₃ FeAl(SiO ₄) _{0.84} (OH) _{8.64}	→ 3Ca ²⁺ + Al(OH) ₄ ⁻ + Fe(OH) ₄ ⁻ + 0.84 SiO(OH) ₃ ⁻ + 3.16OH ⁻ - 2.52H ₂ O
262 C ₃ FS _{1.34} H _{3.32}	-34.20	Ca ₃ Fe ₂ (SiO ₄) _{1.34} (OH) _{6.64}	→ 3Ca ²⁺ + 2Fe(OH) ₄ ⁻ + 1.34 SiO(OH) ₃ ⁻ + 2.66OH ⁻ - 4.02H ₂ O
263			

264	C ₄ AH ₁₉	-25.45	Ca ₄ Al ₂ (OH) ₁₄ ·12H ₂ O	→ 4Ca ²⁺ + 2Al(OH) ₄ ⁻ + 6OH ⁻ + 12H ₂ O
265	C ₄ AH ₁₃	-25.25 ^{***}	Ca ₄ Al ₂ (OH) ₁₄ ·6H ₂ O	→ 4Ca ²⁺ + 2Al(OH) ₄ ⁻ + 6OH ⁻ + 6H ₂ O
266	C ₂ AH _{7.5}	-13.80	Ca ₂ Al ₂ (OH) ₁₀ ·2.5H ₂ O	→ 2Ca ²⁺ + 2Al(OH) ₄ ⁻ + 2OH ⁻ + 2.5H ₂ O
267	CAH ₁₀	-7.60	CaAl ₂ (OH) ₈ ·6H ₂ O	→ Ca ²⁺ + 2Al(OH) ₄ ⁻ + 6H ₂ O
268	C ₄ Ac _{0.5} H ₁₂	-29.13	Ca ₄ Al ₂ (CO ₃) _{0.5} (OH) ₁₃ ·7H ₂ O	→ 4Ca ²⁺ + 2Al(OH) ₄ ⁻ + 0.5CO ₃ ²⁻ + 5OH ⁻ + 7H ₂ O
269	C ₄ AcH ₁₁	-31.47	Ca ₄ Al ₂ (CO ₃)(OH) ₁₂ ·5H ₂ O	→ 4Ca ²⁺ + 2Al(OH) ₄ ⁻ + CO ₃ ²⁻ + 4OH ⁻ + 5H ₂ O
270	C ₄ AsH ₁₄	-29.26	Ca ₄ Al ₂ (SO ₄)(OH) ₁₂ ·6H ₂ O	→ 4Ca ²⁺ + 2Al(OH) ₄ ⁻ + SO ₄ ²⁻ + 4OH ⁻ + 6H ₂ O
271	C ₄ AsH ₁₂	-29.23 ^{***}	Ca ₄ Al ₂ (SO ₄)(OH) ₁₂ ·6H ₂ O	→ 4Ca ²⁺ + 2Al(OH) ₄ ⁻ + SO ₄ ²⁻ + 4OH ⁻ + 6H ₂ O
272	C ₂ ASH ₈	-19.70	Ca ₂ Al ₂ SiO ₂ (OH) ₁₀ ·3H ₂ O	→ 2Ca ²⁺ + 2Al(OH) ₄ ⁻ + 1SiO(OH) ₃ ⁻ + OH ⁻ + 2H ₂ O
273	Friedel's salt	-27.27	Ca ₄ Al ₂ Cl ₂ (OH) ₁₂ ·4H ₂ O	→ 4Ca ²⁺ + 2Al(OH) ₄ ⁻ + 2Cl ⁻ + 4OH ⁻ + 4H ₂ O
274	Kuzel's salt	-28.53	Ca ₄ Al ₂ Cl(SO ₄) _{0.5} (OH) ₁₂ ·6H ₂ O	→ 4Ca ²⁺ + 2Al(OH) ₄ ⁻ + Cl ⁻ + 0.5SO ₄ ²⁻ + 4OH ⁻ + 6H ₂ O
275	Nitrate-AFm	-28.67	Ca ₄ Al ₂ (OH) ₁₂ (NO ₃) ₂ ·4H ₂ O	→ 4Ca ²⁺ + 2Al(OH) ₄ ⁻ + 2NO ₃ ⁻ + 4OH ⁻ + 4H ₂ O
276	Nitrite-AFm	-26.24	Ca ₄ Al ₂ (OH) ₁₂ (NO ₂) ₂ ·4H ₂ O	→ 4Ca ²⁺ + 2Al(OH) ₄ ⁻ + 2NO ₂ ⁻ + 4OH ⁻ + 4H ₂ O
277				
278	C ₄ FH ₁₃	-30.75 ^{**}	Ca ₄ Fe ₂ (OH) ₁₄ ·6H ₂ O	→ 4Ca ²⁺ + 2Fe(OH) ₄ ⁻ + 6OH ⁻ + 6H ₂ O
279	Fe-hemicarbonate	-30.83	Ca ₄ Fe ₂ (CO ₃) _{0.5} (OH) ₁₃ ·3.5H ₂ O	→ 4Ca ²⁺ + 2Fe(OH) ₄ ⁻ + 0.5CO ₃ ²⁻ + 5OH ⁻ + 3.5H ₂ O
280	Fe-monocarbonate	-34.59	Ca ₄ Fe ₂ (CO ₃)(OH) ₁₂ ·6H ₂ O	→ 4Ca ²⁺ + 2Fe(OH) ₄ ⁻ + CO ₃ ²⁻ + 4OH ⁻ + 6H ₂ O
281	Fe-monosulfate	-31.57	Ca ₄ Fe ₂ (SO ₄)(OH) ₁₂ ·6H ₂ O	→ 4Ca ²⁺ + 2Fe(OH) ₄ ⁻ + SO ₄ ²⁻ + 4OH ⁻ + 6H ₂ O
282	Fe-Friedel's salt	-28.62	Ca ₄ Fe ₂ Cl ₂ (OH) ₁₂ ·4H ₂ O	→ 4Ca ²⁺ + 2Fe(OH) ₄ ⁻ + 2Cl ⁻ + 4OH ⁻ + 4H ₂ O
283				
284	Cs (anhydrite)	-4.357	CaSO ₄	→ Ca ²⁺ + SO ₄ ²⁻
285	CsH ₂ (gypsum)	-4.581	CaSO ₄ ·2H ₂ O	→ Ca ²⁺ + SO ₄ ²⁻ + 2H ₂ O
286	CsH _{0.5} (hemihydrate)	-3.59	CaSO ₄ ·0.5H ₂ O	→ Ca ²⁺ + SO ₄ ²⁻ + 0.5H ₂ O
287	syngenite	-7.20	K ₂ Ca(SO ₄) ₂ ·H ₂ O	→ 2K ⁺ + Ca ²⁺ + 2SO ₄ ²⁻ + H ₂ O
288				
289	Al(OH) ₃ (am)	0.24	Al(OH) ₃ (am)	→ Al(OH) ₄ ⁻ - OH ⁻
290	Al(OH) ₃ (mic)	-0.67	Al(OH) ₃ (mic)	→ Al(OH) ₄ ⁻ - OH ⁻
291	Al(OH) ₃ (gibbsite) [*]	-1.12	Al(OH) ₃ (gibbsite)	→ Al(OH) ₄ ⁻ - OH ⁻
292				
293	Fe(OH) ₃ (am)	-2.6	Fe(OH) ₃ (am)	→ Fe(OH) ₄ ⁻ - OH ⁻
294	Fe(OH) ₃ (mic)	-4.6	Fe(OH) ₃ (mic)	→ Fe(OH) ₄ ⁻ - OH ⁻
295	FeOOH(mic)	-5.6	FeOOH(mic)	→ Fe(OH) ₄ ⁻ - OH ⁻ - H ₂ O
296	FeOOH(goethite) [*]	-8.6	FeOOH(goethite)	→ Fe(OH) ₄ ⁻ - OH ⁻ - H ₂ O
297				
298	CH	-5.2	Ca(OH) ₂	→ Ca ²⁺ + 2OH ⁻
299	SiO ₂ (am)	-2.714	SiO ₂ (am)	→ SiO ₂ ⁰
300	SiO ₂ (quartz) [*]	-3.746	SiO ₂ (quartz)	→ SiO ₂ ⁰
301				
302	¹ / ₂ M ₆ AcH ₁₃	-33.29 ^{***}	Mg ₃ Al(OH) ₈ (CO ₃) _{0.5} ·2.5H ₂ O	→ 3Mg ²⁺ + Al(OH) ₄ ⁻ + 0.5CO ₃ ²⁻ + 4OH ⁻ + 2.5H ₂ O
303	¹ / ₂ M ₆ FcH ₁₃	-33.64 ^{***}	Mg ₃ Fe(OH) ₈ (CO ₃) _{0.5} ·2.5H ₂ O	→ 3Mg ²⁺ + Fe(OH) ₄ ⁻ + 0.5CO ₃ ²⁻ + 4OH ⁻ + 2.5H ₂ O
304				
305	M _{1.5} S ₂ H _{2.5}	-28.80	(MgO) _{1.5} (SiO ₂) ₂ (H ₂ O) _{2.5}	→ 1.5Mg ²⁺ + 2SiO ₂ ⁰ + 3OH ⁻ + H ₂ O
306	M _{1.5} SH _{2.5}	-23.57	(MgO) _{1.5} SiO ₂ (H ₂ O) _{2.5}	→ 1.5Mg ²⁺ + SiO ₂ ⁰ + 3OH ⁻ + H ₂ O
307				
308	Zeolite P(Ca) [*]	-20.3	CaAl ₂ Si ₂ O ₈ ·4.5H ₂ O	→ Ca ²⁺ + 2Al(OH) ₄ ⁻ + 2SiO ₂ ⁰ + 0.5H ₂ O
309	Natrolite [*]	-30.2	Na ₂ Al ₂ Si ₃ O ₁₀ ·2H ₂ O	→ 2Na ⁺ + 2Al(OH) ₄ ⁻ + 3SiO ₂ ⁰ - 2H ₂ O
310	Chabazite	-25.8	CaAl ₂ Si ₄ O ₁₂ ·6H ₂ O	→ Ca ²⁺ + 2Al(OH) ₄ ⁻ + 4SiO ₂ ⁰ + 2H ₂ O
311	Zeolite X(Na)	-20.1	Na ₂ Al ₂ Si _{2.5} O ₉ ·6.2H ₂ O	→ 2Na ⁺ + 2Al(OH) ₄ ⁻ + 2.5SiO ₂ ⁰ + 2.2H ₂ O
312	Zeolite Y(Na)	-25.0	Na ₂ Al ₂ Si ₄ O ₁₂ ·8H ₂ O	→ 2Na ⁺ + 2Al(OH) ₄ ⁻ + 4SiO ₂ ⁰ + 4H ₂ O
313				
314	Calcium silicate complexes			
315	CaHSiO ₃ ⁺	1.2 ^{*v}	Ca ²⁺ + HSiO ₃ ²⁻	→ CaHSiO ₃ ⁺
316	CaSiO ₃ ⁰	4.6 ^{*v}	Ca ²⁺ + SiO ₃ ²⁻	→ CaSiO ₃ ⁰

317 * precipitates very slowly at 20°C, generally not included in calculations; ** tentative value; *** recalculated in this pa-
318 per from ΔG_r⁰ values. ^{*v} The formation of less strong calcium silicate complexes have been recently suggested (log
319 K(CaHSiO₃⁺) = 0.5 and log K(CaSiO₃⁰) = 2.9. Within Cemdata18, however, the listed values for calcium silicate
320 complexes have to be used to maintain compatibility with the C-S-H models.

321

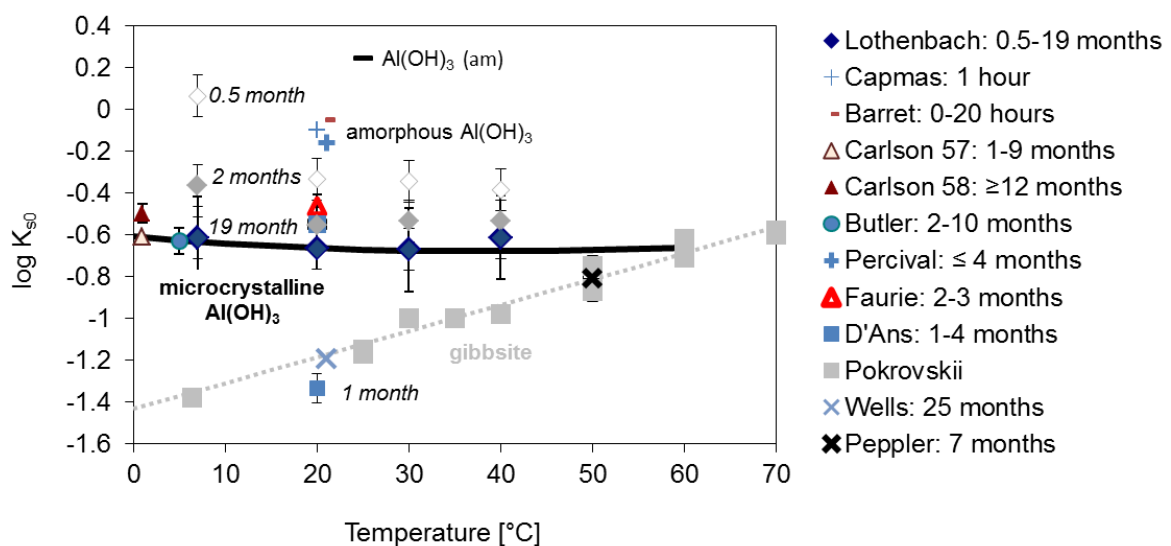
322

323 **2.1 Solubility of Al(OH)₃ and its effect on calcium aluminate and calcium sul-**
 324 **foaluminate cements**

325 The solubility of precipitated Al(OH)₃ decreases with time. Initially “amorphous” or poorly ordered
 326 Al(OH)₃ precipitates with a solubility product of approximately 0±0.2. With time, the degree of order-
 327 ing increases, and microcrystalline Al(OH)₃ forms, while the solubility product decreases to -0.7 after 2
 328 years. The solubility of hydrothermally prepared gibbsite is with -1.1 lower as illustrated in Figure 1,
 329 however its formation is not expected within the timeframe of months to years generally considered
 330 for hydrating cements. At 60°C and above, it is expected that microcrystalline Al(OH)₃ does not persist,
 331 but that gibbsite forms relatively fast (Figure 1). The solubility of Al(OH)₃ determines whether CAH₁₀ (as
 332 in the presence of Al(OH)₃ with log K_{S0} ≥ -0.6 at 25°C) is formed initially in calcium aluminate cements
 333 or whether it converts to C₃AH₆ and microcrystalline Al(OH)₃ [12]. The decrease of the solubility of
 334 Al(OH)₃ with time is also responsible for the initial occurrence of CAH₁₀ and ettringite instead of mono-
 335 sulfate plus microcrystalline Al(OH)₃ in some calcium sulfoaluminate cements, as discussed in more de-
 336 tail in [53].

337 Which Al(OH)₃ modification (see Table 1) should be taken into account depends mainly on the
 338 timeframe and the temperature considered. While gibbsite should be allowed to form at temperatures
 339 above 60°C, its precipitation should be suppressed for calculations at ambient temperatures, where
 340 microcrystalline Al(OH)₃ will form instead. Within very short timeframes (minutes to hour), possibly on-
 341 ly amorphous Al(OH)₃ should be allowed to precipitate. Similarly, also the formation of some other
 342 stable phases such as goethite (FeOOH), hematite (Fe₂O₃) and quartz (SiO₂) should be suppressed in
 343 calculations of hydrated cements in favour of their more disperse counterparts: microcrystalline
 344 FeOOH (or microcrystalline or amorphous Fe(OH)₃, depending on the timeframe considered), and
 345 amorphous SiO₂.

346



347

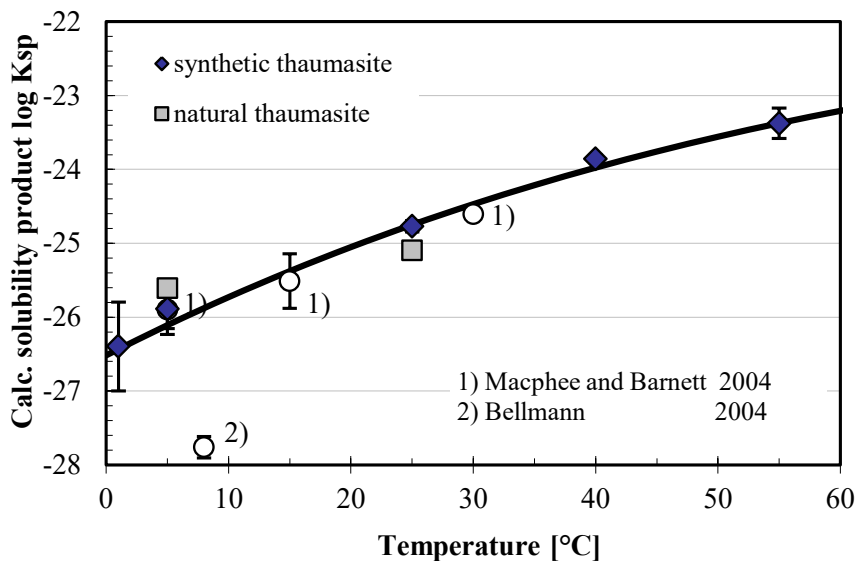
348 Figure 1: Logarithm of the solubility product of Al(OH)₃ (referring to Al(OH)₄⁻ and OH⁻) as a function of
 349 time and temperature calculated from the literature, adapted from [12]. Gibbsite solubility (dotted line)

350 was calculated using data from the GEMS version of the PSI/Nagra 12/07 TDB [22, 23], whereas the
351 solubility of microcrystalline $\text{Al}(\text{OH})_3$ (black line) and amorphous $\text{Al}(\text{OH})_3$ (black hyphen) was calculated
352 based on the data given in Table 1.

353

354 **2.2 Thaumasite**

355 Damidot et al. [54] obtained solubility data to derive a solubility constant for thaumasite at 25°C, at
356 which temperature thaumasite was considered to be stable. Invariant points were calculated for phase
357 assemblages including thaumasite in the system $\text{CaO}-\text{Al}_2\text{O}_3-\text{SiO}_2-\text{CaSO}_4-\text{CaCO}_3-\text{H}_2\text{O}$. Schmidt et al.
358 [55] used the solubility data of Macphee and Barnett [56] to derive thermodynamic data for
359 thaumasite over the temperature range 1 to 30°C to confirm experimental data showing formation of
360 thaumasite in mortars at 8 and 20°C. Another set of solubility data at 8°C for natural thaumasite was
361 reported by Bellmann [57] who also highlighted the potential pathways of formation of thaumasite at
362 this temperature. Macphee and Barnett [56] obtained the solubility data of ettringite-thaumasite solid
363 solutions in the temperature range between 5°C and 30°C; no apparent decomposition of thaumasite
364 and related solid solutions occurred after 6 months storage at 30°C, which suggests the persistence of
365 thaumasite at temperatures at least up to ~30°C. A complete solubility dataset representative for the
366 stability range of thaumasite was missing, as [56] reported the solubility data for thaumasite-ettringite
367 solid-solutions but not for pure thaumasite. Hence, due to a lack of experimental data, no thermody-
368 namic data for thaumasite were included in the Cemdata07 database, but were added in a first update
369 using the data derived in Schmidt et al. [55] based on the solubility data given by Macphee and Bar-
370 nett [49]. In 2015, Matschei and Glasser [28] published a new dataset obtained on apparently pure-
371 phase synthetic thaumasite. It was shown that pure thaumasite was thermally stable up to $68\pm 5^\circ\text{C}$. The
372 obtained new data agreed well, within limits of error, with those obtained by Macphee and Barnett
373 [56], but differs significantly from the data for natural thaumasite reported by Bellmann [57] at 8°C. Ex-
374 periments done by [28, 56] excluded atmospheric carbon dioxide, whereas the solubility determina-
375 tions reported in [57] were made in the presence of air containing carbon dioxide. The contact with the
376 air may lead to the decomposition of thaumasite, which would make the interpretation of the solubility
377 data invalid.



378

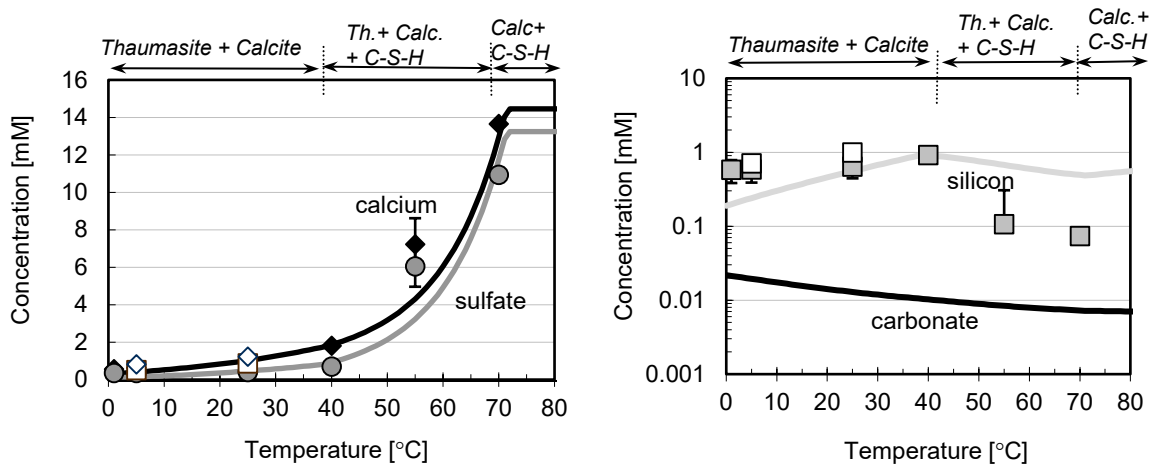
379 Figure 2: Calculated solubility products referring to Ca^{2+} , $\text{SiO}(\text{OH})_3^-$, SO_4^{2-} , CO_3^{2-} , OH^- and H_2O of syn-
 380 thetic and natural thaumasite samples from solubility experiments. The curve shows the calculated
 381 best fit using a three-term temperature extrapolation. Reproduced from [28].

382

383 The heat capacities were estimated using a reference reaction with a solid having a known heat capaci-
 384 ty and similar structure, as discussed in more detail in [55] and [28]. As shown by Helgeson et al. [43],
 385 this principle can be successfully applied to estimate the heat capacity of silicate minerals by formulat-
 386 ing a reaction involving a structurally-related mineral of known heat capacity.

387

388 Finally, it is possible to do an internal consistency check and recalculate solubilities under the chosen
 389 experimental conditions with the thermodynamic data of the Cemdata18 dataset. As illustrated in Fig-
 390 ure 3, the calculated solubility data for thaumasite show generally good agreement with the experi-
 391 mentally-derived dataset. Despite an underestimation of the calculated silicon concentrations at 1°C
 392 and 5°C, both datasets, experimental and calculated, generally agree, proving the internal consistency
 393 of the data. Especially in the temperature range from 1 to ~40°C, where the solid phase assemblage
 394 consists mainly of thaumasite and traces of calcite, differences between experimental calcium and sul-
 395 fate concentrations are within analytical errors. In the temperature range 1°C to ~ 40°C, concentrations
 396 of calcium, sulfate and silicon increase with rising temperature, whereas calculated carbonate concen-
 397 trations show a continuous decrease. At temperatures > ~40°C, calcium and sulfate concentrations in-
 398 crease significantly, whereas silicon concentrations decrease due to the formation of C-S-H.
 399 Thaumasite is absent at temperatures above 70°C.



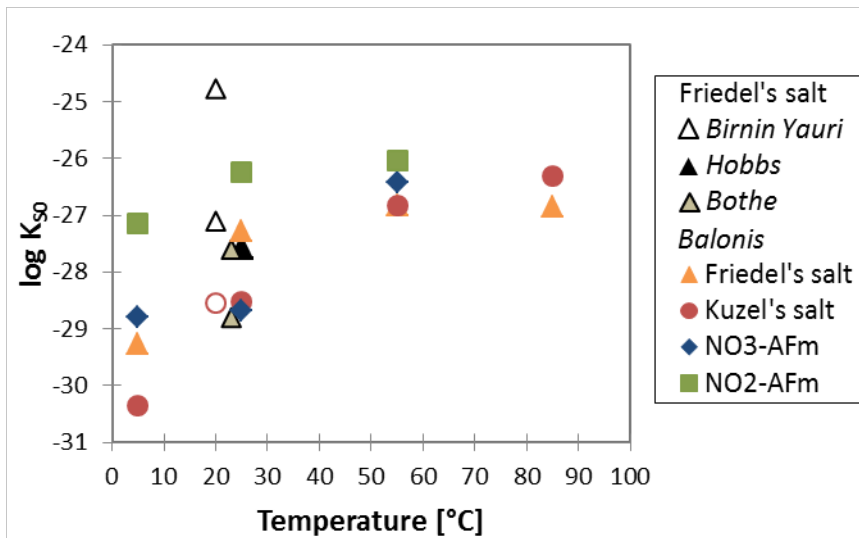
401 Figure 3: Experimentally measured (markers) and re-calculated (lines) solubility data for thaumasite;
 402 (filled markers represent the experimental data for synthetic thaumasite, open markers – the data for
 403 natural thaumasite from [28]). Calculations are based on the new thermodynamic data for thaumasite
 404 complemented with the CSHQ data from Cemdata18 [1, 7]. Predicted solid phases/ phase assemblages
 405 are shown along the top.

406

407 2.3 Chloride-, nitrate-, and nitrite-AFm phases

408 Binding of chloride and the formation of chloride bearing cement hydrates has been widely studied
 409 due to its impact on the corrosion of steel in reinforced concrete. The first comprehensive solubility
 410 data for Friedel's salt ($\text{Ca}_4\text{Al}_2\text{Cl}_2(\text{OH})_{12}\cdot 4\text{H}_2\text{O}$) and Kuzel's salt ($\text{Ca}_4\text{Al}_2\text{Cl}(\text{SO}_4)_{0.5}(\text{OH})_{12}\cdot 6\text{H}_2\text{O}$) were provid-
 411 ed in the late nineties. Birnin-Yauri [58] has described the dissolution of Friedel's salt as congruent and
 412 provided values of $\log K_{S0}$ -27.1 and -24.8 ($K_{S0} = \{\text{Ca}^{2+}\}^4\{\text{Al}(\text{OH})_4\}^2\{\text{Cl}^-\}^2\{\text{OH}^-\}^4\{\text{H}_2\text{O}\}^4$). Hobbs [59] esti-
 413 mated $\log K_{S0}$ as -27.6 ± 0.9 and Bothe [60] has estimated via geochemical modeling that the solubility
 414 product of Friedel's salt should fall within the range $-28.8 < \log K_{S0} < -27.6$. Balonis et al. [27] provid-
 415 ed solubility data for Friedel's salt as a function of time and temperature with an estimated value of
 416 solubility product for an ideal composition and at room temperature to be -27.27 [34, 36]. Compilation
 417 of the available solubility data is shown by triangles on Figure 4.

418 The estimated thermodynamic data [36] ($\Delta_f G^0 \sim -6810.9$ kJ/mol, $\Delta_f H^0 \sim -7604$ kJ/mol, S^0 731 J/mol K)
 419 have similar values (except the entropy) to the dataset published by Blanc et al. [16]
 420 ($\Delta_f G^0 \sim -6815.44$ kJ/mol, $\Delta_f H^0 \sim -7670.04$ kJ/mol, S^0 527.70 J/mol K), and agree reasonably well with
 421 the data obtained by Grishchenko et al. [61] ($\Delta_f G^0$ estimated in a range between 6800 and 6860 kJ/mol,
 422 $S^0 \sim 680$ J/mol K), though it should be kept in mind that Grishchenko's composition is reported to be
 423 slightly contaminated with carbonate ions. Attempts to synthesize Cl-AFt at temperatures above 0°C
 424 were unsuccessful [34], hence no thermodynamic data are available that can be used.



425

426 Figure 4: Solubility products of Friedel's salt, Kuzel's salt, NO₃-AFm and NO₂-AFm (referring to reac-
 427 tions using Ca²⁺, Cl⁻, SO₄²⁻, NO₃⁻, NO₂⁻, OH⁻ and H₂O as indicated in Table 2) as a function of tempera-
 428 ture. Data for Friedel's salt from [27, 58-60, 62], data for other AFm are from Balonis and co-workers
 429 [27, 34-36].

430

431 Glasser et al. [62] first measured the solubility of Kuzel's salt and noted that its dissolution is strongly
 432 incongruent, with ettringite precipitating as a secondary phase. From the solubility data given by
 433 Glasser et al. a log K_{S0} of Kuzel's salt -28.54 ($K_{S0} = \{Ca^{2+}\}^4\{Al(OH)_4\}^{-2}\{Cl\}\{SO_4^{2-}\}^{0.5}\{OH\}^{-4}\{H_2O\}^6$) was esti-
 434 mated [27]. Balonis et al. [27] has also experimentally derived the solubility data and calculated solubil-
 435 ity products for Kuzel's salt at different temperatures ranging from 5 to 85°C for the period between 1-
 436 12 months, with the solubility product at room temperature determined to be log K_{S0} = -28.53. Data for
 437 12 months are shown by the filled circles in Figure 4.

438 In recent years, the impact of soluble nitrate and nitrite corrosion inhibitors on the mineralogy of ce-
 439 ment pastes has been studied [34, 36, 63], and it has been demonstrated that the AFm phase has the
 440 ability to accommodate NO₃⁻ and NO₂⁻ ions in the interlayer position. Solubility data along with ther-
 441 modynamic parameters for the nitrate AFm (NO₃-AFm) and nitrite AFm (NO₂-AFm) published by Balo-
 442 nis et al. [34, 35] are shown in Figure 4. Similarly, as in the case of Cl-AFt, an attempted synthesis of
 443 NO₃- or NO₂-AFt at room temperature was not successful [34].

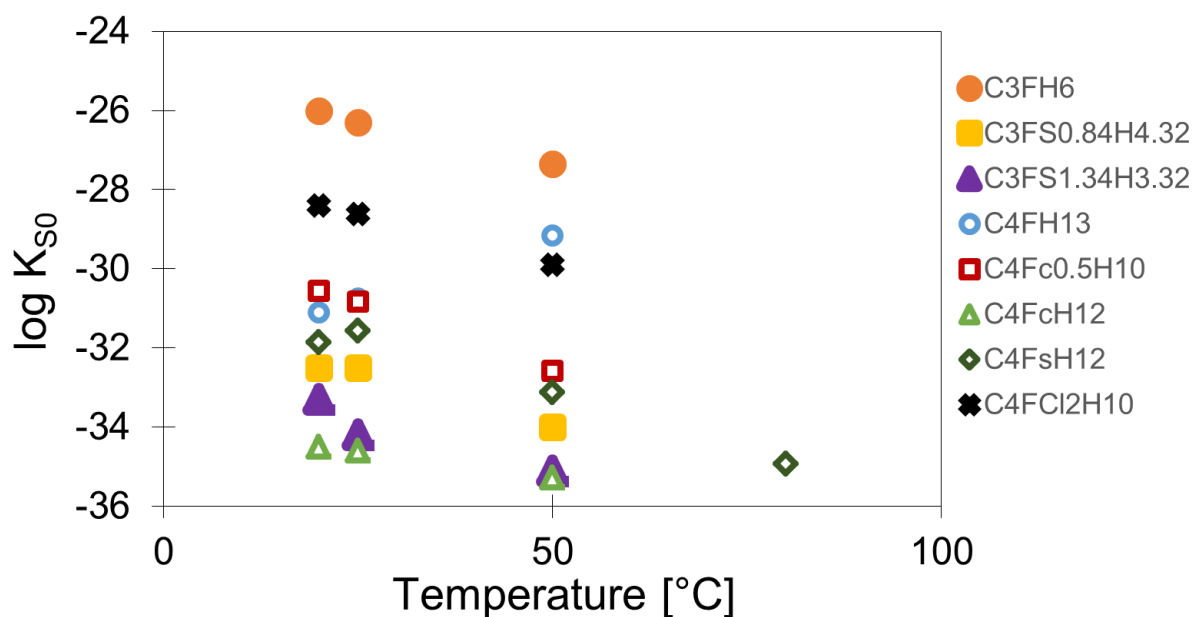
444

445 2.4 Iron containing hydrates

446 The main source of iron in cements is 5-15% ferrite clinker in Portland cements and slag in blended
 447 cements. In synthetic systems containing only water, C₂F, calcium sulfate, calcium carbonate or silica,
 448 different Fe-containing phases like ettringite, monosulfate, monocarbonate, siliceous hydrogarnet can
 449 precipitate, as well as form solid solutions with their Al-containing analogues [8-10, 21].

450 The stability of Fe-containing phases generally is only moderately affected by temperature, as shown
 451 in Figure 5. At ambient temperature, Fe-ettringite (C₆F₃H₃₂), Fe-monosulfate (C₄F₅H₁₂), Fe-

452 monocarbonate (C_4FCH_{12}), Fe-Friedel's salt ($C_4FCI_2H_{10}$), and Fe-siliceous hydrogarnet ($C_3FS_{0.95}H_{4.1}$,
 453 $C_3FS_{1.52}H_{2.96}$) are stable, while Fe-katoite (C_3FH_6) and Fe-hemicarbonate ($C_4Fc_{0.5}H_{10}$) are metastable [8-
 454 10, 21, 37]. Attempts to synthesize Fe-strätlingite (C_2FSH_8) failed, as only portlandite, C-S-H and iron
 455 hydroxide formed, indicating the instability of Fe-strätlingite at ambient conditions. C_4FsH_{12} , C_4FCH_{12} ,
 456 and $C_4FCI_2H_{10}$ are also stable at 50° but not at 80°C, while Fe-siliceous hydrogarnet is stable at up to
 457 110°C. The limited stability field of the Fe-containing AFm and AFt hydrates is related to the very high
 458 stability of goethite ($FeOOH$) and hematite (Fe_2O_3), which form at 50°C within several months and at
 459 80°C within days [9]. Although hematite and portlandite would be more stable than the Fe-katoite, AFt
 460 and AFm phases between 0 and 100°C, the formation of goethite and hematite at ambient tempera-
 461 tures is very slow, such that Fe-containing siliceous hydrogarnet, AFt and AFm phases can be synthe-
 462 sized instead. Figure 3 shows the solubility products of Fe-containing phases calculated based on the
 463 measured composition of the liquid phase at 20, 50 and 80°C; those data were used to derive the
 464 thermodynamic data for standard conditions (25°C, 1 atm) given in Table 1. The formation of solid so-
 465 lutions between Al and Fe-containing endmembers has been observed for ettringite, siliceous hy-
 466 drogarnet, monosulfate, and Friedel's salt, while no solid solution formed between the rhombohedral
 467 Fe-monocarbonate with the triclinic Al-monocarbonate due to the structural differences [8-10, 21, 37].
 468



469
 470 Figure 5: Solubility product (K_{S0}) of Fe-containing hydrogarnet and AFm-phases at different tempera-
 471 tures, referring to reactions using Ca^{2+} , $Fe(OH)_4^-$, $SiO(OH)_3^-$, SO_4^{2-} , CO_3^{2-} , Cl^- , OH^- and H_2O as indicated
 472 in Table 2. Data from Dilnesa and co-workers [8-10, 37].
 473

474 While different Fe-containing hydrates could be synthesized, only Fe-siliceous hydrogarnet is expected
 475 to occur in hydrated cements. The solubility product of Fe-siliceous hydrogarnet (given in Table 1) is 5
 476 to 7 log units lower than that of Al-siliceous hydrogarnet indicating a high stabilization of Fe-siliceous

477 hydrogarnet, while the solubility products of the Fe-containing hydrates are comparable or only
478 somewhat more stable than their Al-containing analogues. In fact, in hydrated PC, Fe(III) precipitates as
479 iron hydroxide during the first hours and as siliceous hydrogarnet ($C_3(A,F)S_{0.84}H_{4.32}$) after 1 day and
480 longer [64-66]. The data for the $C_3FS_{0.84}H_{4.32}$ and for the mixed Al- and Fe-containing $C_3A_{0.5}F_{0.5}S_{0.84}H_{4.32}$
481 determined by Dilnesa et al. [9] are included in Cemdata18, but not the data for the Al-based
482 $C_3AS_{0.84}H_{4.32}$ due to its formation being kinetically hindered at ambient conditions [9].

483

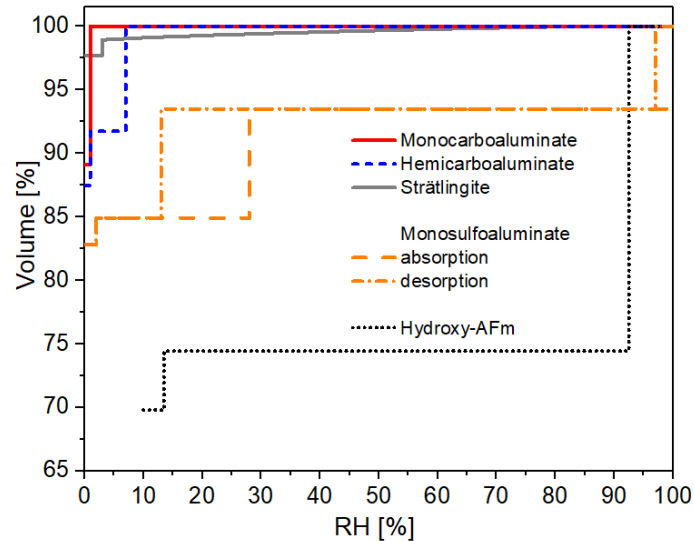
484 **2.5 Effect of relative humidity**

485 Cement hydrates are known to show varying water content as functions of temperature and relative
486 humidity (RH). Some of these hydrates are crystalline phases with layered structure such as the AFm-
487 phases or ettringite-type structures. The AFm and AFt phases have different hydration states (i.e. vary-
488 ing molar water content) depending on the exposure conditions, which can impact the volume stabil-
489 ity, porosity and density of cement paste. The molar volume of some AFm phases can decrease by as
490 much as 20% during drying [31], which may strongly influence the porosity and performance of some
491 cementitious systems.

492 In gel-like phases such as C-S-H, water can be present within the intrinsic gel porosity, as well as in its
493 interlayer. Unfortunately, until now there was no thermodynamic model capable of assessing this vary-
494 ing water content.

495 The crystalline AFm phases have a layered structure and are known for their varying water content in
496 the interlayer, which can be of two types. Firstly, the "space filling", loosely integrated zeolitic water
497 molecules, which are easily removed from the structure upon increase of temperature or at an initial
498 small decrease of RH and have thermodynamic properties close to liquid water. Secondly, the "struc-
499 tural water" molecules, which are strongly bound to calcium cations of the main layer and can only be
500 removed at low water activities and/or high temperatures, typically accompanied by high enthalpies
501 values. Recently, the thermodynamic properties of the different hydration states of the most important
502 AFm phases were determined by Baquerizo et al. [31, 32] and are listed in Table 1. A summary of the
503 volume stability of AFm phases at 25°C is shown in Figure 6.

504

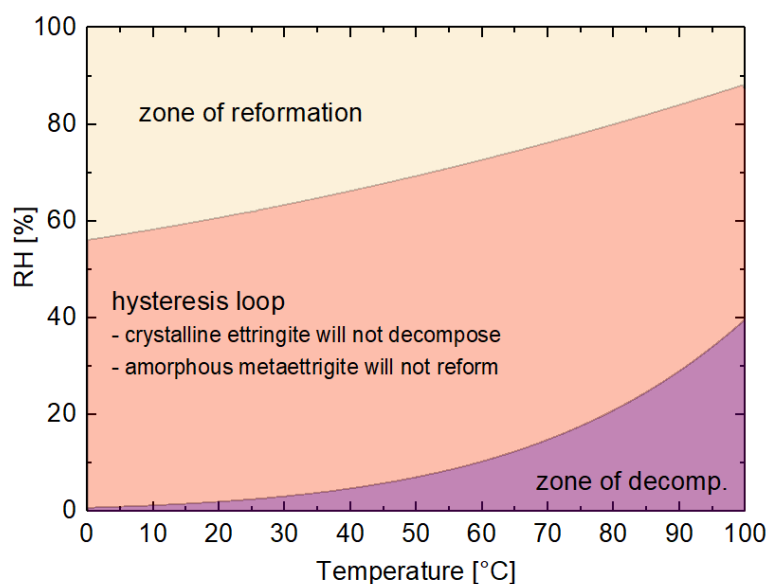


505
 506 Figure 6: Volume changes of the AFm phases studied as function of RH at 25°C. 100% volume corre-
 507 sponds to the higher hydration state of each phase.

508
 509 Ettringite, $C_6As_3H_{32}$, is also known to have varying water content. This hydrate is a common phase oc-
 510 ccurring during the hydration of PC. It is also the main hydration product in calcium sulfoaluminate ce-
 511 ments and calcium aluminate cement blended with gypsum. Understanding the stability of ettringite
 512 during hydration and under different drying conditions is of great importance to assess the perfor-
 513 mance of systems containing large amounts of this phase. In general, ettringite contains 32 H_2O mole-
 514 cules per formula unit: 30 fixed in the columns and 2 H_2O of zeolitic water loosely bound in the chan-
 515 nels. Removal of the two inter-channel water molecules takes place with decreasing relative humidity
 516 (RH) without any significant change of the structure. Nevertheless, a series of structural changes are
 517 observed when the water content is below 30 H_2O , resulting in an amorphous phase commonly known
 518 as metaettringite. The thermodynamic properties of crystalline ettringite, having 32 and 30 H_2O , and
 519 amorphous ettringite (or metaettringite) having 13 H_2O and 9 H_2O were recently derived by Baquerizo
 520 et al. [30] and are listed in Table 1. Something interesting to notice is that decomposition and refor-
 521 mation of ettringite takes place reversibly but with a marked hysteresis, which makes the estimation of
 522 thermodynamic properties difficult. The values presented in Table 1 corresponds to those derived us-
 523 ing the desorption equilibrium properties. Figure 7 shows the stability of ettringite at 25°, presenting
 524 three different zones:

- 525 - The zone of decomposition, which has to be reached in order to decompose ettringite into
- 526 metaettringite.
- 527 - The hysteresis loop, where crystalline ettringite will not undergo decomposition unless the zone of
- 528 decomposition is reached and amorphous metaettringite will not reform unless the zone of refor-
- 529 mation is reached.
- 530 - The zone of reformation, which has to be reached in order to be convert metaettringite back to
- 531 crystalline ettringite.

532



533

534 Figure 7: Stability of ettringite as a function of relative humidity and temperature.

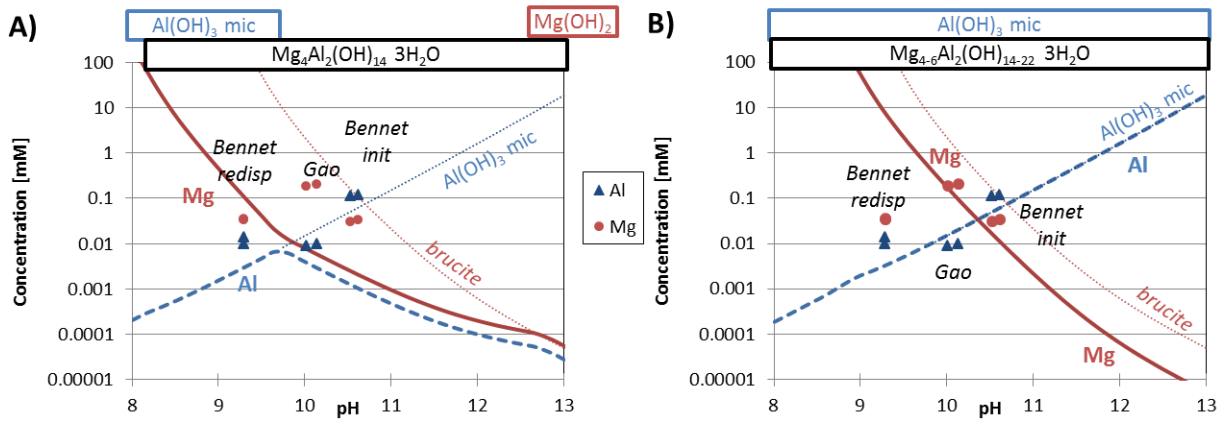
535

536 2.6 Mg-Al layered double hydroxide (hydrotalcite-like phase)

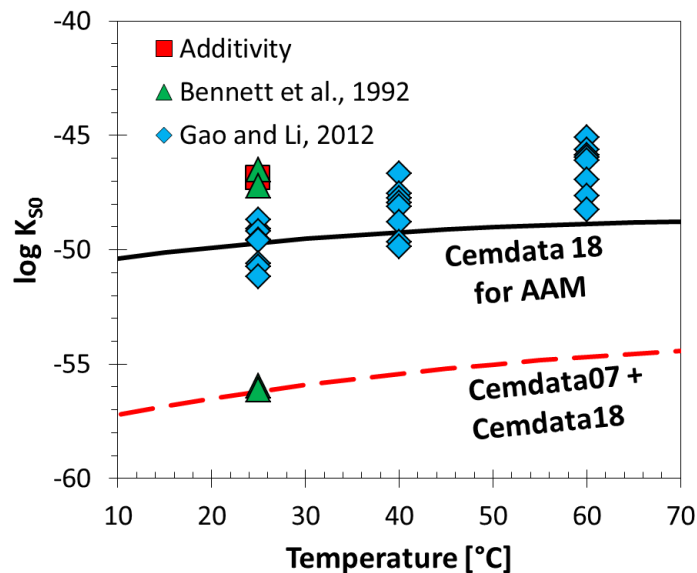
537 Mg-Al layered double hydroxide (LDH) type phases are structurally similar to hydrotalcite and typically
 538 occur as secondary reaction products in hydrated Portland cements [67] and in alkali-activated granu-
 539 lated blast furnace slag (GBFS) [68, 69]. In hydrated or alkali-activated cementitious materials free from
 540 carbonation, Mg-Al LDH phases normally exhibit poor long-range structural order and are thought to
 541 significantly occur along the solid solution series $Mg_{(1-x)}Al_x(OH)_{(2+x)}(H_2O)_4$, where $0.2 \leq x \leq 0.33$ [70, 71]
 542 due to the deficiency of CO_2 in the system. Mg-Al LDH formation is thus often difficult to observe by
 543 conventional X-ray diffraction, particularly at low MgO content.

544 Few solubility data for hydroxide containing hydrotalcite like Mg-Al LDH phases have been measured;
 545 the data at 25°C are summarised in Figure 8A and B. The samples studied by Bennet et al. [72] were
 546 synthesised for 2 days at 80°C, dried, and then re-dispersed in water for 4 weeks at 25°C. This proce-
 547 dure resulted in a solubility product of 10^{-47} for M_4AH_{10} . Further re-dispersion steps lowered the solu-
 548 bility product of M_4AH_{10} to 10^{-56} . This lower solubility product of 10^{-56} for M_4AH_{10} was selected for use
 549 in Cemdata07 [1, 29] (see Figure 8A and Figure 9), and by Bennet et al. [72].

550



551
 552 Figure 8: Solubility of A) $Mg_4Al_2(OH)_{14} \cdot 3H_2O$ and B) of the MgAl-OH-LDH solid solution
 553 compared to the solubility of microcrystalline $Al(OH)_3$ and brucite (dotted lines) and to the experi-
 554 mental data (Mg: circles, Al: triangles) determined by Bennet et al. [72] and Gao and Li [73].



555
 556 Figure 9: Measured and calculated solubility products of Mg_4AH_{10} (reactions refer to Mg^{2+} , $Al(OH)_4^-$, OH^-
 557 and H_2O as indicated in Table 3) at different temperatures. Adapted from Myers et al. [74].

558
 559 Based on the solubility data of Gao and Li [73] for samples precipitated from oversaturated solutions
 560 (equilibration time 2 days), solubility data for hydrotalcite like Mg-Al LDH phases intercalated with OH^-
 561 (MgAl-OH-LDH) were recently recompiled and recalculated [74], as shown in Figure 8B) and Figure 9.
 562 Solubility products for the end members of MgAl-OH-LDH solid solution model were defined using
 563 the available data [72, 73] and guided using experimental observations in alkali activated slag cements
 564 with the high stability of MgAl-OH-LDH and absence of brucite in uncarbonated alkali-activated slag
 565 cements is widely documented and provides a reliable proxy for this task. An ideal (simple mixing) sol-
 566 id solution thermodynamic model (MA-OH-LDH_{ss}) was provisionally defined using these data for
 567 Mg/Al molar ratios between 2 and 4. The use of independent experimental observations to derive the
 568 solid solution model is important because solubility products derived from the available solubility data

569 are scattered by up to $\sim 10 \log_{10}$ units at 25°C, possibly due to the varied equilibration times used (2
570 days [73] to 1 month [72]). We recommend using MgAl-OH-LDH_{ss} for alkali activated materials.

571
572 Usage of the MgAl-OH-LDH_{ss} model (describing hydrotalcite-like phases with variable Mg/Al ratio,
573 and recommended for use in alkali activated material systems) does not lead to hydrotalcite formation
574 under typical PC conditions due to the low aluminium concentrations in the pore solution [29] of PCs,
575 for which brucite would be calculated to precipitate instead. As the formation of hydrotalcite like
576 phases is reported in well hydrated PCs with dolomite [75], the use of a single phase, M₄AH₁₀, with a
577 lower solubility product (see Table 3, Figure 9) derived from the long-term experiments in [72] only, is
578 recommended for hydrated PC. The necessity to use presently two different datasets and the large dif-
579 ferences in the available data indicates that the solubility data selected for M₄AH₁₀ and for MgAl-OH-
580 LDH_{ss} are tentative and may require updating as more data become available. Therefore, we believe
581 that additional solubility measurements for Mg-Al LDH phases are needed.

582
583 Table 3: Standard thermodynamic properties at 25°C and 1 atm for hydrotalcite-like phases (provided
584 in separate modules of Cemdata18 database). The data are consistent with the GEMS version of the
585 PSI/Nagra 12/07 TDB [22, 23] and the data detailed in Table 1 and Table 4.

586	$\Delta_f G^\circ$	$\Delta_f H^\circ$	S°	a_0	a_1	a_2	a_3	V°	Ref
587	[kJ/mol]	[kJ/mol]	[J/K/mol]	[J/K/mol]	[J/mol/K ²]	[J K/mol]	[J/K ^{0.5} /mol]	[cm ³ /mol]	
588									
589	M ₄ AH ₁₀ [*]	-6394.6	-7196	549	-364	4.21	3.75·10 ⁶	629	220 [1, 29]
590									
591	<i>MgAl-OH-LDH (ideal ternary solid solution)**</i>								
592	M ₄ AH ₁₀	-6358.5	-7160.2	548.9	547.6	-	-	-	219.1 [74]
593	M ₆ AH ₁₂	-8022.9	-9006.7	675.2	803.1	-	-	-	305.4 [74]
594	M ₈ AH ₁₄	-9687.4	-10853.3	801.5	957.7	-	-	-	392.4 [74]
595	Mineral	log K ₅₀ Dissolution reactions used to calculate solubility products.							
596	M ₄ AH ₁₀ [*]	-56.02 [*]	Mg ₄ Al ₂ (OH) ₁₄ ·3H ₂ O	→ 4Mg ²⁺ + 2Al(OH) ₄ ⁻ + 6OH ⁻ + 3H ₂ O					
597									
598	M ₄ AH ₁₀ ^{**}	-49.7	Mg ₄ Al ₂ (OH) ₁₄ ·3H ₂ O	→ 4Mg ²⁺ + 2Al(OH) ₄ ⁻ + 6OH ⁻ + 3H ₂ O					
599	M ₆ AH ₁₂ ^{**}	-72.0	Mg ₆ Al ₂ (OH) ₁₈ ·3H ₂ O	→ 6Mg ²⁺ + 2Al(OH) ₄ ⁻ + 10OH ⁻ + 3H ₂ O					
600	M ₈ AH ₁₄ ^{**}	-94.3	Mg ₈ Al ₂ (OH) ₂₂ ·3H ₂ O	→ 8Mg ²⁺ + 2Al(OH) ₄ ⁻ + 14OH ⁻ + 3H ₂ O					

601 a_0, a_1, a_2, a_3 are the empirical coefficients of the heat capacity function: $C_p^\circ = a_0 + a_1T + a_2T^{-2} + a_3T^{-0.5}$; ^{*} tentative value; recom-
602 mended for PC based systems. ^{**} tentative values; recommended for alkali activated materials.

603

604 2.7 C-S-H solid solution models

605 The C-S-H gel-like phase is the major hydrate in PC and blended PC pastes. C-S-H is also the main
606 "sorber" of alkali, alkali-earth, and hazardous cations (Sr²⁺, UO₂²⁺, Zn²⁺, etc.) in hydrated cements used
607 as waste matrices, including engineered barriers in nuclear waste repositories.

608 C-S-H phases have a variable composition that depends on the prevailing Ca/Si ratio in the system
609 that can change by pozzolanic reaction, leaching caused by the ingress of water and/or chemical at-

610 tack, such as carbonation. There are differences between properties of C-S-H samples prepared by (a)
 611 C_3S or C_2S hydration; (b) co-precipitation (double-decomposition) methods [76]. C-S-H has a 'defect-
 612 tobermorite' structure with a mean silicate chain length depending on the Ca/Si ratio, pH and the
 613 presence of aluminum [77]. It has variable "non-gel" water content (i.e. structural water and water pre-
 614 sent in the interlayer [78, 79]), also depending on the Ca/Si ratio and the synthesis route, variable par-
 615 ticle morphology, stacking, and "gel" water content, i.e. water present between C-S-H particles. Many
 616 C-S-H experimental solubility data sets available to date have been critically analyzed [80], including C-
 617 S-H type phases with variable aluminum and alkali contents [76, 81-84].

618 C-S-H solubility can be reliably modelled using either solid solution models [11, 80, 85] or (to a limited
 619 extent) using a surface complexation approach [86, 87]. Quantitative knowledge of C-S-H solubility is
 620 needed in essentially all studies of cement hydration and of waste-cement interactions, which explains
 621 why measuring and modeling the C-S-H solubility and water content is a major topic in cement chem-
 622 istry [76].

623 In Table 4, five alternative C-S-H solid solution models are represented, in part for backward compati-
 624 bility with previous versions of Cemdata (Cemdata07 and Cemdata14); they are provided in the
 625 Cemdata18 database. Here we provide a brief overview of those models with some recommendations
 626 for their use.

627

628 Table 4: Solid solution models of C-S-H (provided in separate modules of Cemdata18 database).

629	Phase,	$\Delta_f G^\circ$	$\Delta_f H^\circ$	S°	a_0	a_1	a_2	V°	Ref
630	End member	[kJ/mol]	[kJ/mol]	[J/K/mol]	[J/K/mol]	[J/mol/K ²]	[J K/mol]	[cm ³ /mol]	
631	<u>C-S-H (CSH-II solid solution)</u>								
632	Tob: $C_{0.83}SH_{1.3}$	-1744.36	-1916	80	85	0.160		59	[1]
633	Jen: $C_{1.67}SH_{2.1}$	-2480.81	-2723	140	210	0.120	$-3.07 \cdot 10^6$	78	[1]
634									
635	<u>C-S-H-K-N (ECSH-1 solid solution)</u>								
636	TobCa-1: $C_{0.83}SH_{1.83}$	-1863.62	-2059.5	114.6	170.4			68	[85]
637	SH: SH (SiO_2H_2O)	-1085.45	-1188.6	111.3	119.8			34	[85]
638	NaSH-1: $N_{0.5}S_{0.2}H_{0.45}$	-433.57	-480.4	41.2	37.9			10.5	[88]
639	KSH-1: $K_{0.5}S_{0.2}H_{0.45}$	-443.35	-490.0	48.4	40.6			12.4	[88]
640	SrSH-1: $SrSH_2$	-2020.89	-2231.6	141.9	174.8			64	[88]
641		(-2017.47 ^b)	(-2228 ^b)						
642									
643	<u>C-S-H-K-N (ECSH-2 solid solution)</u>								
644	TobCa-2: $C_{0.83}SH_{1.83}$	-1863.62	-2059.5	114.6	170.4			68	[85]
645	JenCa: $CS_{0.6}H_{1.1}$	-1569.05	-1741.6	73.0	114.5			36	[85]
646	NaSH-2: $N_{0.5}S_{0.2}H_{0.45}$	-430.72	-477.6	41.2	37.9			10.5	[88]
647	KSH-2: $K_{0.5}S_{0.2}H_{0.45}$	-440.49	-487.2	48.4	40.6			12.4	[88]
648	SrSH-2: $SrSH_2$	-2019.75	-2230.5	141.9	174.8			64	[88]
649		(-2016.33 ^b)	(-2227 ^b)						
650									
651	<u>C-S-H (CSHQ solid solution)</u>								
652	TobH Ca/Si=0.67: $C_{2/3}SH_{1.5}$	-1668.56	-1841.5	89.9	141.6			55	[11]
653	TobD Ca/Si = 1.25: $C_{5/6}S_{2/3}H_{1.83}$	-1570.89	-1742.4	121.8	166.9			48	[11]
654	JenH Ca/Si = 1.33: $C_{1.33}SH_{2.17}$	-2273.99	-2506.3	142.5	207.9			76	[11]

658	JenD Ca/Si=2.25: C _{1.5} S _{0.67} H _{2.5}	-2169.56	-2400.7	173.4	232.8				81	[11]
659	NaSH: N _{0.5} S _{0.2} H _{0.45}	-431.20	-478.0	41.2	37.9				10.5	[88, 89]
660	KSH: K _{0.5} S _{0.2} H _{0.45}	-440.80	-489.6	48.4	40.6				12.4	[88, 89]
661										
662										
663	<u>C-S-H (CSH3T solid solution)</u>									
664	TobH Ca/Si=0.67: C ₁ S _{3/2} H _{5/2}	-2561.53	-2832.97	152.8	231.2				85	[11]
665	T5C Ca/Si=1.0: C _{5/4} S _{5/4} H _{5/2}	-2518.66	-2782.03	159.9	234.1				79	[11]
666	T2C Ca/Si=1.5: C _{3/2} S ₁ H _{5/2}	-2467.08	-2722.40	167.0	237.0				81	[11]
667										
668										
669	<u>C-(N-)A-S-H (CNASH solid solution)</u>									
670	TobH ^c : C ₁ S _{3/2} H _{5/2}	-2560.00	-2831.4	152.8	231.2	-	-	-	85.0	[90]
671	INFCA: C ₁ A _{5/32} S _{38/32} H _{53/32}	-2342.90	-2551.3	154.5	180.9	-	-	-	59.3	[90]
672	INFNCN: C ₁ N _{5/16} S _{3/2} H _{19/16}	-2452.46	-2642.0	185.6	183.7	-	-	-	71.1	[90]
673	INFCA: C ₁ A _{5/32} N _{11/32} S _{38/32} H _{42/32}	-2474.28	-2666.7	198.4	179.7	-	-	-	69.3	[90]
674	T5C ^c : C _{5/4} S _{5/4} H _{5/2}	-2516.90	-2780.3	159.9	234.1	-	-	-	79.3	[90]
675	5CA: C _{5/4} A _{1/8} S ₁ H _{13/8}	-2292.82	-2491.3	163.1	177.1	-	-	-	57.3	[90]
676	5CNA: C _{5/4} N _{1/4} A _{1/8} S ₁ H _{11/8}	-2381.81	-2568.7	195.0	176.2	-	-	-	64.5	[90]
677	T2C ^c : C _{3/2} S ₁ H _{5/2}	-2465.40	-2720.7	167.0	237.0	-	-	-	80.6	[90]
678										

679 a₀, a₁, a₂, are the empirical coefficients of the heat capacity equation: C_p^o= a₀ +a₁T+a₂T⁻²; no value = 0.

680 ^a Only CSH-II solid solution included in Cemdata'07.03 database. ^b for the ACW conditions. ^c Thermodynamic
681 properties were slightly modified relative to the T2C, T5C, and TobH end members of the downscaled CSH3T
682 thermodynamic model [11].

683

684 **CSH-II model.** This simple ideal C-S-H solid solution model [85] has been used for many years, and
685 was included (with a modified stability to better describe the changes in the calcium concentrations
686 with pH and less water to correspond to the composition of C-S-H present in cements) into Cemda-
687 ta07 database [1, 29]. The original model [85] consisted of two binary ideal solutions CSH-I and CSH-II.
688 CSH-I used end-members of amorphous silica (SH; SiO₂) and a tobermorite-like C-S-H gel phase (Tob-
689 I; (Ca(OH)₂)₂(SiO₂)_{2.4}·2H₂O). CSH-II used end-members of tobermorite-like (Tob-II;
690 (Ca(OH)₂)_{0.8333}SiO_{2.0.8333}·H₂O) and jennite-like (Jen; (Ca(OH)₂)_{1.6666}SiO₂·H₂O) C-S-H gel phases. The CSH-II
691 phase co-exists with CH (portlandite) at Ca/Si ratios above 1.5 to 1.7. The CSH-I solid solution has been
692 shown to be unrealistic ([80] and references therein) and amorphous SiO₂ co-exists with C-S-H gel of
693 Ca/Si ratios = 0.4-0.8. The water content in this C-S-H II is lower than in the other models discussed
694 below, but corresponds well to the water present in the interlayer of C-S-H as measured by ¹H-NMR
695 [78, 79]. In Cemdata18, we provide the CSH-II solid solution model only, covering the range of Ca/Si
696 ratios from 0.83 to 1.67, for backward compatibility with the Cemdata07 database and as an alternative
697 to the newer models.

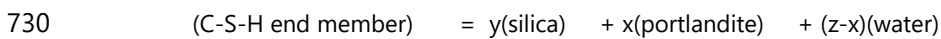
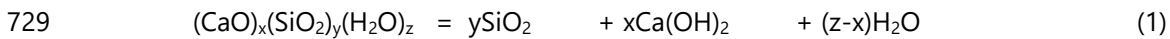
698

699 **ECSH-1 and ECSH-2 models** extend both CSH-I and CSH-II models with Na-, K- and Sr- containing
700 end members. Aimed at pragmatic description of uptake of minor cations, these provisional ideal solid
701 solution models [88] were constructed with help of the statistical dual-thermodynamic method [91]
702 based on GEM-Selektor calculations. With this method, one can retrieve both the unknown stoichiometry
703 and the standard molar Gibbs energy Δ_fG₂₉₈^o of ideal solid solution end members from the exper-
704 imental bulk compositions of the aqueous solution and co-existing solid solution. In total, 13 possible

705 end member stoichiometries with the general formula
 706 $[(\text{Ca}(\text{OH})_2)_{n_{\text{Ca}}}(\text{Sr}(\text{OH})_2)_{n_{\text{Sr}}}(\text{KOH})_{n_{\text{K}}}(\text{NaOH})_{n_{\text{Na}}}\text{SiO}_2\text{H}_2\text{O}]_{n_{\text{Si}}}$ were considered for these models. To develop
 707 these models, the n_{Ca} , n_{Sr} , ... coefficients were adjusted in order to minimize the standard deviations
 708 of estimated G°_{298} values for model end members in trial GEM calculations for a number of experi-
 709 mental data points. These trial GEM calculations employed: (1) the Nagra-PSI database [24]; (2) many
 710 experimental data points at different Ca/Si, Sr/Si, Na/Si, K/Si ratios; and (3) varying stoichiometry coef-
 711 ficients of solid solution end members within the ranges of $0.1 < n_{\text{Si}} < 2$, $0 < n_{\text{Ca}} < 1.6$, $0 < n_{\text{Sr}} < 2$, $0 < n_{\text{K}}$
 712 < 2 , and $0 < n_{\text{Na}} < 2$.

713 Followed by ‘forward GEM modelling’ of Sr uptake data in pure water and in artificial cement water
 714 (ACW), this procedure resulted in ideal ECSH-II and ECSH-I solid solution models that provided the op-
 715 timal description of data (over 96 experiments published in [92] and additional in-house Sr uptake da-
 716 ta on C-S-H in water and in ACW). $\Delta_r G^\circ_{298}$ values for Na- and K-containing end members were also fi-
 717 ne-tuned using literature data [81] on Na and K uptake isotherms in C-S-H (Figure 10). The ECSH-1
 718 and ECSH-2 models can realistically describe the uptake of cations and the decrease of (maximum)
 719 Ca/Si ratios in equilibrium with portlandite upon increasing alkali concentration in aqueous solution.
 720 However, it was not possible to use the same $\Delta_r G^\circ_{298}$ of SrSH end member to model isotherms of Sr
 721 uptake in C-S-H prepared in water and in the artificial cement pore water (ACW with pH ≈ 13.3 at 25 °C,
 722 containing 0.18 M KOH, 0.114 M NaOH and 1.2 mM $\text{Ca}(\text{OH})_2$). We believe that the $\Delta_r G^\circ_{298}(\text{SrSH})$ differ-
 723 ence (up to 3.4 kJ mol⁻¹) can probably be explained by different silica polymerization and cation ex-
 724 change capacity of C-S-H due to the presence of alkali. We anticipate that ECSH-1 and ECSH-2 will be
 725 replaced by more accurate C-S-H-K-Na models in the near future.

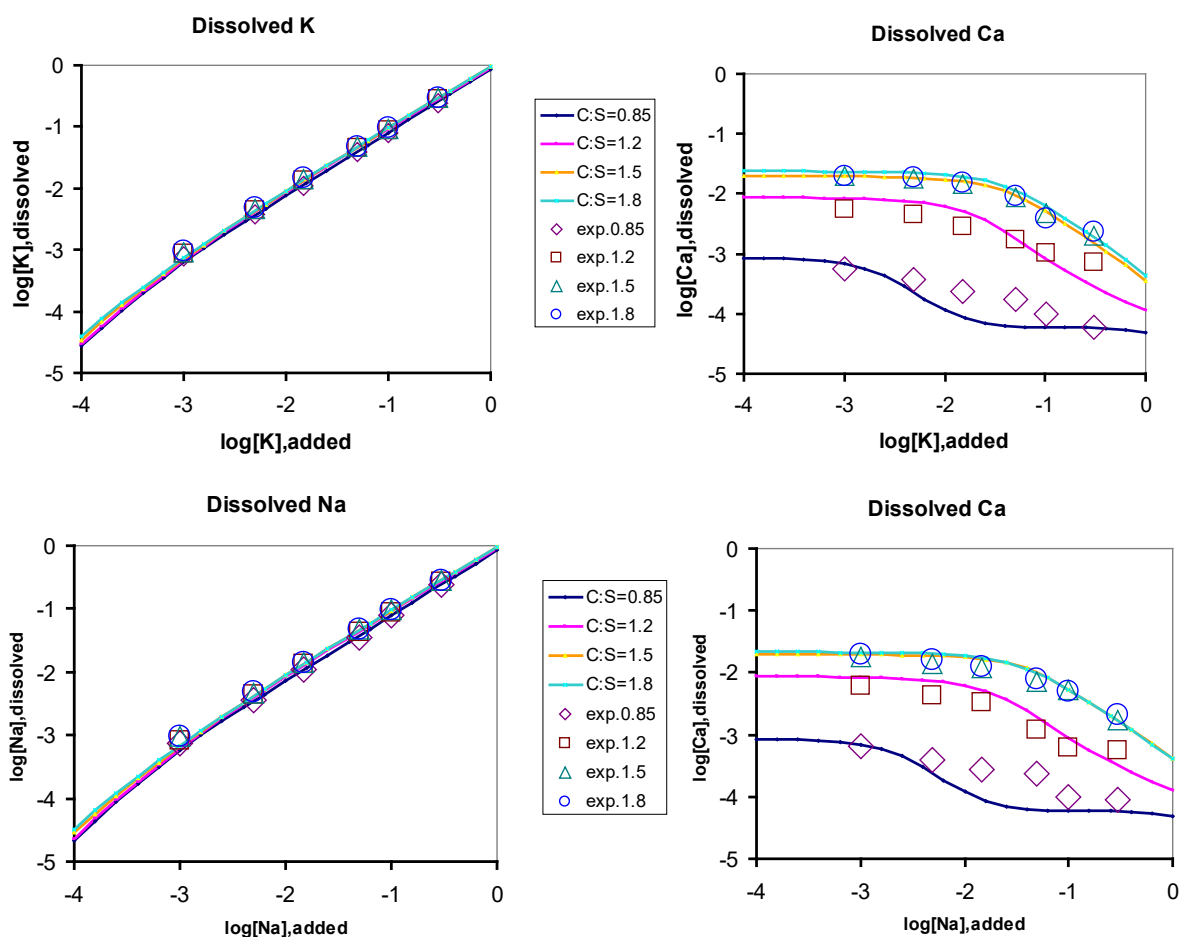
726 With no known thermodynamic properties of structural analogues available, the standard entropy and
 727 heat capacity of the ECSH end members were estimated assuming linear dependencies of entropy and
 728 heat capacity effects of reactions on the Ca/Si ratio in C-S-H [11]:



$$731 \quad \Delta_r S^\circ_{298} = y (61.054 + 5.357 x/y) \quad (2a)$$

$$732 \quad \Delta_r Cp^\circ_{298} = y (31.881 - 11.905 x/y) \quad (2b)$$

733 Using eqs (2a,b), $\Delta_r S^\circ_{298}$ and $\Delta_r Cp^\circ_{298}$ were calculated and rounded off to the nearest whole numbers.
 734 The $\Delta_r H^\circ_{298}$ values were calculated from $\log_{10} K^\circ_{298}$ and $\Delta_r S^\circ_{298}$ values together with the S° , Cp° , $\Delta_r H^\circ$ and
 735 $\Delta_r G^\circ$ values at $T_r = 298.15$ K using the ReacDC module of GEM-Selektor code and thermodynamic
 736 properties of water, portlandite and amorphous silica from the GEMS version of the PSI/Nagra 12/07
 737 TDB [22, 23] and Cemdata18 databases. The resulting thermodynamic properties (Table 4) are ex-
 738 pected to suffice for temperatures between 0 and 90 °C within 0.5 pK units uncertainty.



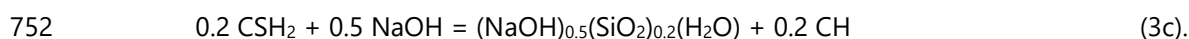
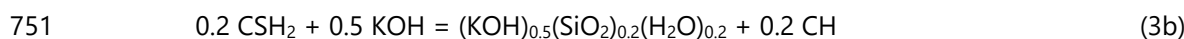
739

740

741 Figure 10: Comparison of sorption isotherms for K or Na calculated using the ECSH-II Aq-SS model
 742 (curves) with the data for K and Na sorption [81] (scattered symbols). Abscissa: \log_{10} moles of added K
 743 or Na per 1 kg H_2O ; ordinate: \log_{10} molar.

744

745 Next, the S_{298}° , Cp_{298}° and values of the SrSH, NaSH and KSH end members of ECSH phases were eval-
 746 uated. This was done by taking the properties of their reference calcium hydroxide counterpart $\text{C}_1\text{S}_1\text{H}_2$
 747 and then either subtracting or adding respective properties of solid portlandite $\text{Ca}(\text{OH})_2$, as well as
 748 solid $\text{Sr}(\text{OH})_2$, solid NaOH or solid KOH from Wagman et al. [93]. This is equivalent to assuming $\Delta_r S_{298}^{\circ}$
 749 = 0 and $\Delta_r Cp_{298}^{\circ} = 0$ for the reactions:



753 For these calculations, $\Delta_r S_{298}^{\circ}$, and $\Delta_r Cp_{298}^{\circ}$, S_{298}° , Cp_{298}° of the reference compound CSH_2 were com-
 754 puted using Eqs 1, 2a and 2b. Note that the stoichiometries of the K and Na C-S-H end members de-
 755 fined by reactions 3b and 3c correspond to $\text{N}_{0.25}\text{S}_{0.2}\text{H}_{0.45}$ or $\text{K}_{0.25}\text{S}_{0.2}\text{H}_{0.45}$, but not $\text{N}_{0.25}\text{S}_{0.2}\text{H}_{0.3}$ or
 756 $\text{K}_{0.25}\text{S}_{0.2}\text{H}_{0.3}$ as defined in Kulik et al. [88]. The respective values for $\Delta_r G_{298}^{\circ}$, and $\Delta_r H_{298}^{\circ}$ are summarised
 757 in Table 4.

758

759 **CSHQ model** [11] was developed in order to address some known shortcomings of earlier CSH-I and
760 CSH-II models [29, 85], namely insufficient connection to the C-S-H structure and the unrealistic as-
761 sumption of ideal mixing between tobermorite-like and amorphous silica end members. It was based
762 on structural data supporting the defect-tobermorite model [94-96], represented as a solid solution
763 model with four different structural sites (sublattices) [11]: $[BTI^{+2}]_1:[TU^-]_2:[CU^0]_2:[IW^0]_5$. The main as-
764 sumption was that in BTI sites, the incorporation of Ca^{2+} ion in the interlayer occurs simultaneously
765 with the removal of a bridging tetrahedron in the silica "dreierketten" chain, and this process is re-
766 versible. Excess calcium can also be incorporated as a $Ca(OH)_2$ moiety, either interstitially in the tober-
767 morite interlayer, or forming domains of jennite-like structure. This was accounted for by an exchange
768 of a vacancy with $Ca(OH)_2$ in CU sites. The occupation of TU and IW sublattices was fixed as $2CaSiO_{3.5}^-$
769 and $4H_2O+vacancy$, respectively. This led to four end members with stoichiometries depending on the
770 assumed Ca^{2+}/H^+ ratio in BTI sites.

771 This solid solution model has a correct built-in dependence of the mean silica chain length (MCL) on
772 Ca/Si ratios. By downscaling the end-member stoichiometries to $Si = 1.0$ and adjusting the G°_{298} values
773 of end members, the CSHQ model could be fine-tuned to various C-S-H solubility data sets [11]. In this
774 Cemdata18 database, two end members for K and Na (similar to those from the ECSH model) were
775 provisionally added to improve predictions of pH and composition of the PC porewater.

776 The downscaled ideal CSHQ model (Table 4) provides a reasonable fit to the variety of C-S-H solubility
777 data in the $[Ca]-[Si]$, $[Ca]-C/S$ and $[Si]-Ca/Si$ spaces as discussed in more detail in [11].

778 An extension to cover the uptake of alkalis by C-S-H was based on an ideal solid solution model be-
779 tween jennite, tobermorite, $[(KOH)_{2.5}SiO_2H_2O]_{0.2}$ and $[(NaOH)_{2.5}SiO_2H_2O]_{0.2}$ as proposed by Kulik et al.
780 [88] and using the thermodynamic data reported in [89]: $\Delta_rG^{\circ} = -440'800 \text{ J/mol}$ and $-431'200 \text{ J/mol}$ (at
781 $20^{\circ}C$) for $[(KOH)_{2.5}SiO_2H_2O]_{0.2}$ and $[(NaOH)_{2.5}SiO_2H_2O]_{0.2}$, respectively.

782

783 **CSH3T model** [11] was aimed at more consistency with the tobermorite-like structure of C-S-H phases
784 at $Ca/Si < 1.5$. The evidence of interlayer ordering in tobermorite-like C-S-H with $0.9 < C/S < 1.25$ [96]
785 has led to setting the CU sites always vacant, and to splitting the BTI sublattice into two
786 $([BTI1^+]_1:[BTI2^+]_1:[TU^-]_2:[IW^0]_4)$ with substitutions of $Si_{0.5}OH^+$ by $HO_{0.5}Ca_{0.5}^+$. This yielded a solid solution
787 model with end members TobH ($C_2S_3H_5$), T5C ($C_{2.5}S_{2.5}H_5$), T2C ($C_3S_2H_5$), connected by an ordering reac-
788 tion $\frac{1}{2}TobH + \frac{1}{2}T2C = T5C$. The model has a built-in dependence of the mean chain length on the
789 composition, consistent with measured values [95] for the co-precipitated tobermorite-like C-S-H. The
790 CSH3T model [11] in its downscaled form (Table 4) can be computed just using a simple ideal mixing
791 model. The CSH3T model has been later extended with U(VI) end members [97] and with Al and Na
792 end members [90]. The ideal CSH3T SS model [11] produces quite realistic curves for solubility of the
793 synthetic C-S-H co-precipitation (double decomposition) data. More accurate C-S-H multi-site solid
794 solution models are in development.

795

796 **CNASH_{ss} model** [90] includes Al and Na and represents an extension of the CSH3T model that was
797 optimised for alkali activated systems. The calcium (alkali) aluminosilicate hydrate (C-(N-)A-S-H) gel-
798 like phase that precipitates in alkali-activated cements contains significantly less Ca, more Al and alkali

799 and has a more densely packed structure than the C-(A-)S-H which forms in hydrated PC-based mate-
800 rials [98, 99]. However, both phases are based on the same defect-tobermorite structure. In alkali-
801 activated slag cements (an exemplary 'high-Ca' alkali-activated material [100]), the C-(N-)A-S-H phase
802 typically has a $\text{Ca/Si} \approx 1$ and an $\text{Al/Si} \leq 0.25$ [90].

803 Many solubility and chemical composition data for the C-(N-)A-S-H system have been published.
804 Much of this data was used to develop an ideal solid solution thermodynamic model (CNASH_{ss}), in-
805 cluding configurational entropy terms, which explicitly includes mixing of Al and Na [90]. The
806 CNASH_{ss} model enables Al incorporation into C-(N-)A-S-H gel to be explicitly considered in thermo-
807 dynamic modelling simulations. The CNASH_{ss} model has been applied to simulate phase assemblag-
808 es in NaOH, sodium silicate, Na_2CO_3 , and Na_2SO_4 -activated slag systems [74, 101]. This model is also
809 applicable to thermodynamic modelling of PC-based materials; however, it less closely represents the
810 full body of available solubility data for the C-S-H phase [102] at $\text{Ca/Si} > \sim 1.3$ than other C-S-H ther-
811 modynamic models, e.g. [11, 80]. CNASH_{ss} closely represents the full set of solubility data for the C-
812 (N-)A-S-H gel phase down to $\text{Ca/Si} = 0.67$. Therefore, we recommend using CNASH_{ss} for alkali acti-
813 vated systems rather than hydrated PC systems, where we recommend the use of CSHQ or C-S-H-II.

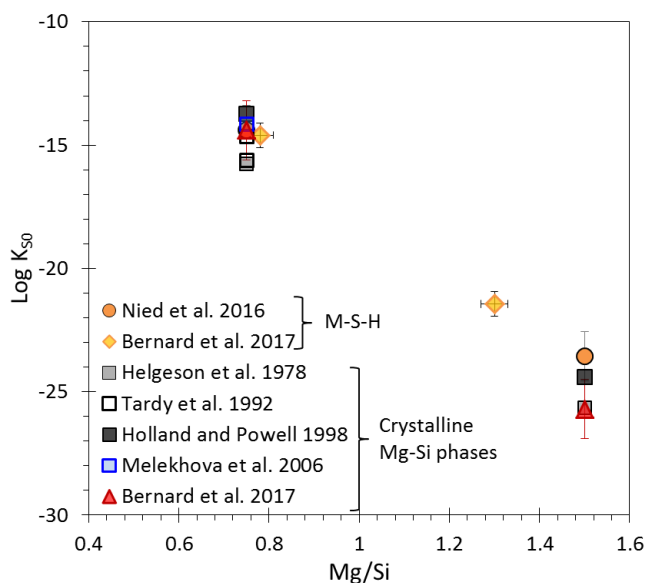
814 Additional solubility data for C-(N-)A-S-H gel not used to validate CNASH_{ss} were recently published,
815 including for C-(N-)A-S-H gels at synthesis temperatures of 7°C, 50°C and 80°C [103, 104] and using K
816 rather than Na [84, 105]. Future refinement to the CNASH_{ss} thermodynamic model should include
817 these data and formally extend the model to different temperatures and alkali type.

818 During the last 20 years, ideal solid solution models of C-S-H have evolved starting from simple ideal
819 solid solutions using full end-member mixing up to recent truly multi-site mixing models consistent
820 with both solubility data and structural/spectroscopic data. Because end members in multi-site solid
821 solutions are constructed of moieties substituting each other on different sublattices, such models
822 have the best potential for: (1) extension by adding moieties for other elements of interest (e.g. K, Na,
823 Al, U, Sr) in their respective sites; (2) generating all possible end members; and (3) parameterizing end
824 members based on available solubility, element uptake, and spectroscopic data (e.g. using the
825 GEMSFITS code [106]) and are the subjects of ongoing research.

826 For the calcium silicate hydrate complexes, $\text{CaH}_3\text{SiO}_4^+$ ($\text{CaHSiO}_3^+ + 2\text{H}_2\text{O}$) and $\text{CaH}_2\text{SiO}_4^0$ (CaSiO_3^0
827 $+ 2\text{H}_2\text{O}$), the reported complex formation data show a significant scatter. In particular, complex for-
828 mation constants for $\text{CaH}_2\text{SiO}_4^0$ vary by more than one log unit. While the PSI/Nagra TDB [22, 23] re-
829 ports a complex formation constant of $10^{4.6}$ for the reaction $\text{Ca}^{2+} + \text{SiO}_3^{2-} \rightarrow \text{CaSiO}_3^0$ (see Table 2),
830 which has a large effect on the silicon concentrations in presence of C-S-H at $\text{Ca/Si} > 1$ [80], no such
831 constant is defined in the PHREEQC database [18]. Walker et al. [80] recommended to use a constant
832 of $10^{4.0}$, making the complex less important, while recently an even lower complex formation constant
833 of $10^{2.9}$ has been derived based on titration experiments [107]. This large scatter of data results in very
834 diverging assessment of the importance of the CaSiO_3^0 complex at $\text{Ca/Si} > 1$ and has a significant im-
835 pact on the C-S-H solubility as this complex accounts for about 90% of aqueous dissolved silicon in
836 equilibrium with both C-S-H and portlandite. Dedicated investigations not only of calcium silicate hy-
837 drate complexes but also of other possible complexes between aluminum, calcium and silicate at high
838 pH values are urgently needed.

840 2.8 Magnesium silicate hydrates

841 The formation of magnesium silicates hydrate (M-S-H) has been observed at the interfacial zone of
 842 cement paste with clays [67, 108, 109] and/or as secondary products from the degradation of cement
 843 pastes by groundwater or seawater [110-112]. The combination of leaching and carbonation of the
 844 cement paste decreases pH at the surface of the cement, decalcifies C-S-H and leads the formation of
 845 a Mg-enriched phase, M-S-H. M-S-H phases are poorly ordered but have a layered structure with tet-
 846 rahedral silica arranged in sheets similar to clay minerals, have variable Mg/Si from ≈ 0.8 to $\text{Mg/Si} \approx 1.2$
 847 and are stable at pH values between 7.5 to 11.5 [40, 113-115]. Given the difference in structure and pH
 848 domains, most studies [114-117] observed the precipitation of distinct C-S-H and M-S-H phases and
 849 not of a mixed magnesium calcium silicate hydrate phase. Solubility measurements [40, 113, 118] indi-
 850 cated an only slightly higher solubility of the poorly ordered M-S-H in comparison to crystalline mag-
 851 nesium-silicates such as talc, antigorite or chrysotile as shown in Figure 11. The ideal solid solution
 852 model for M-S-H published by Nied et al. [40] has been selected for the present version of the data-
 853 base. As several groups [113, 114, 118] are currently working on thermodynamic data for M-S-H, we
 854 expect that more sophisticated models will be published in the coming years.



855

856 Figure 11: Evolution of the solubility product (K_{S0}) of magnesium silicate hydrates at room temperature
 857 as a function of the total Mg/Si; referring to reactions using Mg^{2+} , SiO_2 and H_2O as indicated in Table
 858 2. Adapted from [118].

859

860 2.9 Zeolites

861 Interactions of highly alkaline solutions in hydrated PC systems with service environments will likely re-
 862 sult in the partial dissolution of aluminosilicate minerals from adjacent rocks and the formation of sec-
 863 ondary zeolite minerals [119] in the context of deep underground nuclear waste repositories. Zeolite

864 formation also occurs in alkali activated cement systems. These zeolites are often related to the poorly
865 crystalline N-A-S-H (sodium-aluminium-silicate-hydrate) and K-A-S-H (potassium-aluminium-silicate-
866 hydrate) gels that form in these systems [74, 103]; the type of gel formed depends on the presence of
867 Na^+ or K^+ , cation concentrations, the relative degree of saturation of the liquid phase with respect to
868 silica, pH and temperature [120]. Several papers in recent years estimated solubility data for different
869 zeolites, based mainly on heat capacity and enthalpy measurements [47, 74, 121]. This may lead to
870 considerable bias in the estimated solubility data in the range of several log units due to uncertainties
871 associated with the measurements of enthalpy data. The determination of solubility data for zeolites
872 has been hindered by variability in cation composition (Ca, Na, K), Al/Si ratios, H_2O contents and atom-
873 ic structure, and also their slow reaction kinetics.

874 In 2017, two independent studies [41, 103] reported very similar solubility products for zeolite Y and X
875 (or for N-A-S-H gel with Al/Si = 0.5 and Al/Si = 0.8) based on experimental data. The data for zeolite
876 X(Na), zeolite Y(Na) and chabazite [41] make it possible to predict zeolite formation in sodium activat-
877 ed cements; data for potassium-based zeolites are still missing in the Cemdata18 database. Also data
878 for natrolite and zeolite P(Ca) have been included [41]. In experiments with high pH values their for-
879 mation was kinetically hindered (although natrolite and zeolite P(Ca) were more stable than zeolite
880 X(Na), zeolite Y(Na) and chabazite). Thus we recommend that natrolite and zeolite P(Ca) should be
881 considered in modelling the interface between cement and adjacent rocks. However, their formation
882 may be suppressed in models for alkali activated systems, where zeolite X(Na), zeolite Y(Na) and chaba-
883 zite or their amorphous or nanocrystalline precursors are formed [122].

884

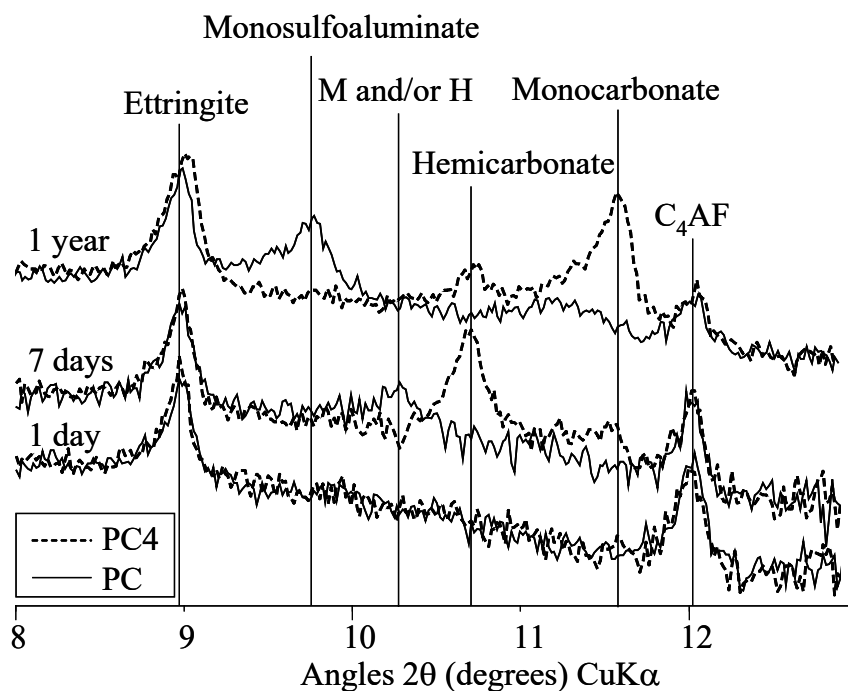
885 **3 Comparison Cemdata07 with Cemdata18**

886 The updates since the first cemdata version, cemdata07 (published in 2008), are significant. In particu-
887 lar, the distribution of iron and aluminium, the volume and Ca/Si in C-S-H as well as the alkali concen-
888 trations in the pore solution in PC can significantly affect thermodynamic modelling results. To illus-
889 trate these differences, the effect of limestone on the same PC was calculated with Cemdata07 and
890 Cemdata18 and compared below. The effect of relative humidity on calculated hydrates is used below
891 as a second example. These comparisons concentrate on PC, as compiled specific data for alkali acti-
892 vated materials are only now available (in this paper).

893 **3.1 Effect of limestone on solid and liquid phase composition**

894 The influence of limestone on cement hydration has been widely studied and was the subject of sever-
895 al publications by the authors [2, 20, 123]. Experimental investigations showed that the presence of
896 calcium carbonate prevents the destabilisation of ettringite to monosulfate at long hydrations times
897 and stabilises monocarbonate together with ettringite (see e.g. [123-125] and Figure 12).

898



899
900

901 Figure 12: Experimentally observed phase assemblage in a PC without additional limestone (PC) and
902 with 4 wt.% of limestone (PC4); reproduced from [123].

903

904 Also thermodynamic modelling [2, 20, 123] (mainly using the Cemdata2007 database) showed that the
905 presence of small amounts of limestone significantly impacted the mineralogy of hydrated cements. In
906 the absence of any limestone no ettringite but only monosulfate as well as of a small amount of
907 katoite ($C_3(A,F)H_6$) was predicted as shown in Figure 13A. The presence of a small amount of limestone
908 was calculated to stabilise hemicarbonate and at higher dosages monocarbonate plus ettringite, re-
909 sulting in an increase of the total volume. The higher volume in the presence of a small amount of
910 limestone due to the stabilization of ettringite has been found to have a positive effect on the me-
911 chanical properties of PC and blended cements [20, 124].

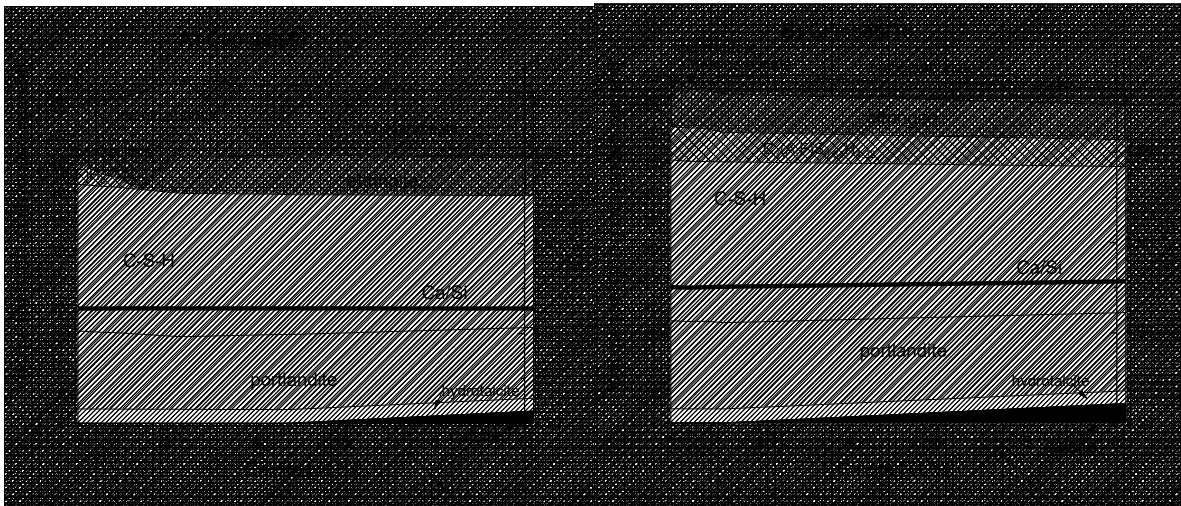
912 The stability of siliceous hydrogarnet was a matter of debate during the development of Cemdata07
913 and in most calculations with Cemdata07 the formation of siliceous hydrogarnet $C_3AS_{0.8}H_{4.4}$ had been
914 suppressed assuming kinetic hindrance. Based on the data compiled in Cemdata07, which originated
915 from measurements from [7, 72, 126], ettringite and siliceous hydrogarnet were calculated to be signif-
916 icantly more stable than monosulfate, hemi- or monocarboaluminate thus theoretically preventing
917 their presence. Since monosulfate, hemi- and monocarboaluminate are experimentally observed in hy-
918 drated PC, it was assumed that this was due to a kinetic hindrance in the formation of siliceous hy-
919 drogarnet and that possibly a later conversion of hemi- and monocarboaluminate to siliceous hy-
920 drogarnet could occur.

921

922 The new data for $(C_3A_{0.5}F_{0.5}S_{0.84}H_{4.32})$ by Dilnesa et al. [9], included in Cemdata18, suggest that mixed
923 Al- and Fe-containing siliceous hydrogarnet can coexist with monosulfate, hemi- and monocarboalu-
924 minate at ambient conditions, which is in better agreement with the observed experimental data pre-

925 sented in Figure 12 and elsewhere [123-125]. Figure 13B displays the predicted phase assemblage of a
 926 hydrated PC with limestone using Cemdata18 as given in Table 1- Table 4; employing CSHQ and
 927 M_4AH_{10} . The formation of hemi- and monocarboaluminate accompanied by a stabilisation of ettringite
 928 instead of monosulfoaluminate was correctly predicted by both datasets. As shown in Figure 13 the
 929 biggest difference between the two datasets is the prediction of a katoite-type siliceous hydrogarnet
 930 phase ($C_3A_{0.5}F_{0.5}S_{0.84}H_{4.32}$), modelled as solid solution with a varying alumina and iron by using Cemda-
 931 ta18, together with hemi- and monocarboaluminate and ettringite throughout the modelled composi-
 932 tion range independently of the $CaCO_3$ content.

933

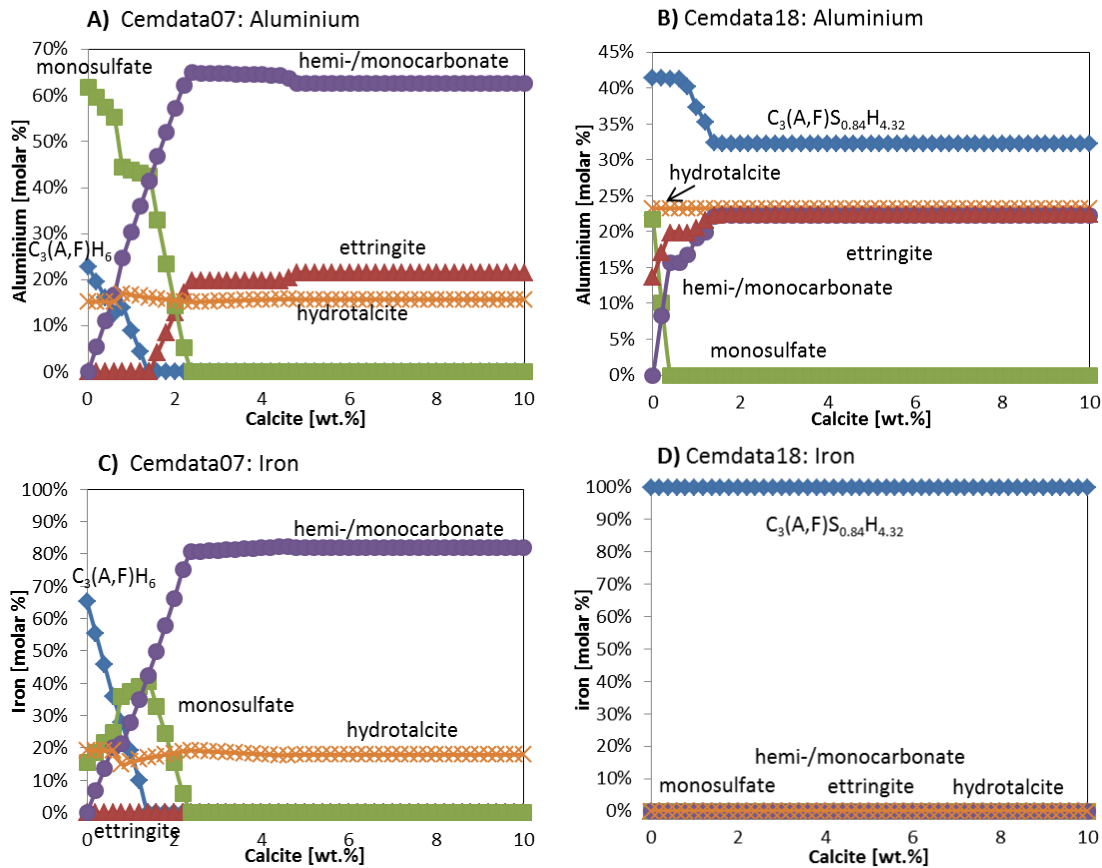


934

935 Figure 13: Comparison of calculated solid phase assemblage using A) Cemdata07 and B) Cemdata18
 936 assuming complete hydration of PC using the composition reported in [123].

937

938 The consideration of the siliceous hydrogarnet solid solution in Cemdata18 led to a quite significant
 939 redistribution of alumina and iron within the phase assemblage. Whereas with Cemdata07 around 70%
 940 of the available alumina was bound in AFm phases (see Figure 14A) the predictions based on Cemda-
 941 ta18 suggest that only about 25% of alumina is bound in AFm phases and ~30% in the hydrogarnet
 942 phase (Figure 14B). For iron, the difference is even more drastic. The predictions with Cemdata18 sug-
 943 gest that close to 100% of the iron is bound by the siliceous hydrogarnet solid solution (Figure 14D)
 944 which is also in agreement with experimental observations [64-66], where predominantly the formation
 945 of mixed aluminum and iron containing hydrogarnet phases in close proximity to the original ferrite
 946 phases was observed in hydrated cements.



947

948

949 Figure 14: Effect of the amount of limestone on the phase assemblage and the distribution of aluminium
 950 and iron in hydrated PC calculated using Cemdata07 (A, C) and Cemdata18 (B, D).

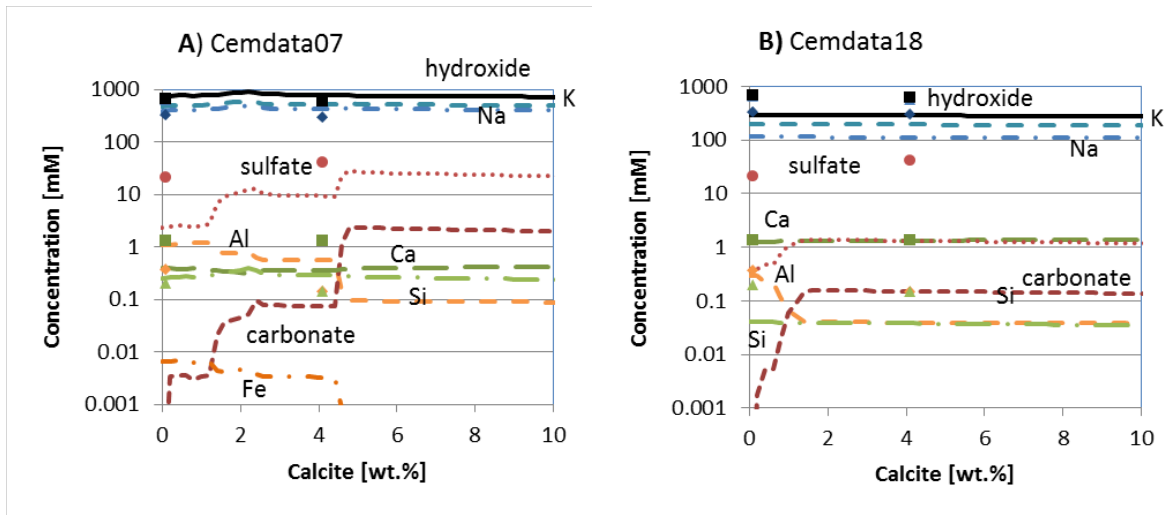
951

952 The binding of alkalis in C-S-H lowers the alkali and hydroxide concentrations [81, 84, 88] in the pore
 953 solution of hydrated PC and thus the pH values from above 14 to ~13 to 13.5 [1, 29, 123, 127]. The dis-
 954 regard of alkali binding by C-S-H would result in very high predicted pH values of 14 and above, which
 955 does not agree with measurements of the pore solution composition [5, 29]. As in 2007 no thermody-
 956 namic models to describe the uptake of alkali in C-S-H were available, distribution coefficients (K_d val-
 957 ues) were used together with Cemdata07 in most calculations of hydrated cements as described in de-
 958 tails e.g. in [1, 29, 123]. The use of distribution coefficient allowed predicting the alkali concentrations
 959 in PC relatively well as shown in Figure 15A, but the approach was not adequate to predict alkali up-
 960 take in low Ca/Si C-S-H present in blended cements. K_d values do not account for competitive sorption
 961 on specific sites as would be expected for the C-S-H gel, and also tend to be experiment-specific and
 962 so cannot generally be applied to other systems under different conditions. In the Cemdata18, the up-
 963 take of alkalis by C-S-H is modelled by introducing additional Na- and K-endmembers
 964 ($[(NaOH)_{2.5}SiO_2H_2O]_{0.2}$ and $[(KOH)_{2.5}SiO_2H_2O]_{0.2}$) in the CSHQ model, as described above (section 2.7).
 965 The introduction of these provisional data simplify the modelling, as no additional K_d values have to be
 966 introduced in the models, and allows the calculation of alkali uptake over the whole range of Ca/Si ra-
 967 tios, although the agreement between measured and calculated alkali concentrations is only satisfacto-
 968 rily, as shown in Figure 15B. Due to the lack of appropriate models for sodium and potassium uptake

969 in C-S-H valid over the complete range of Ca/Si, the modelling of alkali and hydroxide concentrations
970 in the pore solution remains a challenge.

971 The trends in the concentrations of calcium, sulfate, silicon and aluminium are generally correctly re-
972 produced by both models (see e.g. [1, 29, 123, 127], Figure 15) although there are differences between
973 measured and calculated values, in particular for Ca and Al for Cemdata07 and for sulfate and silicon
974 for Cemdata18.

975



976

977 Figure 15: Effect of the amount of limestone on the phase assemblage and the distribution of alumin-
978 ium and iron in hydrated PC calculated using A) Cemdata07 and B) Cemdata18.

979

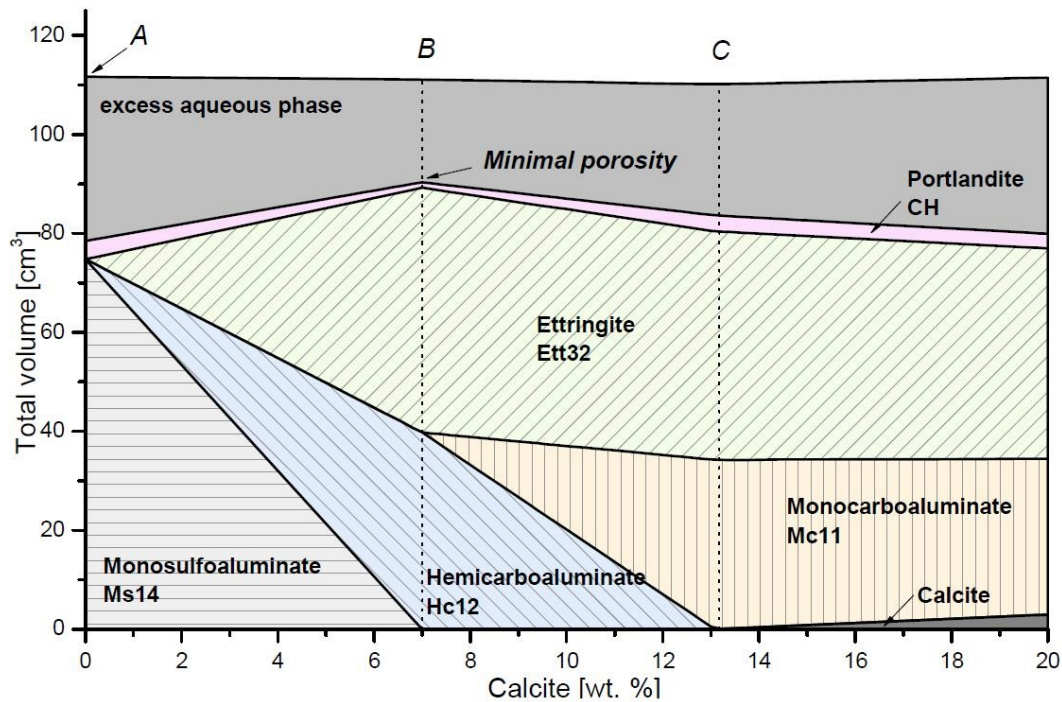
980

981 3.2 Effect of relative humidity on hydrated cements

982 Using the thermodynamic properties of phases with different water contents described in Section 2.5
983 and Table 1 it was possible to predict the drying behaviour of hydrated systems.

984 Drying of the $\text{CaO-Al}_2\text{O}_3\text{-SO}_3\text{-CO}_2\text{-H}_2\text{O}$ was simulated because it is directly relevant to PC and lime-
985 stone blended cements. The initial model mixture contained C_3A , portlandite (CH), calcium sulfate
986 ($\text{SO}_3/\text{Al}_2\text{O}_3=1$ molar bulk ratio), and varying amounts of calcite at 25°C. The amount of solids was kept
987 constant at 100 g and reacted with 90 g water. A diagram of the specific volume changes of the hy-
988 drated mixture with respect to calcite content is shown in Figure 16.

989



990

991 Figure 16 Calculated specific volume changes of a hydrated model mixture consisting of C_3A , portland-
 992 ite and with fixed sulfate ratio ($SO_3/Al_2O_3=1$, molar bulk ratio) in dependence of changing calcite con-
 993 tent at 25°C.

994

995 Due to their differing AFm-AFt mineralogy hydrate phase assemblages A, B and C in Figure 16, with
 996 0%, 7% and 13.2% of calcite respectively, were selected as initial hydrated systems for the drying mod-
 997 eling. Drying was simulated by continuously removing water from the assemblages until a RH of zero
 998 was reached. The investigated systems were:

999

- System A: monosulfoaluminate (Ms14) and portlandite (CH)
- System B: ettringite (Ett32), hemicarboaluminate (Hc12) and portlandite (CH)
- System C: ettringite (Ett32), monocarboaluminate (Mc11) and portlandite (CH)

1000

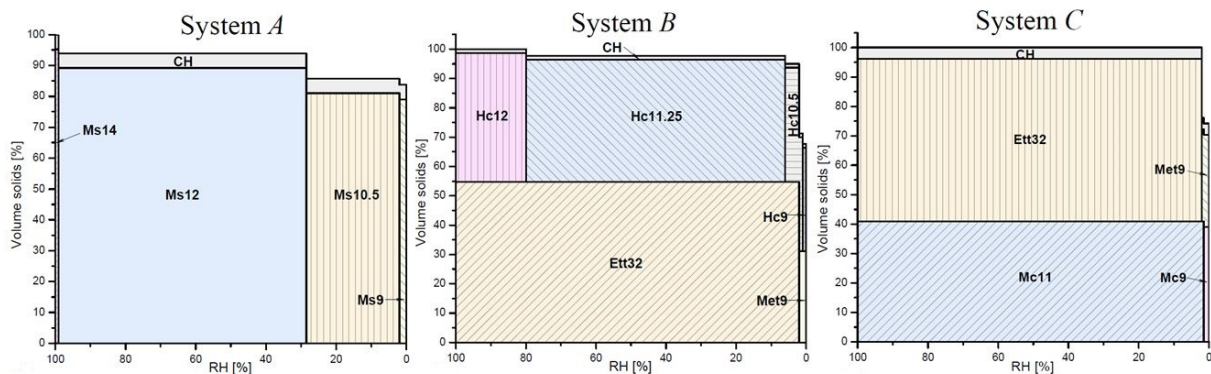
1001

1002

1003 Figure 17 a, b and c present the evolution of specific solid volume as a function of RH. We can see that
 1004 dehydration happens stepwise at critical RH stability limits of the phase assemblages, representing in-
 1005 variant points where the RH is fixed due to phase rule restrictions. At this critical RH two hydration
 1006 states of the same cement hydrate coexist and buffer the humidity in a similar manner as conventional
 1007 drying agents. Another important finding is that the addition of calcite and the formation of carboalu-
 1008 minates and ettringite will enhance the dimensional stability of hydrated cement paste and makes it
 1009 less sensitive to humidity fluctuations, which appears to be relevant for limestone blended cements.
 1010 Due to the presence of monocarboaluminate and ettringite system C is the most stable phase assem-
 1011 blage, which only decomposes at very low humidities (below 2% RH) whereas monosulfoaluminate
 1012 quickly loses part of its interlayer water at <99% RH.

1013

1014 Something important to keep in mind is that, although experimentally we observe the changes shown
 1015 in Figure 17, several of these dehydration processes are metastable with respect to other phase as-
 1016 semblages. This has to be considered when predicting the drying behaviour of cementitious systems.



1017
 1018 Figure 17: Calculated specific volume changes of a hydrated model mixture consisting of C₃A, port-
 1019 landite and with fixed sulfate ratio (SO₃/Al₂O₃=1, molar bulk ratio) in dependence of changing calcite
 1020 content at 25°C. , as shown in Figure 16 for the Systems A, B and C.

1021
 1022
 1023

1024 4 Conclusions

1025 The Cemdata18 database summarised in this paper can reliably calculate the type, composition,
 1026 amount and volume of hydrates formed and the pH and composition of the pore solution during hy-
 1027 dration and degradation of cementitious systems. The Cemdata18 database, as compiled in Table 1 to
 1028 Table 4, includes carefully selected thermodynamic data published in the literature based on critical re-
 1029 views supplemented with new experimental data. Data for solids commonly encountered in cement
 1030 systems in the temperature range 0-100°C, including C-S-H, M-S-H, hydrogarnet, hydrocalcite-like
 1031 phases, some zeolite, AFm and AFt phases and their respective solid solutions has been compiled. The
 1032 Cemdata18 database is an update of the Cemdata07 and Cemdata14 databases, and is compatible
 1033 with the GEMS version of the PSI/Nagra 12/07 TDB [22, 23]. Cemdata18 TDB is freely downloadable
 1034 (<http://www.empa.ch/cemdata>) in formats supporting the computer programs GEM-Selektor [13, 14]
 1035 and PHREEQC [18]. Further details are available in Appendix A and B.

1036

1037 The most important additions to the Cemdata18 TDB include:

- 1038 • C-S-H:
 - 1039 ○ CSHQ model for Portland and blended cements, the uptake of alkalis by C-S-H is mod-
 1040 elled by additional Na- and K-containing end members
 - 1041 ○ CSH3T model that corresponds to pure defect-tobermorite structure with ordering at
 1042 Ca/Si ratio close to 1.0, and forms the basis for CNASH-ss model

- 1043 ○ C-(N-)A-S-H model for alkali activated materials (CNASH-ss), which calculates the uptake
- 1044 of aluminium and sodium in low Ca/Si C-S-H
- 1045 • iron-containing hydrates, in particular for the mixed Fe-Al-hydrogarnet solid solution, $C_3FS_{0.84}H_{4.32}-$
- 1046 $C_3A_{0.5}F_{0.5}S_{0.84}H_{4.32}$, which takes up iron and a part of the aluminium in hydrated cements
- 1047 • AFm and AFt-phases with different water contents to describe the effect of water activity and dry-
- 1048 ing on hydrates
- 1049 • amorphous, microcrystalline AH_3 and for gibbsite to study the effect of AH_3 solubility on the hy-
- 1050 drates in calcium aluminate and calcium sulfoaluminate cements
- 1051 • chloride, nitrate and nitrate-containing AFm phases
- 1052 • thaumasite and for the uptake of carbonates in SO_4 -ettringite.
- 1053 • description of the variation in Mg/Al in layered double hydroxides (hydrotalcite-like phases) ob-
- 1054 served in alkali activated materials
- 1055 • data for M-S-H and some Na- and Ca-based zeolites, which can form at the interaction zone of
- 1056 cement with clays, rocks or seawater and in alkali activated materials.

1057 These additions improve the reliability of thermodynamic modelling of cement systems, in particular
 1058 for alkali activated materials and for processes at cement/environment interfaces, where hydrates such
 1059 as thaumasite, Friedel's salt, M-S-H, and zeolites may form.

1060 The consideration of siliceous hydrogarnet solid solution in Cemdata18 leads to a quite significant re-
 1061 distribution of alumina and iron within the phase assemblage in PC; the predictions based on Cemda-
 1062 ta18 suggest that alumina is bound not only in AFt, AFm phases and hydrotalcite but also in siliceous
 1063 hydrogarnet phase while all hydrated iron is present in siliceous hydrogarnet.

1064

1065 Several C-S-H solubility models as well two models for hydroxide-hydrotalcite are available (Table 4,
 1066 Appendix A and B). The CSHQ and the OH-hydrotalcite with Mg/Al = 2 are well adapted for PC sys-
 1067 tems. Although CSHQ is able to describe the entire range of Ca/Si ratios encountered, it is best used
 1068 for high Ca/Si C-S-H as it lacks the ability to predict aluminium uptake, however, this is less important
 1069 in PC where the aluminium content is relatively low. For alkali activated binders, the CNASH model has
 1070 been developed for C-S-H type calcium (alkali) aluminosilicate hydrate gels with lower calcium but
 1071 higher aluminium and alkali content. An Mg-Al layered double hydroxide model with variable Mg/Al
 1072 ratio is also available for use in alkali activated cement systems.

1073

1074 Despite significant additions to the Cemdata18 TDB, several important gaps still exist in the database.
 1075 In particular, reliable thermodynamic data for alkali, aluminium and water uptake in C-S-H applicable
 1076 to high and low Ca/Si C-S-H and M-S-H, data for hydrotalcite-like phases of variable composition and
 1077 for different interlayer ions, data for further zeolites derived from experimental solubility measure-
 1078 ments, data for aqueous complexes which possibly form at high pH values as well as data for the reac-
 1079 tion products of alkali silica reaction are needed. However, these data gaps should be viewed as possi-
 1080 ble future improvements rather than barriers to use thermodynamic modelling: Cemdata18 database
 1081 has already been successfully applied to model hydrated PC, calcium aluminate, calcium sulfoalumi-
 1082 nate and blended cements, and also alkali activated materials. Cemdata18, therefore, enables im-

1083 proved characterisation and understanding of the chemistry and related in-service performance prop-
1084 erties of a wide range of cement systems, including the most common types.

1085

1086 **Acknowledgements**

1087 The partial financial support from the NANOCEM consortium (www.nanocem.org), the Swiss National
1088 Foundation (SNF grants No. 117605, 132559, 130419 and 200021_169014), from Nagra, Wettingen,
1089 Switzerland, and from the BMBF ThermAc3 Verbundprojekt (Germany) are gratefully acknowledged.

1090 The authors thank also Tres Thoenen, Ravi Patel and Andres Idiart for their support on the PHREEQC
1091 version.

1092

1093

1094 **References**

- 1095 [1] B. Lothenbach, T. Matschei, G. Möschner, F.P. Glasser, Thermodynamic modelling of the effect of
 1096 temperature on the hydration and porosity of Portland cement, *Cem Concr Res*, 38 (2008) 1-18.
- 1097 [2] T. Matschei, B. Lothenbach, F.P. Glasser, The role of calcium carbonate in cement hydration, *Cem*
 1098 *Concr Res*, 37 (2007) 551-558.
- 1099 [3] M. Moesgaard, D. Herfort, M. Steenberg, L.F. Kirkegaard, Y. Yue, Physical performance of blended
 1100 cements containing calcium aluminosilicate glass powder and limestone, *Cem Concr Res*, 41 (2011)
 1101 359-364.
- 1102 [4] T. Matschei, F.P. Glasser, Temperature dependence, 0 to 40 °C, of the mineralogy of Portland
 1103 cement paste in the presence of calcium carbonate, *Cem Concr Res*, 40 (2010) 763-777.
- 1104 [5] B. Lothenbach, F. Winnefeld, C. Alder, E. Wieland, P. Lunk, Effect of temperature on the pore
 1105 solution, microstructure and hydration products of Portland cement pastes, *Cem Concr Res*, 37 (2007)
 1106 483-491.
- 1107 [6] F. Deschner, B. Lothenbach, F. Winnefeld, J. Neubauer, Effect of temperature on the hydration
 1108 Portland cement blended with siliceous fly ash, *Cem Concr Res*, 52 (2013) 169-181.
- 1109 [7] T. Matschei, B. Lothenbach, F.P. Glasser, Thermodynamic properties of Portland cement hydrates in
 1110 the system $\text{CaO-Al}_2\text{O}_3\text{-SiO}_2\text{-CaSO}_4\text{-CaCO}_3\text{-H}_2\text{O}$, *Cem Concr Res*, 37 (2007) 1379-1410.
- 1111 [8] B.Z. Dilnesa, B. Lothenbach, G. Le Saout, G. Renaudin, A. Mesbah, Y. Filinchuk, A. Wichser, E.
 1112 Wieland, Iron in carbonate containing AFm phases, *Cem Concr Res*, 41 (2011) 311-323.
- 1113 [9] B.Z. Dilnesa, B. Lothenbach, G. Renaudin, A. Wichser, D. Kulik, Synthesis and characterization of
 1114 hydrogarnet $\text{Ca}_3(\text{Al}_x\text{Fe}_{1-x})_2(\text{SiO}_4)_y(\text{OH})_{4(3-y)}$, *Cem Concr Res*, 59 (2014) 96-111.
- 1115 [10] B.Z. Dilnesa, B. Lothenbach, G. Renaudin, A. Wichser, E. Wieland, Stability of monosulfate in the
 1116 presence of iron, *J Am Ceram Soc*, 95 (2012) 3305-3316.
- 1117 [11] D.A. Kulik, Improving the structural consistency of C-S-H solid solution thermodynamic models,
 1118 *Cem Concr Res*, 41 (2011) 477-495.
- 1119 [12] B. Lothenbach, L. Pelletier-Chaignat, F. Winnefeld, Stability in the system $\text{CaO-Al}_2\text{O}_3\text{-H}_2\text{O}$, *Cem*
 1120 *Concr Res*, 42 (2012) 1621-1634.
- 1121 [13] D. Kulik, T. Wagner, S. Dmytrieva, G. Kosakowski, F. Hingerl, K. Chudnenko, U. Berner, GEM-
 1122 Selektor geochemical modeling package: revised algorithm and GEMS3K numerical kernel for coupled
 1123 simulation codes, *Computational Geosciences*, 17 (2013) 1-24.
- 1124 [14] T. Wagner, D.A. Kulik, F.F. Hingerl, S.V. Dmytrieva, GEM-Selektor geochemical modeling package:
 1125 TSolMod library and data interface for multicomponent phase models, *Canadian Mineralogist*, 50
 1126 (2012) 1173-1195.
- 1127 [15] P. Blanc, X. Bourbon, A. Lassin, E. Gaucher, Chemical model for cement-based materials:
 1128 Temperature dependence of thermodynamic functions for nanocrystalline and crystalline C-S-H
 1129 phases, *Cem Concr Res*, 40 (2010) 851-866.
- 1130 [16] P. Blanc, X. Bourbon, A. Lassin, E. Gaucher, Chemical model for cement-based materials:
 1131 Thermodynamic data assessment for phases other than CSH, *Cem Concr Res*, 40 (2010) 1360-1374.
- 1132 [17] C.M. Bethke, *Geochemical and Biogeochemical Reaction Modeling*, (2nd Ed.), Cambridge
 1133 University Press, New York, NY, USA, 2008.
- 1134 [18] D.J. Parkhurst, C.A.J. Appelo, Description of input and examples for PHREEQC version 3 - A
 1135 computer program for speciation, batch-reaction, one-dimensional transport, and inverse geochemical
 1136 calculations, 6, USGS, Denver, CO, USA., 2013.
- 1137 [19] J.E. Cross, F.T. Ewart, HATCHES - A thermodynamic database and management system, *Radiochim*
 1138 *Acta*, 52/53 (1991) 421-422.
- 1139 [20] D. Damidot, B. Lothenbach, D. Herfort, F.P. Glasser, Thermodynamics and cement science, *Cem*
 1140 *Concr Res*, 41 (2011) 679-695.

- 1141 [21] G. Möschner, B. Lothenbach, J. Rose, A. Ulrich, R. Figi, R. Kretzschmar, Solubility of Fe-ettringite
1142 ($\text{Ca}_6[\text{Fe}(\text{OH})_6]_2(\text{SO}_4)_3 \cdot 26\text{H}_2\text{O}$), *Geochim Cosmochim Acta*, 72 (2008) 1-18.
- 1143 [22] T. Thoenen, W. Hummel, U. Berner, E. Curti, The PSI/Nagra Chemical Thermodynamic Data Base
1144 12/07, PSI report 14-04, Villigen PSI, Switzerland, 2014.
- 1145 [23] T. Thoenen, D.A. Kulik, Nagra/PSI Chemical Thermodynamic Data Base 01/01 for the GEM-Selektor
1146 (V.2- PSI) Geochemical Modeling Code: Release 28-02-03. Internal Report TM-44-03-04, available from
1147 <http://gems.web.psi.ch/TDB/doc/pdf/TM-44-03-04-web.pdf> (checked 2018-04-19), (2003).
- 1148 [24] W. Hummel, U. Berner, E. Curti, F.J. Pearson, T. Thoenen, Nagra/PSI Chemical Thermodynamic Data
1149 Base 01/01, Universal Publishers/uPUBLISH.com, USA, also published as Nagra Technical Report NTB
1150 02-16, Wetingen, Switzerland, 2002.
- 1151 [25] E. Shock, D. Sassani, M. Willis, D. Sverjensky, Inorganic species in geologic fluids: Correlations
1152 among standard molal thermodynamic properties of aqueous ions and hydroxide complexes, *Geochim*
1153 *Cosmochim Acta*, 61 (1997) 907-950.
- 1154 [26] D. Sverjensky, E. Shock, H. Helgeson, Prediction of the thermodynamic properties of aqueous
1155 metal complexes to 1000 C and 5 kb, *Geochim Cosmochim Acta*, 61 (1997) 1359-1412.
- 1156 [27] M. Balonis, B. Lothenbach, G. Le Saout, F.P. Glasser, Impact of chloride on the mineralogy of
1157 hydrated Portland cement systems, *Cem Concr Res*, 40 (2010) 1009-1022.
- 1158 [28] T. Matschei, F.P. Glasser, The thermal stability of thaumasite, *Mater Struct*, 48 (2015) 2277–2289.
- 1159 [29] B. Lothenbach, F. Winnefeld, Thermodynamic modelling of the hydration of Portland cement, *Cem*
1160 *Concr Res*, 36 (2006) 209-226.
- 1161 [30] L.G. Baquerizo, T. Matschei, K.L. Scrivener, Impact of water activity on the stability of ettringite,
1162 *Cem Concr Res*, 76 (2016) 31-44.
- 1163 [31] L.G. Baquerizo, T. Matschei, K.L. Scrivener, Hydration states of AFm cement phases, *Cem Concr Res*,
1164 73 (2015) 143-157.
- 1165 [32] L.G. Baquerizo, T. Matschei, K.L. Scrivener, M. Saeidpour, A. Thorell, L. Wadsö, Methods to
1166 determine hydration states of minerals and cement hydrates, *Cem Concr Res*, 65 (2014) 85-95.
- 1167 [33] M. Balonis, F.P. Glasser, The density of cement phases, *Cem Concr Res*, 39 (2009) 733-739.
- 1168 [34] M. Balonis, The influence of inorganic chemical accelerators and corrosion inhibitors on the
1169 mineralogy of hydrated Portland cement systems, Thesis, University of Aberdeen, Aberdeen, UK, 2010.
- 1170 [35] M. Balonis, M. Medala, F.P. Glasser, Influence of calcium nitrate and nitrite on the constitution of
1171 AFm and AFt cement hydrates, *Adv Cem Res*, 23 (2011) 129-143.
- 1172 [36] M. Balonis, F.P. Glasser, Calcium nitrite corrosion inhibitor in portland cement: influence of nitrite
1173 on chloride binding and mineralogy, *J Am Ceram Soc*, 94 (2011) 2230-2241.
- 1174 [37] B.Z. Dilnesa, Fe-containing hydrates and their fate during cement hydration: thermodynamic data
1175 and experimental study, Thesis, EPFL, Lausanne, 2012.
- 1176 [38] D. Garvin, V.B. Parker, H.J. White, CODATA thermodynamic tables. Selections for some compounds
1177 of calcium and related mixtures: a prototype set of tables, Springer Verlag, Berlin, 1987.
- 1178 [39] K.B. Rozov, U. Berner, D.A. Kulik, L.W. Diamond, Solubility and thermodynamic properties of
1179 carbonate-bearing hydrotalcite-pyroaurite solid solutions with a 3:1 Mg/(Al+Fe) mole ratio, *Clay Clay*
1180 *Miner*, 59 (2011) 215-232.
- 1181 [40] D. Nied, K. Enemark-Rasmussen, E. L'Hôpital, J. Skibsted, B. Lothenbach, Properties of magnesium
1182 silicate hydrates (M-S-H), *Cem Concr Res*, 79 (2016) 323-332.
- 1183 [41] B. Lothenbach, E. Bernard, U. Mäder, Zeolite formation in the presence of cement hydrates and
1184 albite, *Phys Chem Earth*, 99 (2017) 77-94.
- 1185 [42] V.J. Babushkin, G.M. Matveyev, O.P. Mchedlov-Petrosyan, Thermodynamics of Silicates. Springer-
1186 Verlag, Berlin, H, (1985).
- 1187 [43] H.C. Helgeson, J.M. Delany, H.W. Nesbitt, D.K. Bird, Summary and critique of the thermodynamic
1188 properties of rock-forming minerals, *Am J Sci*, 278-A (1978) 1-229.

- 1189 [44] R.A. Robie, B.S. Hemingway, Thermodynamic properties of minerals and related substances at
1190 298.15 K and 1 bar (105 Pascals) pressures and at higher temperatures, US Geol Surv Bull, 2131 (1995)
1191 1-461.
- 1192 [45] G. Möschner, B. Lothenbach, A. Ulrich, R. Figi, R. Kretschmar, Solid solution between Al-ettringite
1193 and Fe-ettringite ($\text{Ca}_6[\text{Al}_{1-x}\text{Fe}_x(\text{OH})_6]_2(\text{SO}_4)_3 \cdot 26\text{H}_2\text{O}$), *Cem Concr Res*, 39 (2009) 482-489.
- 1194 [46] E. Corazza, C. Sabelli, The crystal structure of syngenite, $\text{K}_2\text{Ca}(\text{SO}_4)_2 \cdot \text{H}_2\text{O}$, *Z Kristallog*, 124 (1967)
1195 398-408.
- 1196 [47] P. Blanc, P. Vieillard, H. Gailhanou, S. Gaboreau, N. Marty, F. Claret, B. Made, E. Giffaut,
1197 ThermoChimie database developments in the framework of cement/clay interactions, *Appl Geochem*,
1198 55 (2015) 95-107.
- 1199 [48] R.M. Milton, Molecular sieve adsorbents, US Patent No (1959) 2,882,244.
- 1200 [49] G. Gottardi, E. Galli, Natural Zeolites, *Mineral and Rocks*, 18 (1985).
- 1201 [50] H. Boysen, M. Lerch, A. Stys, A. Senyshyn, Structure and oxygen mobility in mayenite ($\text{Ca}_{12}\text{Al}_{14}\text{O}_{33}$):
1202 a high-temperature neutron powder diffraction study, *Acta Crystallogr*, B63 (2007) 675-682.
- 1203 [51] W. Hörkner, H. Müller-Buschbaum, Zur Kristallstruktur von CaAl_2O_4 , *J Inorg Nucl Chem*, 38 (1976)
1204 983-984.
- 1205 [52] D.W. Goodwin, A.J. Lindop, The crystal structure of $\text{CaO} \cdot 2\text{Al}_2\text{O}_3$, *Acta Crystallogr B*, 26 (1970) 1230-
1206 1235.
- 1207 [53] F. Winnefeld, B. Lothenbach, Phase equilibria in the system $\text{Ca}_4\text{Al}_6\text{O}_{12}\text{SO}_4 - \text{Ca}_2\text{SiO}_4 - \text{CaSO}_4 - \text{H}_2\text{O}$
1208 referring to the hydration of calcium sulfoaluminate cements, *RILEM Technical Letters*, 1 (2016) 10-16.
- 1209 [54] D. Damidot, S.J. Barnett, F.P. Glasser, D.E. Macphee, Investigation of the $\text{CaO}-\text{Al}_2\text{O}_3-\text{SiO}_2-\text{CaSO}_4-$
1210 $\text{CaCO}_3-\text{H}_2\text{O}$ system at 25°C by thermodynamic calculation, *Adv Cem Res*, 16 (2004) 69-76.
- 1211 [55] T. Schmidt, B. Lothenbach, M. Romer, K.L. Scrivener, D. Rentsch, R. Figi, A thermodynamic and
1212 experimental study of the conditions of thaumasite formation, *Cem Concr Res*, 38 (2008) 337-349.
- 1213 [56] D.E. Macphee, S.J. Barnett, Solution properties of solids in the ettringite-thaumasite solid solution
1214 series, *Cem Concr Res*, 34 (2004) 1591-1598.
- 1215 [57] F. Bellmann, On the formation of thaumasite $\text{CaSiO}_3 \cdot \text{CaSO}_4 \cdot \text{CaCO}_3 \cdot 15\text{H}_2\text{O}$: Part I, *Adv Cem Res*, 16
1216 (2004) 55-60.
- 1217 [58] U.A. Birnin-Yauri, F.P. Glasser, Friedel's salt, $\text{Ca}_2\text{Al}(\text{OH})_6(\text{Cl},\text{OH}) \cdot 2\text{H}_2\text{O}$: its solid solutions and their
1218 role in chloride binding, *Cem Concr Res*, 28 (1998) 1713-1723.
- 1219 [59] M.Y. Hobbs, Solubilities and ion exchange properties of solid solutions between OH, Cl and CO_3
1220 end members of the monocalcium aluminate hydrates, Thesis, University of Waterloo, Ontario, Canada,
1221 2001.
- 1222 [60] J.V. Bothe Jr, P.W. Brown, PhreeqC modeling of Friedel's salt equilibria at 23 ± 1 °C, *Cem Concr*
1223 *Res*, 34 (2004) 1057-1063.
- 1224 [61] R.O. Grishchenko, A.L. Emelina, P.Y. Makarov, Thermodynamic properties and thermal behavior of
1225 Friedel's salt, *Thermochim Acta*, 570 (2013) 74-79.
- 1226 [62] F.P. Glasser, A. Kindness, S.A. Stronach, Stability and solubility relationships in AFm phases. Part I.
1227 Chloride, sulfate and hydroxide, *Cem Concr Res*, 29 (1999) 861-866.
- 1228 [63] G. Falzone, M. Balonis, G. Sant, X-AFm stabilization as a mechanism of bypassing conversion
1229 phenomena in calcium aluminate cements, *Cem Concr Res*, 72 (2015) 54-68.
- 1230 [64] B.Z. Dilnesa, E. Wieland, B. Lothenbach, R. Dähn, K. Scrivener, Fe-containing phases in hydrated
1231 cements, *Cem Concr Res*, 58 (2014) 45-55.
- 1232 [65] M. Vespa, E. Wieland, R. Dähn, B. Lothenbach, Identification of the thermodynamically stable Fe-
1233 containing phase in aged cement pastes, *J Am Ceram Soc*, 98 (2015) 2286-2294.
- 1234 [66] H.F.W. Taylor, D.E. Newbury, An electron microprobe study of a mature cement paste, *Cem Concr*
1235 *Res*, 14 (1984) 565-573.

- 1236 [67] U. Mäder, A. Jenni, C. Lerouge, S. Gaboreau, S. Miyoshi, Y. Kimura, V. Cloet, M. Fukaya, F. Claret, T.
 1237 Otake, M. Shibata, B. Lothenbach, 5-year chemico-physical evolution of concrete–claystone interfaces,
 1238 Mont Terri rock laboratory (Switzerland), *Swiss J Geosci*, 110 (2017) 307-327.
- 1239 [68] S.A. Bernal, R. San Nicols, R.J. Myers, R. Mejia de Gutierrez, F. Puertas, J.S.J. Van Deventer, J.L.
 1240 Provis, MgO content of slag controls phase evolution and structural changes induced by accelerated
 1241 carbonation in alkali-activated binders, *Cem Concr Res*, 57 (2014) 33-43.
- 1242 [69] I.G. Richardson, A.R. Brough, G.W. Groves, C.M. Dobson, The characterization of hardened alkali-
 1243 activated blast-furnace slag pastes and the nature of the calcium silicate hydrate (C-S-H) phase, *Cem*
 1244 *Concr Res*, 24 (1994) 813-829.
- 1245 [70] H. Taylor, Crystal structures of some double hydroxide minerals, *Mineral Mag*, 39 (1973) 377-389.
- 1246 [71] I. Richardson, Clarification of possible ordered distributions of trivalent cations in layered double
 1247 hydroxides and an explanation for the observed variation in the lower solid-solution limit, *Acta*
 1248 *Crystallogr B*, 69 (2013) 629-633.
- 1249 [72] D.G. Bennett, D. Read, M. Atkins, F.P. Glasser, A thermodynamic model for blended cements. II:
 1250 Cement hydrate phases; thermodynamic values and modelling studies, *J Nucl Mater*, 190 (1992) 315-
 1251 325.
- 1252 [73] W. Gao, Z. Li, Solubility and K SP of $Mg_4Al_2(OH)_{14} \cdot 3H_2O$ at the various ionic strengths,
 1253 *Hydrometallurgy*, 117-118 (2012) 36-46.
- 1254 [74] R.J. Myers, B. Lothenbach, S. Bernal, J.L. Provis, Thermodynamic modelling of alkali-activated slag-
 1255 based cements, *Appl Geochem*, 61 (2015) 233-247.
- 1256 [75] M. Zajac, S.K. Bremseth, M. Whitehead, M. Ben Haha, Effect of $CaMg(CO_3)_2$ on hydrate
 1257 assemblages and mechanical properties of hydrated cement pastes at 40°C and 60°C, *Cem Concr Res*,
 1258 65 (2014) 21-29.
- 1259 [76] B. Lothenbach, A. Nonat, Calcium silicate hydrates: solid and liquid phase composition, *Cem Concr*
 1260 *Res*, 78 (2015) 57-70.
- 1261 [77] I. Richardson, Tobermorite/jennite-and tobermorite/calcium hydroxide-based models for the
 1262 structure of CSH: applicability to hardened pastes of tricalcium silicate, β -dicalcium silicate, Portland
 1263 cement, and blends of Portland cement with blast-furnace slag, metakaolin, or silica fume, *Cem Concr*
 1264 *Res*, 34 (2004) 1733-1777.
- 1265 [78] A. Muller, K. Scrivener, A. Gajewicz, P. McDonald, Use of bench-top NMR to measure the density,
 1266 composition and desorption isotherm of C–S–H in cement paste, *Microporous and Mesoporous*
 1267 *Materials*, 178 (2013) 99-103.
- 1268 [79] A. Muller, K. Scrivener, J. Skibsted, A. Gajewicz, P. McDonald, Influence of silica fume on the
 1269 microstructure of cement pastes: New insights from 1H NMR relaxometry, *Cem Concr Res*, 74 (2015)
 1270 116-125.
- 1271 [80] C.S. Walker, S. Sutou, C. Oda, M. Mihara, A. Honda, Calcium silicate hydrate (C-S-H) gel solubility
 1272 data and a discrete solid phase model at 25 °C based on two binary non-ideal solid solutions, *Cem*
 1273 *Concr Res*, 79 (2016) 1-30.
- 1274 [81] S.-Y. Hong, F.P. Glasser, Alkali binding in cement pastes: Part I. The C-S-H phase, *Cem Concr Res*,
 1275 29 (1999) 1893-1903.
- 1276 [82] E. L'Hôpital, B. Lothenbach, D. Kulik, K. Scrivener, Influence of calcium to silica ratio on aluminium
 1277 uptake in calcium silicate hydrate, *Cem Concr Res*, 85 (2016) 111-121.
- 1278 [83] E. L'Hôpital, B. Lothenbach, G. Le Saout, D.A. Kulik, K. Scrivener, Incorporation of aluminium in
 1279 calcium-silicate hydrate, *Cem Concr Res*, 75 (2015) 91-103.
- 1280 [84] E. L'Hôpital, B. Lothenbach, K. Scrivener, D.A. Kulik, Alkali uptake in calcium alumina silicate
 1281 hydrate (C-A-S-H), *Cem Concr Res*, 85 (2016) 122-136.
- 1282 [85] D.A. Kulik, M. Kersten, Aqueous solubility diagrams for cementitious waste stabilization systems: II,
 1283 End-member stoichiometries of ideal calcium silicates hydrate solid solutions, *J Am Ceram Soc*, 84
 1284 (2001) 3017-3026.

1285 [86] J. Haas, A. Nonat, From C–S–H to C–A–S–H: Experimental study and thermodynamic modelling,
1286 Cem Concr Res, 68 (2015) 124-138.

1287 [87] S.V. Churakov, C. Labbez, Thermodynamics and molecular mechanism of Al incorporation in
1288 calcium silicate hydrates, J Phys Chem C, 121 (2017) 4412-4419.

1289 [88] D. Kulik, J. Tits, E. Wieland, Aqueous-solid solution model of strontium uptake in C-S-H phases,
1290 Geochim Cosmochim Acta, 71 (2007) A530.

1291 [89] B. Lothenbach, G. Le Saout, M. Ben Haha, R. Figi, E. Wieland, Hydration of a low-alkali CEM III/B-
1292 SiO₂ cement (LAC), Cem Concr Res, 42 (2012) 410-423.

1293 [90] R. Myers, S.A. Bernal, J.L. Provis, A thermodynamic model for C-(N-)A-S-H gel: CNASH_ss.
1294 Derivation and validation, Cem Concr Res, 66 (2014) 27-47.

1295 [91] D. Kulik, Dual-thermodynamic estimation of stoichiometry and stability of solid solution end
1296 members in aqueous-solid solution systems, Chem Geol, 225 (2006) 189-212.

1297 [92] J. Tits, E. Wieland, C.J. Müller, C. Landesman, M.H. Bradbury, Strontium binding by calcium silicate
1298 hydrates, J Colloid Interface Sci, 300 (2006) 78-87.

1299 [93] D.D. Wagman, E.H. Evans, V.B. Parker, R.H. Schumm, I. Halow, Bailey S.M, Churney K.L., N.R. L., The
1300 NBS tables of chemical thermodynamic properties. Selected values for inorganic and C1 and C2
1301 organic substances in SI units, J Phys Chem Ref Data, 11, Suppl. 2 (1982) 1-392.

1302 [94] I.G. Richardson, The calcium silicate hydrates, Cem Concr Res, 38 (2008) 137-158.

1303 [95] J.J. Chen, J.J. Thomas, H.F.W. Taylor, H.M. Jennings, Solubility and structure of calcium silicate
1304 hydrate, Cem Concr Res, 34 (2004) 1499-1519.

1305 [96] K. Garbev, M. Bornefeld, G. Beuchle, P. Stemmermann, Cell dimensions and composition of
1306 nanocrystalline calcium silicate hydrate solid solutions. part 2: X-Ray and thermogravimetry study, J Am
1307 Ceram Soc, 91 (2008) 3015-3023.

1308 [97] X. Gaona, D.A. Kulik, N. Macé, E. Wieland, Aqueous–solid solution thermodynamic model of U(VI)
1309 uptake in C–S–H phases, Appl Geochem, 27 (2012) 81-95.

1310 [98] A.J. Allen, J.J. Thomas, H.M. Jennings, Composition and density of nanoscale calcium–silicate–
1311 hydrate in cement, Nat Mater, 6 (2007) 311-316.

1312 [99] J.J. Thomas, A.J. Allen, H.M. Jennings, Density and water content of nanoscale solid C–S–H formed
1313 in alkali-activated slag (AAS) paste and implications for chemical shrinkage, Cem Concr Res, 42 (2012)
1314 377-383.

1315 [100] J.L. Provis, S.A. Bernal, Geopolymers and related alkali-activated materials, Annu Rev Mater Res,
1316 44 (2014) 299-327.

1317 [101] R.J. Myers, S.A. Bernal, J.L. Provis, Phase diagrams for alkali-activated slag binders, Cem Concr
1318 Res, 95 (2017) 30-38.

1319 [102] C.S. Walker, D. Savage, M. Tyrer, K.V. Ragnarsdottir, Non-ideal solid solution aqueous solution
1320 modeling of synthetic calcium silicate hydrate, Cem Concr Res, 37 (2007) 502-511.

1321 [103] L. Gomez-Zamorano, M. Balonis, B. Erdemli, N. Neithalath, G. Sant, C–(N)–S–H and N–A–S–H gels:
1322 Compositions and solubility data at 25°C and 50°C, J Am Ceram Soc, 100 (2017) 2700-2711.

1323 [104] R.J. Myers, E. L'Hôpital, J.L. Provis, B. Lothenbach, Effect of temperature and aluminium on
1324 calcium (alumino)silicate hydrate chemistry under equilibrium conditions, Cem Concr Res, 68 (2015)
1325 83-93.

1326 [105] R.J. Myers, E. L'Hôpital, J.L. Provis, B. Lothenbach, Composition-solubility-structure relationships
1327 in calcium (alkali) aluminosilicate hydrate (C-(N,K-)A-S-H), Dalton Trans, 44 (2015) 13530-13544.

1328 [106] G.D. Miron, D.A. Kulik, S.V. Dmytrieva, T. Wagner, GEMSFITS: Code package for optimization of
1329 geochemical model parameters and inverse modeling., Appl Geochem, 55 (2015) 28-45.

1330 [107] L. Nicoleau, E. Schreiner, Determination of Ca²⁺ complexation constants by monomeric silicate
1331 species at 25°C with a Ca²⁺ ion selective electrode, Cem Concr Res, 98 (2017) 36-43.

- 1332 [108] A. Jenni, U. Mäder, C. Lerouge, S. Gaboreau, B. Schwyn, In situ interaction between different
1333 concretes and Opalinus clay, *Phys Chem Earth*, 70-71 (2014) 71-83.
- 1334 [109] A. Dauzères, G. Achiedo, D. Nied, E. Bernard, S. Alahrache, B. Lothenbach, Magnesium
1335 perturbation in low-pH concretes placed in clayey environment—solid characterizations and modeling,
1336 *Cem Concr Res*, 79 (2016) 137-150.
- 1337 [110] D. Bonen, M.D. Cohen, Magnesium sulfate attack on portland cement paste—II. Chemical and
1338 mineralogical analyses, *Cem Concr Res*, 22 (1992) 707-718.
- 1339 [111] M. Santhanam, M.D. Cohen, J. Olek, Mechanism of sulfate attack: a fresh look: part 1: summary of
1340 experimental results, *Cem Concr Res*, 32 (2002) 915-921.
- 1341 [112] U.H. Jakobsen, K. De Weerd, M.R. Geiker, Elemental zonation in marine concrete, *Cem Concr Res*,
1342 85 (2016) 12-27.
- 1343 [113] C. Roos, S. Grangeon, P. Blanc, V. Montouillout, B. Lothenbach, P. Henocq, E. Giffaut, P. Vieillard,
1344 S. Gaboreau, Crystal structure of magnesium silicate hydrates (M S H): the relation with 2:1 Mg–Si
1345 phyllosilicates, *Cem Concr Res*, 73 (2015) 228-237.
- 1346 [114] E. Bernard, B. Lothenbach, F. Le Goff, I. Pochard, A. Dauzères, Effect of magnesium on calcium
1347 silicate hydrates (C-S-H), *Cem Concr Res*, 97 (2017) 61-72.
- 1348 [115] D.R.M. Brew, F.P. Glasser, Synthesis and characterisation of magnesium silicate hydrate gels, *Cem
1349 Concr Res*, 35 (2005) 85-98.
- 1350 [116] B. Lothenbach, D. Nied, E. L'Hôpital, G. Achiedo, A. Dauzères, Magnesium and calcium silicate
1351 hydrates *Cem Concr Res*, 77 (2015) 60-68.
- 1352 [117] W.-S. Chiang, G. Ferraro, E. Fratini, F. Ridi, Y.-Q. Yeh, U. Jeng, S.-H. Chen, P. Baglioni, Multiscale
1353 structure of calcium-and magnesium-silicate-hydrate gels, *J Mater Chem A*, 2 (2014) 12991-12998.
- 1354 [118] E. Bernard, B. Lothenbach, D. Rentsch, I. Pochard, A. Dauzères, Formation of magnesium silicate
1355 hydrates (M-S-H), *Phys Chem Earth*, 99 (2017) 142-157.
- 1356 [119] J.A.T. Smellie, Maqarin Natural Analogue Study: Phase III, SKB, SKB Technical Report 98-04,
1357 Stockholm, Sweden, 1998.
- 1358 [120] S.J. Chipera, J.A. Apps, Geochemical stability of natural zeolites, *Reviews in Mineralogy and
1359 Geochemistry*, 45 (2001) 117-161.
- 1360 [121] R. Arthur, H. Sasamoto, C. Walker, M. Yui, Polymer model of zeolite thermochemical stability, *Clay
1361 Clay Miner*, 59 (2011) 626-639.
- 1362 [122] J.L. Provis, G.C. Lukey, J.S. van Deventer, Do geopolymers actually contain nanocrystalline
1363 zeolites? A reexamination of existing results, *Chem Mater*, 17 (2005) 3075-3085.
- 1364 [123] B. Lothenbach, G. Le Saout, E. Gallucci, K. Scrivener, Influence of limestone on the hydration of
1365 Portland cements, *Cem Concr Res*, 38 (2008) 848-860.
- 1366 [124] K. De Weerd, M. Ben Haha, G. Le Saout, K.O. Kjellsen, H. Justnes, B. Lothenbach, Hydration
1367 mechanisms of ternary Portland cements containing limestone powder and fly ash, *Cem Concr Res*, 41
1368 (2011) 279-291.
- 1369 [125] F. Deschner, F. Winnefeld, B. Lothenbach, S. Seufert, P. Schwesig, S. Dittrich, F. Goetz-
1370 Neunhoffer, J. Neubauer, Hydration of a Portland cement with high replacement by siliceous fly ash
1371 *Cem Concr Res*, 42 (2012) 1389-1400.
- 1372 [126] T.G. Jappy, F.P. Glasser, Synthesis and stability of silica-substituted hydrogarnet $\text{Ca}_3\text{Al}_2\text{Si}_{3-x}\text{O}_{12-4x}(\text{OH})_{4x}$, *Adv Cem Res*, 4 (1991) 1-8.
- 1374 [127] A. Vollpracht, B. Lothenbach, R. Snellings, J. Haufe, The pore solution of blended cements: a
1375 review, *Mater Struct*, 49 (2016) 3341-3367.
- 1376 [128] W.R. Smith, R.W. Missen, *Chemical Reaction Equilibrium Analysis: Theory and Algorithms*, Wiley-
1377 Interscience, New York 1982. reprinted with corrections, Krieger, Malabar, FL., 1991.
- 1378 [129] T. Matschei, F.P. Glasser, New approaches to quantification of cement hydration, in: J. Stark (Ed.)
1379 16 Internationale Baustofftagung (ibautil), Weimar, Germany, 2006, pp. 390-400.

- 1380 [130] B.J. Merkel, B. Planer-Friederich, Groundwater Geochemistry. A Practical Guide to Modeling of
1381 Natural and Contaminated Aquatic Systems, Springer Berlin, 2008.
- 1382 [131] G.M. Anderson, D.A. Crerar, Thermodynamics in Geochemistry: the Equilibrium Model, Oxford
1383 University Press, Oxford, 1993.
- 1384 [132] D. Kulik, Minimising uncertainty induced by temperature extrapolations of thermodynamic data:
1385 a pragmatic view on the integration of thermodynamic databases into geochemical computer codes,
1386 in: The use of thermodynamic databases in performance assessment, OECD, Barcelona, 2002, pp. 125-
1387 137.
- 1388 [133] J.W. Johnson, E.H. Oelkers, H.C. Helgeson, SUPCRT92: A software package for calculating the
1389 standard molal thermodynamic properties of minerals, gases, aqueous species, and reactions from 1 to
1390 5000 bar and 0 to 1000°C, Comput Geosci, 18 (1992) 899-947.

1391

1392

1393 **Appendix: Cemdata18 thermodynamic dataset**

1394 **A Cemdata18 dataset in GEMS format**

1395 Cemdata18 database in GEM-Selektor v.3 format can be freely downloaded
1396 (<http://www.empa.ch/cemdata>) and is fully compatible with the GEMS version of the PSI/Nagra 12/07
1397 TDB [22, 23] (<http://gems.web.psi.ch>). As several alternative C-S-H models, as well as two models for
1398 hydroxide-hydrotalcite are available, the user needs to select the appropriate models during the gen-
1399 eration of new projects, as illustrated in Figure A.1. The CSHQ and the OH-hydrotalcite with Mg/Al = 2
1400 are well adapted for Portland cement systems (select cemdata, pc, ht and cshq as indicated at the left
1401 hand side of Figure A.1).

1402 For alkali activated binders, the CNASH model has been developed for C-S-H type calcium (alkali) alu-
1403 minosilicate hydrate gels with lower calcium but higher aluminium and alkali content. An Mg-Al lay-
1404 ered double hydroxide model with variable Mg/Al ratio is also available for use in alkali activated ce-
1405 ment systems. For alkali activated binders, the selection of cemdata and aam and deselection of pc is
1406 recommended as illustrated at the right hand side of Figure A.1.

1407

Built-in Database	Version	Built-in Database	Version
<input checked="" type="checkbox"/> support		<input checked="" type="checkbox"/> support	
<input checked="" type="checkbox"/> template		<input checked="" type="checkbox"/> template	
<input type="checkbox"/> supcrt		<input type="checkbox"/> supcrt	
<input checked="" type="checkbox"/> psi-nagra		<input checked="" type="checkbox"/> psi-nagra	
<input checked="" type="checkbox"/> 3rdparty		<input checked="" type="checkbox"/> 3rdparty	
<input checked="" type="checkbox"/> cemdata	18.01	<input checked="" type="checkbox"/> cemdata	18.01
<input checked="" type="checkbox"/> .		<input checked="" type="checkbox"/> .	
<input checked="" type="checkbox"/> pc	18.01	<input type="checkbox"/> pc	18.01
<input checked="" type="checkbox"/> .		<input type="checkbox"/> .	
<input checked="" type="checkbox"/> ht	18.01	<input type="checkbox"/> ht	18.01
<input checked="" type="checkbox"/> csh		<input type="checkbox"/> csh	
<input checked="" type="checkbox"/> cshq	18.01	<input type="checkbox"/> cshq	18.01
<input type="checkbox"/> cshkn	18.01	<input type="checkbox"/> cshkn	18.01
<input type="checkbox"/> csh3t	18.01	<input type="checkbox"/> csh3t	18.01
<input type="checkbox"/> csh2o	18.01	<input type="checkbox"/> csh2o	18.01
<input type="checkbox"/> aam	18.01	<input checked="" type="checkbox"/> aam	18.01
<input type="checkbox"/> .		<input checked="" type="checkbox"/> .	
<input type="checkbox"/> csh+ht	18.01	<input checked="" type="checkbox"/> csh+ht	18.01
<input checked="" type="checkbox"/> ss	18.01	<input checked="" type="checkbox"/> ss	18.01
<input checked="" type="checkbox"/> ss-fe3	18.01	<input checked="" type="checkbox"/> ss-fe3	18.01

1408

1409 Figure A.1: Selection of modules of Cemdata18 and related databases in GEM-Selektor to model PC
 1410 (Portland-cement) systems (left) and to model AAM (alkali-activated materials). For PC systems, one of
 1411 four alternative solid solution models of C-S-H should be selected (see Section 2.7); selection of Fe-
 1412 containing solid solutions ("ss-fe3" module) is also optional.

1413

1414 B Cemdata18 dataset in PHREEQC format

1415 To enable users to model cementitious systems using the Cemdata18 dataset with the popular
 1416 PHREEQC geochemical speciation code [18], a PHREEQC ".dat" format database of the Cemdata18 da-
 1417 taset (CEMDATA18-09-10-2017.dat) is provided for download from <http://www.empa.ch/cemdata>. This
 1418 LMA (Law of Mass Action) type dataset has been generated using the reaction generator module of
 1419 the ThermoMatch code (Miron et al. in preparation) and exported into the PHREEQC format ".dat" file
 1420 using the ThermoMatch database export module. The reaction generator algorithm is based on the
 1421 matrix "row reduce" method described by Smith and Missen [128]. In this process, all aqueous and sol-
 1422 id species from the Cemdata18 GEM-Selektor database were considered. The supplementary data for
 1423 aqueous, gaseous and solid species corresponding to the list of elements covered by Cemdata18 were
 1424 selected from the GEMS version of the PSI/Nagra TDB [22, 23]. The latter and the Cemdata18 GEM da-
 1425 tabase are mutually consistent, and should be used together in GEMS codes for modelling cementi-
 1426 tious systems.

1427 To generate PHREEQC-style reactions for product species, firstly the following master species were se-
 1428 lected based on their generic predominance: Ca^{+2} , Mg^{+2} , Sr^{+2} , Na^+ , K^+ , H^+ , CO_3^{-2} , SO_4^{-2} , Cl^- , NO_3^- , AlO_2^- ,
 1429 FeO_2^- , SiO_2^0 , H_2O^0 . Using selected master species, the reactions were automatically generated for the
 1430 remaining (product) species, and their properties at 25°C and 1 bar were calculated. Formation reac-
 1431 tions were generated for aqueous product species, and dissolution reactions - for gaseous and solid
 1432 product species. The LMA dataset of reactions was then exported into a PHREEQC "dat" file (CEMDA-
 1433 TA18-09-10-2017.dat) using the ThermoMatch database export module. Parameters for the $\log K^0=f(T)$

1434 analytical expressions were calculated for the 3-term extrapolation method that assumes the $\Delta_r C_p^\circ$ to
 1435 be not zero and independent of temperature. These reported parameters are used by PHREEQC for
 1436 calculating the $\log_{10}K^\circ$ as a function of temperature. Such temperature extrapolations of $\log_{10}K^\circ$ should
 1437 be valid at least up to 100°C.

1438 Table B.1 contains the generated formation reactions for the aqueous product species, together with
 1439 the values for reaction standard effects at 25°C and 1 bar. Table B.2 contains the generated dissolution
 1440 reactions for gaseous and solid product species, together with the reaction standard effects at 25°C
 1441 and 1 bar. Table B.2 contains, in addition to the Cemdata18 database as detailed in Table 1 to Table 4,
 1442 also the thermodynamic data of all solids composed of Al, C, Ca, Cl, Fe, H, K, Mg, N, Na, S, Si or Sr
 1443 compiled in the GEMS version of the PSI/Nagra 12/07 TDB [22, 23], needed to allow the generation of
 1444 a compatible dataset in PHREEQC. Figures B.1, B.2, and B.3 show comparisons of cement-related mod-
 1445 elling problems between GEM-Selektor (using GEM-type Cemdata18) and PHREEQC (using LMA-type
 1446 Cemdata18 CEMDATA18-09-10-2017.dat). For the PHREEQC calculations, PHREEQC for Windows ver-
 1447 sion 2.18.00 (uses PHREEQC-2 source version 2.18.3-5570) was used. In all three cases, the considered
 1448 solid solutions were modelled in PHREEQC using the simple ideal mixing model.

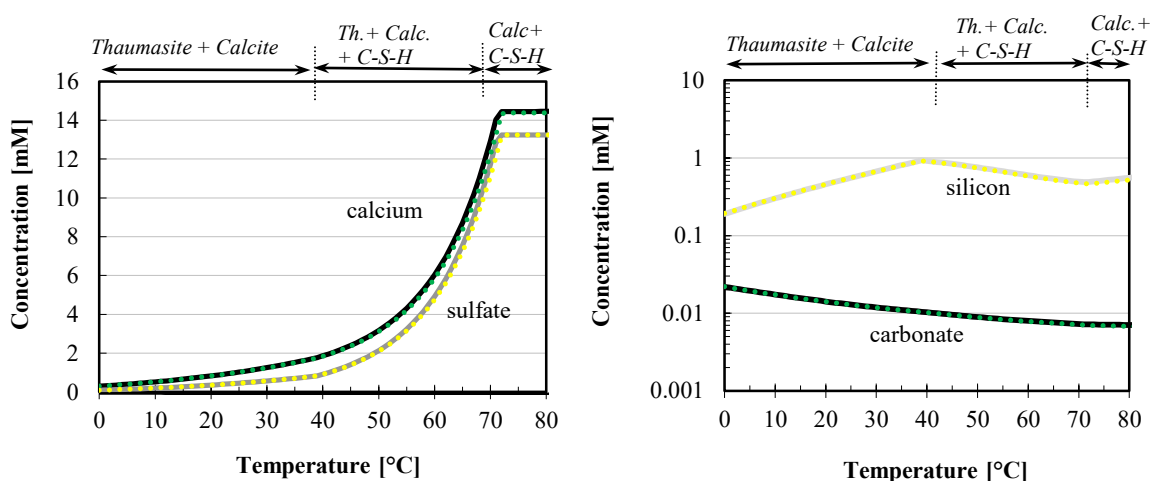
1449

1450 Table B.1 (in separate file)

1451

1452 Table B.2 (in separate file)

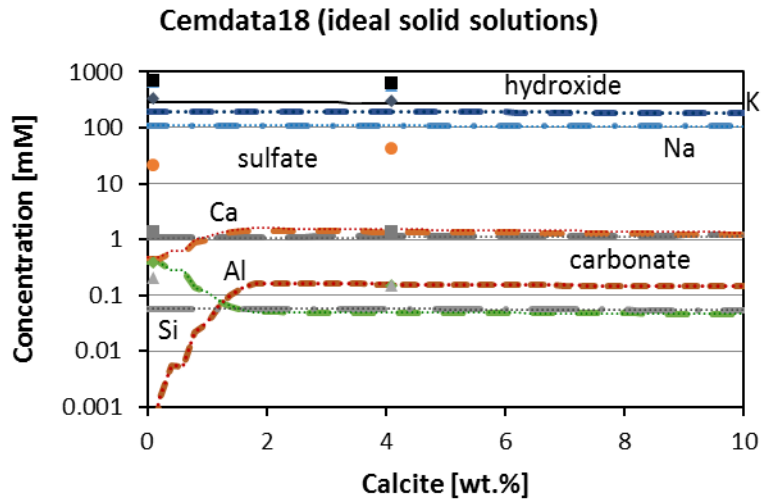
1453



1454

1455 **Figure B1.** Calculated (curves) solubility data for thaumasite, based on the new thermodynamic data
 1456 for thaumasite complemented with the CSHQ data from Cemdata18 [1, 7] in GEM format; Calculated
 1457 (dotted lines) solubility data for thaumasite, based on data Cemdata18 [1, 7] in PHREEQC format.

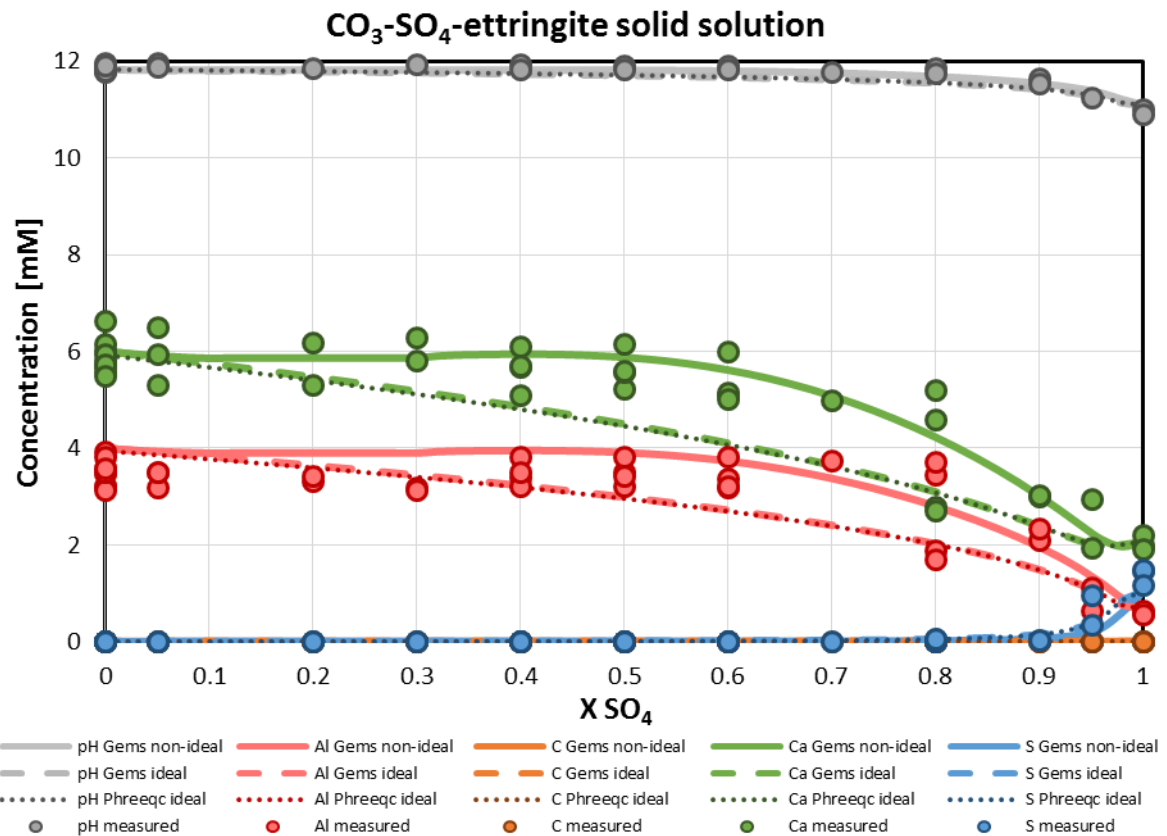
1458



1459

1460 **Figure B2:** Effect of the amount of limestone on the phase assemblage and the distribution of alumin-
 1461 ium and iron in hydrated Portland cement calculated using Cemdata18 GEM format (dashed lines) and
 1462 Cemdata18 PHREEQC format (dotted lines), in both cases using ideal solid solutions.

1463



1464

1465 **Figure B3.** Calculated aqueous composition in equilibrium with $\text{CO}_3\text{-SO}_4\text{-ettringite}$ solid solution as a
 1466 function of SO_4 in the solid. Solid lines calculated using the Cemdata18 GEM format using non ideal
 1467 solid solution; Dashed lines calculated using the Cemdata18 GEM format using ideal solid solution;
 1468 Dotted lines calculated using the Cemdata18 PHREEQC format using ideal solid solution; Circles: ex-
 1469 perimental data [7, 129]

1470 **C Thermodynamic equations and assumptions**

1471 The solubility products compiled in Cemdata18 have generally been derived from solutions composi-
 1472 tion measured at different temperatures, as documented in detail in [1, 7-10, 12, 27, 28, 30, 31, 34-37,
 1473 39-41]. The activity of a species i , a_i , has been calculated with GEMS from the measured concentrations
 1474 considering the formation of aqueous complexes. By definition $a_i = \gamma_i^* m_i$, where γ_i is the activity coeffi-
 1475 cient and m_i the concentration in mol/kg H₂O. Activity coefficients of aqueous species γ_i were comput-
 1476 ed using the built-in extended Debye-Hückel equation with the common ion-size parameter a_i of 3.67
 1477 Å for KOH and 3.31 Å for NaOH solutions and the common third parameter b_y according to the equa-
 1478 tion (C.1):

$$1479 \log \gamma_i = \frac{-A_y z_i^2 \sqrt{I}}{1 + B_y a_i \sqrt{I}} + b_y I \quad (C.1)$$

1480 where z_i denotes the charge of species i , I is the effective molal ionic strength, b_y is a semi-empirical
 1481 parameter (~ 0.123 for KOH and ~ 0.098 for NaOH electrolyte at 25°C), and A_y and B_y are P, T -
 1482 dependent coefficients. For uncharged species, equation (C.1) reduces to $\log \gamma_i = b_y I$. This extended
 1483 Debye-Hückel activity correction is applicable up to approx. 1 m ionic strength [130].
 1484 From the solubility products K of solids calculated at different temperatures T , the Gibbs free energy of
 1485 reaction, $\Delta_r G^\circ$, the Gibbs free energy of formation, $\Delta_f G^\circ$, and the absolute entropy, S° , at $T_0=298.15$ K
 1486 were obtained according to equations (C.2) and (C.3):

$$1487 \Delta_r G^\circ = \sum_i \nu_i \Delta_f G^\circ = -RT \ln K \quad (C.2)$$

$$1488 \Delta_a G_T^\circ = \Delta_f G_{T_0}^\circ - S_{T_0}^\circ (T - T_0) + \int_{T_0}^T C_p^0 dT - \int_{T_0}^T \frac{C_p^0}{T} dT \quad (C.3)$$

1489 Using $C_p^0 = a_0 + a_1 T + a_2 T^2 + a_3 T^{0.5}$ [131], where a_{0-3} are the empirical parameters defined for each
 1490 mineral, the two integral terms of equation (C.3) can be solved to give equation (C.4):

$$1491 \Delta_a G_T^\circ = \Delta_f G_{T_0}^\circ - S_{T_0}^\circ (T - T_0) - a_0 \left(T \ln \frac{T}{T_0} - T + T_0 \right) - 0.5 a_1 (T - T_0)^2 - a_2 \frac{(T - T_0)^2}{2T \cdot T_0^2} - a_3 \frac{2(\sqrt{T} - \sqrt{T_0})^2}{\sqrt{T_0}} \quad (C.4)$$

1493 where ν_i are the stoichiometric reaction coefficients, $R = 8.31451$ J/mol/K, T is the temperature in K,
 1494 and C_p^0 is the heat capacity at constant pressure. The apparent Gibbs free energy of formation, $\Delta_a G_T^\circ$,
 1495 refers to standard Gibbs energies of elements at 298.15 K. A more detailed description of the deriva-
 1496 tion of the dependence of the Gibbs free energy on temperature is available in [131, 132].

1497

1498 Dependence of the solubility product on temperature, consistent to Eq C.4 can be expressed as:

$$1499 \log K_T = A_0 + A_1 T + \frac{A_2}{T} + A_3 \ln T + \frac{A_4}{T^2} + A_5 T^2 + A_6 \sqrt{T} \quad (C.5)$$

1500 [131], where A_0, \dots, A_6 are empirical coefficients. If the entropy (S°), the enthalpy ($\Delta_r H^\circ$), and the coeffi-
 1501 cients (a_0, a_1, \dots) of the heat capacity equation ($C_p^\circ = a_0 + a_1 T + a_2 T^{-2} + a_3 T^{-0.5} + a_4 T^2$) of the species are
 1502 available, the coefficients A_0, \dots, A_6 can be calculated directly (see [131]). These calculations involving
 1503 Eqs C.4 and C.5 are all implemented in the GEM-Selektor.

1504 The heat capacity function, $C_p = f(T)$ is usually obtained from calorimetry experiments. In many cases,
 1505 the heat capacity has to be estimated by using a reference reaction with a solid having a known heat
 1506 capacity and similar structure, as described in publications [1, 7-10, 12, 27, 28, 30, 31, 34-37, 39-41].
 1507 Helgeson et al. [43] applied this principle successfully to estimate heat capacities of silicate minerals by
 1508 formulating reactions involving structurally-related minerals with known heat capacity functions. This
 1509 method has limitations due to the differing thermodynamic properties of "water" varieties, bound
 1510 loosely as a hydration water, or structurally as OH-groups. To minimize errors associated with the vary-
 1511 ing strengths of bonding for "water", reference reactions had been formulated to involve no "free" wa-
 1512 ter as a substituent in reactions, wherever appropriate.

1513 The value of $\Delta_r C_p^0$ has little influence on the calculated log K value in the temperature range 0-100°C
 1514 and is thus often assumed to be constant in a narrow temperature range: $\Delta_r C_p^0_T = \Delta_r C_p^0_{T_0} = \Delta a_0$. This
 1515 simplifies Eq. C.5 to the so called 3-term approximation of the temperature dependence, see Eq. C.6,
 1516 which can be used to compute the standard thermodynamic properties of each solid [132] to obtain a
 1517 temperature-dependent "log K" function using equations C.6-C.12 (implemented in GEMS).

$$1518 \quad \log K_T = A_0 + A_2 T^{-1} + A_3 \ln T \quad (C.6)$$

$$1519 \quad \text{and} \quad A_0 = \frac{0.4343}{R} \cdot \left[\Delta_r S_{T_0}^0 - \Delta_r C_p^0_{T_0} (1 + \ln T_0) \right] \quad (C.7)$$

$$1520 \quad A_2 = \frac{0.4343}{R} \cdot (\Delta_r H_{T_0}^0 - \Delta_r C_p^0_{T_0} T_0) \quad (C.8)$$

$$1521 \quad A_3 = \frac{0.4343}{R} \cdot \Delta_r C_p^0_{T_0} \quad (C.9)$$

$$1522 \quad \Delta_r S_T^0 = \Delta_r S_{T_0}^0 + \Delta_r C_p^0_{T_0} \ln \frac{T}{T_0} \quad (C.10)$$

$$1523 \quad \Delta_r H_T^0 = \Delta_r H_{T_0}^0 + \Delta_r C_p^0_{T_0} (T - T_0) \quad (C.11)$$

$$1524 \quad \Delta_r G_T^0 = \Delta_r H_T^0 + T \Delta_r S_T^0 \quad (C.12)$$

1525 Within the relatively narrow temperature range of 0 to 100°C, where the Cemdata18 database is valid,
 1526 this simplification has a negligible influence on the resulting solubility products, also for non-
 1527 isoelectric reactions as exemplified for ettringite in [20].

1528

1529 **D Thermodynamic data for aqueous and gaseous species**

1530 The thermodynamic data for aqueous and gaseous species compatible with Cemdata18 are summa-
 1531 rized in Table D.1 and D.2.

1532

1533 **Table D.1** Standard (partial molal) thermodynamic properties and equation of state parameters of
 1534 aqueous species at 25°C, 1 bar used in GEM calculations, as detailed in the GEMS version of the
 1535 PSI/Nagra 12/07 TDB [22, 23]. Numbers referring to the charge of aqueous species are written after the
 1536 plus or minus signs to avoid any ambiguity; "@" is used to represent a neutral aqueous species.

Species	ΔG^0	ΔH^0	S^0	C_p^0	V^0	$a_1 \cdot 10^*$	$a_2 \cdot 10^{-2^*}$	a_3	$a_4 \cdot 10^{-4}$	c_1	$c_2 \cdot 10^{-4}$	$\omega_0 \cdot 10^{-5}$
	(kJ/mol)	(kJ/mol)	(J/mol-K)	(J/mol-K)	(J/bar)	(cal/mol/ba	(cal/mol)	(cal-K/mol/bar)	(cal-K/mol)	(cal/mol/K)	(cal-K/mol)	(cal/mol)
Al(SO ₄) ⁺	-1250.43	-1422.67	-172.38	-204.01	-6.02	1.3869	-4.3920	7.4693	-2.5974	-11.6742	-12.9914	1.1729
Al(SO ₄) ²⁻	-2006.30	-2338.40	-135.50	-268.37	31.11	6.8275	8.8925	2.2479	-3.1466	-12.0220	-16.1447	2.1199
Al ⁺³	-483.71	-530.63	-325.10	-128.70	-45.24	-3.3802	-17.0071	14.5185	-2.0758	10.7000	-8.0600	2.7530
AlO ⁺	-660.42	-713.64	-112.97	-125.11	0.31	2.1705	-2.4811	6.7241	-2.6763	-2.5983	-9.1455	0.9570
AlO ₂ ⁻	-827.48	-925.57	-30.21	-49.04	9.47	3.7221	3.9954	-1.5879	-2.9441	15.2391	-5.4585	1.7418
AlO ₂ H [⊙]	-864.28	-947.13	20.92	-209.21	13.01	3.5338	0.8485	5.4132	-2.8140	-23.4129	-13.2195	-0.0300
AlOH ⁺²	-692.60	-767.27	-184.93	55.97	-2.73	2.0469	-2.7813	6.8376	-2.6639	29.7923	-0.3457	1.7247
Ca(CO ₃) [⊙]	-1099.18	-1201.92	10.46	-123.86	-15.65	-0.3907	-8.7325	9.1753	-2.4179	-11.5309	-9.0641	-0.0380
Ca(HCO ₃)	-1146.04	-1231.94	66.94	233.70	13.33	3.7060	1.2670	5.2520	-2.8310	41.7220	8.3360	0.3080
Ca(HSiO ₃)	-1574.24	-1686.48	-8.33	137.80	-6.74	1.0647	-5.1787	7.7785	-2.5649	30.8048	3.6619	0.5831
Ca(SO ₄) [⊙]	-1310.38	-1448.43	20.92	-104.60	4.70	2.4079	-1.8992	6.4895	-2.7004	-8.4942	-8.1271	-0.0010
Ca ⁺²	-552.79	-543.07	-56.48	-30.92	-18.44	-0.1947	-7.2520	5.2966	-2.4792	9.0000	-2.5220	1.2366
CaOH ⁺	-717.02	-751.65	28.03	6.05	5.76	2.7243	-1.1303	6.1958	-2.7322	11.1286	-2.7493	0.4496
CH ₄ [⊙]	-34.35	-87.81	87.82	277.26	37.40	6.7617	8.7279	2.3212	-3.1397	42.0941	10.4707	-0.3179
Cl ⁻	-131.29	-167.11	56.74	-122.49	17.34	4.0320	4.8010	5.5630	-2.8470	-4.4000	-5.7140	1.4560
ClO ₄ ⁻	-8.54	-129.33	182.00	-24.00	43.90	8.1411	15.5654	-7.8077	-3.4224	16.4500	-6.5700	0.9699
CO ₂ [⊙]	-386.02	-413.84	117.57	243.08	32.81	6.2466	7.4711	2.8136	-3.0879	40.0325	8.8004	-0.0200
CO ₃ ⁻²	-527.98	-675.31	-50.00	-289.33	-6.06	2.8524	-3.9844	6.4142	-2.6143	-3.3206	-17.1917	3.3914
e ⁻	0	0	65.34	14.42	0	0	0	0	0	0	0	0
Fe(CO ₃) [⊙]	-644.49	-763.51	-58.45	-123.03	-17.23	-0.6069	-9.2604	9.3828	-2.3961	-11.4137	-9.0233	-0.0380
Fe(HCO ₃) ⁺	-689.86	-794.10	-8.87	231.41	8.18	3.1064	-0.1934	5.8191	-2.7710	43.9175	8.2195	0.5831
Fe(HSO ₄) ⁺	-853.48	-990.45	10.21	338.23	18.81	4.5330	3.2897	4.4500	-2.9149	58.2305	13.4217	0.5121
Fe(HSO ₄) ⁺	-787.15	-981.91	-248.95	426.71	2.32	2.8251	-0.8804	6.0891	-2.7426	83.8315	17.6994	1.9551
Fe(SO ₄) [⊙]	-848.81	-993.86	-16.86	-101.60	1.67	1.9794	-2.9454	6.9007	-2.6572	-8.4131	-7.9804	-0.0380
Fe(SO ₄) ⁺	-784.71	-942.42	-124.68	-145.93	-2.64	1.7837	-3.4232	7.0885	-2.6374	-5.1341	-10.1600	0.9986
Fe(SO ₄) ₂ ⁻	-1536.81	-1854.38	-87.78	-210.37	30.49	6.6756	8.5215	2.3937	-3.1312	-5.4923	-13.3173	1.9457
Fe ⁺²	-91.50	-92.24	-105.86	-32.44	-22.64	-0.7867	-9.6969	9.5479	-2.3780	14.7860	-4.6437	1.4382
Fe ⁺³	-17.19	-49.58	-277.40	-76.71	-37.79	-2.4256	-13.6961	11.1141	-2.2127	19.0459	-6.8233	2.5812
FeCl ⁺	-223.59	-258.05	-42.09	86.49	0.85	2.1468	-2.5367	6.7401	-2.6741	24.6912	1.1617	0.7003
FeCl ⁺²	-156.92	-212.67	-178.82	14.83	-22.86	-0.7164	-9.5277	9.4878	-2.3851	23.8149	-2.3482	1.7013
FeCl ₂ ⁺	-291.92	-385.75	-129.66	300.72	10.27	3.5610	0.9165	5.3828	-2.8168	57.6940	11.5846	1.0276

FeCl ₃ [®]	-417.51	-564.39	-131.06	368.22	35.94	6.6686	8.5038	2.4024	-3.1304	57.3959	14.8930	-0.0380
FeO ⁺	-222.00	-255.09	-46.44	-200.94	-42.02	-3.7118	-16.8408	12.3595	-2.0827	-15.3982	-12.8325	0.7191
FeO ₂ ⁻	-368.26	-443.82	44.35	-234.93	0.45	2.3837	-1.9602	6.5182	-2.6979	-13.3207	-14.5028	1.4662
FeO ₂ H [®]	-419.86	-480.95	92.88	-312.14	7.21	2.7401	-1.0905	6.1776	-2.7338	-37.8300	-18.2305	-0.0300
FeOH ⁺	-274.46	-325.65	-41.84	63.06	-16.71	-0.2561	-8.4029	9.0457	-2.4315	21.4093	0.0209	0.7003
FeOH ⁺²	-241.87	-292.79	-106.27	-33.69	-25.34	-1.1562	-10.6009	9.9077	-2.3407	14.6102	-4.7048	1.4382
H ⁺	0	0	0	0	0	0	0	0	0	0	0	0
H ₂ [®]	17.73	-4.02	57.74	166.85	25.26	5.1427	4.7758	3.8729	-2.9764	27.6251	5.0930	-0.2090
H ₂ O [®]	-237.18	-285.88	69.92	75.36	18.07	0	0	0	0	0	0	0
H ₂ S [®]	-27.93	-39.03	125.52	179.17	34.95	6.5097	6.7724	5.9646	-3.0590	32.3000	4.7300	-0.1000
HCN [®]	114.37	103.75	131.30	0	0	0	0	0	0	0	0	0
HCO ₃ ⁻	-586.94	-690.01	98.45	-34.85	24.21	7.5621	1.1505	1.2346	-2.8266	12.9395	-4.7579	1.2733
HS ⁻	11.97	-16.22	68.20	-93.93	20.21	5.0119	4.9799	3.4765	-2.9849	3.4200	-6.2700	1.4410
HSiO ₃ ⁻	-1014.60	-1144.68	20.92	-87.20	4.53	2.9735	-0.5181	5.9467	-2.7575	8.1489	-7.3123	1.5511
HSO ₃ ⁻	-529.10	-627.70	139.75	-5.38	32.96	6.7014	8.5816	2.3771	-3.1338	15.6949	-3.3198	1.1233
HSO ₄ ⁻	-755.81	-889.23	125.52	22.68	34.84	6.9788	9.2590	2.1108	-3.1618	20.0961	-1.9550	1.1748
K(SO ₄) ⁻	-1031.77	-1158.77	146.44	-45.13	27.46	5.9408	6.7274	3.0989	-3.0571	9.9089	-5.2549	1.0996
K ⁺	-282.46	-252.14	101.04	8.39	9.01	3.5590	-1.4730	5.4350	-2.7120	7.4000	-1.7910	0.1927
KOH [®]	-437.11	-474.15	108.37	-85.02	14.96	3.7938	1.4839	5.1619	-2.8402	-6.1240	-7.2104	-0.0500
Mg(CO ₃) [®]	-998.98	-1132.12	-100.42	-116.50	-16.78	-0.5450	-9.1130	9.3320	-2.4020	-10.4990	-8.7060	-0.0380
Mg(HCO ₃)	-1047.02	-1153.97	-12.55	254.42	9.34	3.2710	0.2060	5.6690	-2.7880	47.2840	9.3400	0.5990
Mg(HSiO ₃)	-1477.15	-1613.91	-99.50	158.65	-10.85	0.6289	-6.2428	8.1967	-2.5209	36.7882	4.6702	0.9177
Mg ⁺²	-453.99	-465.93	-138.07	-21.66	-22.01	-0.8217	-8.5990	8.3900	-2.3900	20.8000	-5.8920	1.5372
MgOH ⁺	-625.87	-690.02	-79.91	129.23	1.64	2.3105	-2.1365	6.5827	-2.6906	32.0008	3.2394	0.8449
MgSO ₄ [®]	-1211.97	-1368.77	-50.88	-90.31	1.81	1.9985	-2.8987	6.8823	-2.6591	-6.8307	-7.4304	-0.0380
N ₂ [®]	18.19	-10.37	95.81	234.16	33.41	6.2046	7.3685	2.8539	-3.0836	35.7911	8.3726	-0.3468
Na(CO ₃) ⁻	-797.11	-938.56	-44.31	-51.28	-0.42	2.3862	-1.9521	6.5103	-2.6982	15.3395	-5.5686	1.7870
Na(HCO ₃)	-847.39	-929.50	154.72	200.33	32.32	6.1730	7.2943	2.8760	-3.0805	33.8790	6.7193	-0.0380
Na(SO ₄) ⁻	-1010.34	-1146.66	101.75	-30.09	18.64	4.7945	3.9284	4.1990	-2.9414	13.4899	-4.5256	1.2606
Na ⁺	-261.88	-240.28	58.41	38.12	-1.21	1.8390	-2.2850	3.2560	-2.7260	18.1800	-2.9810	0.3306
NaOH [®]	-418.12	-470.14	44.77	-13.40	3.51	2.2338	-2.3287	6.6683	-2.6826	4.0146	-3.6863	-0.0300
NH ₃ [®]	-26.67	-81.53	107.82	76.89	24.45	5.0911	2.7970	8.6248	-2.8946	20.3000	-1.1700	-0.0500
NH ₄ ⁺	-79.40	-133.26	111.17	67.11	18.08	3.8763	2.3448	8.5605	-2.8759	17.4500	-0.0210	0.1502
NO ₃ ⁻	-110.91	-206.89	146.94	-66.80	28.66	7.3161	6.7824	-4.6838	-3.0594	7.7000	-6.7250	1.0977
O ₂ [®]	16.45	-12.24	108.95	234.13	30.50	5.7889	6.3536	3.2528	-3.0417	35.3530	8.3726	-0.3943
OH ⁻	-157.27	-230.01	-10.71	-136.34	-4.71	1.2527	0.0738	1.8423	-2.7821	4.1500	-10.3460	1.7246
S ₂ O ₃ ⁻²	-519.99	-649.86	66.94	-238.47	27.59	6.6685	12.4951	-7.7281	-3.2955	-0.0577	-14.7066	2.9694
SCN ⁻	92.70	76.40	144.01	-39.69	35.36	7.0244	9.3687	2.0708	-3.1662	10.7414	-4.9900	1.1073
SO ₃ ⁻²	-487.89	-636.89	-29.29	-280.99	-4.12	2.4632	-1.7691	6.4494	-2.7058	-2.7967	-16.7843	3.3210
SO ₄ ⁻²	-744.46	-909.70	18.83	-266.09	12.92	8.3014	-1.9846	-6.2122	-2.6970	1.6400	-17.9980	3.1463
Sr(CO ₃) [®]	-1107.83	-1207.29	35.56	-134.32	-15.23	-0.3332	-8.5922	9.1201	-2.4237	-12.9961	-9.5733	-0.0380
Sr(HCO ₃) ⁺	-1157.54	-1239.00	95.94	210.07	14.08	3.7702	1.4274	5.1820	-2.8380	37.4746	7.1883	0.2058
Sr(SO ₄) [®]	-1321.37	-1451.50	61.59	-110.60	5.02	2.4382	-1.8251	6.4604	-2.7035	-9.6731	-8.4183	-0.0380
Sr ⁺²	-563.84	-550.87	-31.51	-41.56	-17.76	0.7071	-10.1508	7.0027	-2.3594	10.7452	-5.0818	1.1363
SrOH ⁺	-725.16	-754.14	61.09	-31.66	7.10	2.8620	-0.7922	6.0586	-2.7462	4.7576	-4.5826	0.3306

Temperature correction using Cp(T) integration						a ₀	a ₁	a ₂	(Cp ⁰ = a ₀ + a ₁ T + a ₂ T ²)
SiO ₂ ^{@**}	-833.41	-887.86*	41.34	44.47	1.61	46.94	0.034	-1.13E+06	
Temperature correction using logK(T)						A ₀	A ₁	A ₂	(logK _T = A ₀ + A ₁ T + A ₂ T ⁻¹)
SiO ₃ ^{-2**}	-938.51	-1098.74	-80.20	119.83	0	-10.0006	0	-3917.5	
Si ₄ O ₁₀ ^{-4***}	-3600.81	-3915.99	305.20	328.58	0	0	0	-10822.8	
CaSiO ₃ ^{@**}	-1517.56	-1668.06	-136.68	88.90	0	0	0	1371.49	
MgSiO ₃ [@]	-1425.03	-1554.54	-75.17	-264.79	0	5.7	0	0	
AlSiO ₅ ^{-3***}	-1769.01	-2027.33	-110.41	70.78	-3.41	0	0	158.02	
AlHSiO ₃ ⁺²	-1540.55	-1634.31	-24.99	-215.896	0	14.5828	0	-2141.57	
FeHSiO ₃ ⁺²	-1087.15	-1194.26	-70.77	-163.91	0	9.7	0	0	
Fe ₂ (OH) ₂ ⁺⁴	-491.9	-614.44	-281.97	-2.71	0	6.94586	0	-2950.45	
Fe ₃ (OH) ₄ ⁺⁵	-964.33	-1232.44	-472.43	71.30	0	4.1824	0	-3125.33	
SrSiO ₃ ^{@***}	-1527.29	-1617.43	79.92	78.39	1.64	0	0	1302.92	
S ⁻²	120.42	-16.22	-295.55	-93.93	0	-19	0	0	

1537 * parameters of the HKF-equation of state; given in original calorimetric units (see [25, 26, 133]) as used in GEM.

1538 ** calculated in Matschei et al. [7] assuming Δ_rS° = Δ_rC_p° = 0 using S° and C_p° from SiO₂ (quartz) for the reactions: SiO₂⁰ ->

1539 SiO₂(quartz) Δ_rG° = Δ_rH° = -21.386; SiO₃²⁻ + 2H⁺ -> SiO₂⁰ + H₂O Δ_rG° = 132.08, Δ_rH° = 75, Δ_rS° = -191.46, Δ_rC_p° = 0; SiO₃²⁻ + Ca²⁺ -> Ca-

1540 SiO₃⁰ Δ_rG° = Δ_rH° = -26.257, Δ_rS° = 0, Δ_rC_p° = 0;

1541 *** calculated in this paper assuming Δ_rS° = Δ_rC_p° = 0 using S° and C_p° from SiO₂ (quartz) for the reactions: SiO₃²⁻ + AlO₂⁻ -> AlSiO₅⁻³

1542 Δ_rG° = Δ_rH° = -3.025, Δ_rS° = 0, Δ_rC_p° = 0; Si₄O₁₀⁻⁴ + 4H⁺ -> 4SiO₂⁰ + 2H₂O Δ_rG° = Δ_rH° = 207.2, Δ_rS° = 0, Δ_rC_p° = 0; SiO₃²⁻ + Mg²⁺ ->

1543 MgSiO₃⁰ Δ_rG° = -32.54, Δ_rH° = 0, Δ_rS° = 109.126, Δ_rC_p° = 0; SiO₃²⁻ + Sr²⁺ -> SrSiO₃⁰ Δ_rG° = Δ_rH° = -29.944, Δ_rS° = 0, Δ_rC_p° = 0;

1544 ^v From the GEMS version of the PSI/Nagra 12/07 TDB [22, 23]: Al⁺³ + HSiO₃⁻ -> AlHSiO₃⁺² Δ_rG° = -42.24, Δ_rH° = 41, Δ_rS° = 279.19,

1545 Δ_rC_p° = 0; Fe⁺³ + HSiO₃⁻ -> FeHSiO₃⁺² Δ_rG° = -55.37, Δ_rH° = 0, Δ_rS° = 185.7, Δ_rC_p° = 0; 2Fe⁺³ + 2H₂O -> Fe₂(OH)₂⁺⁴ + 2H⁺ Δ_rG° =

1546 16.84, Δ_rH° = 56.486, Δ_rS° = 132.98, Δ_rC_p° = 0; 3Fe⁺³ + 4H₂O -> Fe₃(OH)₄⁺⁵ + 4H⁺ Δ_rG° = 35.96, Δ_rH° = 59.834, Δ_rS° = 80.07, Δ_rC_p° = 0;

1547

1548

1549 **Table D.2** Standard (partial molal) thermodynamic properties and heat capacity coefficients

1550 (Cp⁰ = a₀ + a₁T + a₂T²) of gaseous species at 25°C, 1 bar used in GEM calculations, as used in

1551 the GEMS version of the PSI/Nagra 12/07 TDB [22, 23].

Species	ΔG ⁰	ΔH ⁰	S ⁰	Cp ⁰	V ⁰	a ₀	a ₁	a ₂
	(kJ/mol)	(kJ/mol)	(J/mol·K)	(J/mol·K)	(J/bar)	(J/mol·K)	(J/mol·K ²)	(J·K/mol)
CH ₄	-50.66	-74.81	186.26	35.75	2479	23.64	0.0479	-192464
CO ₂	-394.39	-393.51	213.74	37.15	2479	44.22	0.0088	-861904
H ₂	0	0	130.68	28.82	2479	27.28	0.0033	50208
H ₂ O	-228.68	-242.40	187.25	40.07	2479	52.99	-0.0435	5472
H ₂ S	-33.75	-20.63	205.79	34.20	2479	32.68	0.0124	-192464
N ₂	0	0	191.61	29.13	2479	28.58	0.0038	-50208
O ₂	0	0	205.14	29.32	2479	29.96	0.0042	-167360

1552

1553